

DISS. ETH NO. 22981

MICROFLUIDIC DEVICES FOR BIOMOLECULE QUANTIFICATION IN SINGLE MICROBES

A thesis submitted to attain the degree of

DOCTOR OF SCIENCES of ETH ZURICH

(Dr. sc. ETH Zurich)

presented by

Simone Stratz

MSc Chemistry, University of Basel

born on 29.03.1988

citizen of Germany

accepted on the recommendation of

Prof. Dr. Petra S. Dittrich, examiner

Prof. Dr. Viola Vogel, co-examiner

2015

A scientist in his laboratory is not a mere technician: he is also a child confronting natural phenomena that impress him as though they were fairy tales.

Marie Curie

Dedicated to my family and friends
with gratitude for their love and support

Denn die einen sind im Dunkeln
und die andern sind im Licht
und man siehet die im Lichte
die im Dunkeln sieht man nicht.

Bertolt Brecht, Dreigroschenoper

Acknowledgements

I would like to express my gratitude to Prof. Petra S. Dittrich for the great supervision of my PhD thesis. I am particular thankful for the following two aspects that made my research stay in the Dittrich group to a highly instructive experience: The high degree of granted research freedom and trust that enabled me to develop an autonomous and independent working style and the “open office door”-mentality that allowed me anytime to step in and discuss scientific issues.

In addition, I would like to thank the entire Dittrich group for the great team spirit and the excellent collegial working atmosphere. My special thanks go to Klaus Eyer, Felix Kurth, Pascal Verboket, Mario Lenz and Karina Hasler. Klaus Eyer supervised my Master thesis and taught me the basics of immunoassays, microscopy and how to prepare a typical Swiss cheese fondue. His tremendous cooperativeness and cordial openness facilitated my first steps at ETH. Felix Kurth explained me the basics of mammalian cell cultivation and microbiology. Moreover, he was a role model for me with regard to his disciplined and structured working style. Pascal Verboket shared with me for more than 3 years the same office. During that time, he provided IT-support, delicious tea products, cleaning tissues for eyewear and, most important, good humor. Mario Lenz, the real “ETH-veteran” of our group, always shared his enormous knowledge about ETH services and available training opportunities and thereby supported the broadening of the own scientific horizon. My particular thanks go to Karina Hasler who performed her semester- and master thesis under my supervision. Due to her quick perception, technical skills and open-minded nature, working together with her was an enormous enrichment.

Aside from the professional environment, I would like to thank my personal surroundings. First of all Michael, who was always on my side. Mastering the numerous new challenges I was faced during my PhD was considerably facilitated by his love and encouragement. Moreover, I am particular grateful for the multifaceted support provided by my parents and my sisters who followed my research projects with great interest. Last but not least, I would like to thank my little niece and nephews for reminding me of the importance of life’s little pleasures like eating ice cream on a hot summer day.

Abstract

In the last decades, numerous studies were undertaken to investigate the behavior of individual cells. The obtained findings clearly confirm the phenotypic heterogeneity in isogenic cell populations. Consequently, current research issues go beyond the pure demonstration of phenotypic differences among cells of a seemingly homogenous population. An additional challenge is to determine which factors of observed cellular heterogeneity fulfill an important biological function and through what underlying control mechanisms are they regulated. In this context, research methods are required that enable the comprehensive characterization of a population on the single-cell level. For this purpose, microfluidic techniques are particularly advantageous, as they allow the accurate handling of small fluid volumes matching those of individual cells. Moreover, microfluidic systems are suitable for long-term cell studies. Consequently, biological information can be provided that is not accessible by snapshot methods relying on single point in time observations such as flow cytometry. Although several microfluidic platforms adapted for single cell analysis have already been presented, a major challenge remains the construction of devices that cover a broad application range.

The work presented in this thesis discusses the development of microfluidic platforms that exceed the functional scope of existing systems. Particular emphasis is placed on two aspects. The precise handling of single microbes characterized by volumes in the low femtoliter range is aimed. Furthermore, multifunctional device designs that enable the comprehensive analysis of single cells are focused.

First, a microfluidic system optimized for bacterial cell studies was developed. The chip design was adapted to the well-studied eukaryotic model organism *Escherichia coli* (*E. coli*). Key feature of the device was a set of microanalysis chambers equipped with cell traps for hydrodynamic capture of a single *E. coli* and ring-shaped valves which, when actuated, isolated the bacterium in a volume of only 155 pL. In addition, a surface modification protocol was implemented for immunoassay-based analysis of the single-cell lysates. The platform was used to quantify the enzyme β -galactosidase in individual *E. coli* cultured under varying nutrient conditions. The results were compared with literature values of bulk measurements whereas our findings additionally enabled to measure the heterogeneous gene expression.

A second device design focused on multifunctional usage. The micrometer-sized cell traps were optimized for the geometry of single *Saccharomyces cerevisiae* (*S. cerevisiae*) cells. Main characteristic was the implemented double-valve configuration surrounding each cell trap. This design feature enabled to switch within milliseconds between complete and partial isolation of the captured cell. Functionality of the platform was demonstrated by on-chip cultivation of *S. cerevisiae* cells grown under differing nutrient conditions. The observed growth rates were comparable to literature values. Moreover, our system allowed the identification of individual cells with diverging growth behavior. In addition, a fluorimetric assay was carried out to quantify the cofactor NAD(P)H in single cells and in mother- and daughter cells that were previously exposed to hydrogen peroxide. The obtained findings indicate that the device can be used to distinguish between healthy and oxidatively-stressed cells.

The third platform prioritized the investigation of a particular source of cell-to-cell differences. The aim was to investigate the influence of inheritance noise. The term refers to the uneven partitioning of cellular biomolecules during cell division. For this purpose, a device design was engineered that allowed the on-chip separation of budding *S. cerevisiae* mother cells from their daughters. The separation process was followed by chemical analysis of the corresponding single cell lysates.

Another set of experiments was carried out on a previously designed platform for mammalian cells. The device was used to measure the effect of different sample matrices on target molecule detection in immunoassays. In previous projects the analysis of cell lysates by immunological methods has proved to be very sensitive, and extremely low limits of detection were achieved. Although immunoassays typically show a high specificity for the target analyte, the question has been raised whether matrix effects; i.e. molecules of the cell lysate, affect the results. First indications of the above-mentioned interferences were obtained by series of experiments measuring the analyte β -galactosidase in different matrices.

In summary, focus of the studies presented in this thesis is on the development of strategies for the comprehensive analysis of single microbes on microfluidic systems.

Zusammenfassung

In den letzten Jahrzehnten wurden zahlreiche Studien durchgeführt, um das Verhalten einzelner Zellen zu untersuchen. Die gewonnenen Erkenntnisse bestätigen eindeutig die phänotypische Heterogenität in isogenen Zellpopulationen. Folglich gehen aktuelle Forschungsfragen über das reine Veranschaulichen von phänotypischen Unterschieden zwischen Zellen einer homogen erscheinenden Population hinaus. Eine zusätzliche Herausforderung ist es zu bestimmen, welche Faktoren der beobachteten zellulären Heterogenität eine wichtige biologische Funktion erfüllen und durch welche zugrundeliegenden Kontrollmechanismen sie reguliert werden. In diesem Zusammenhang werden Forschungsmethoden benötigt, die die umfassende Charakterisierung einer Zellpopulation auf dem Einzel-Zell-Niveau ermöglichen. Für diesen Zweck sind mikrofluidische Methoden besonders vorteilhaft, da sie die genaue Handhabung von geringen Flüssigkeitsvolumen, die denen einer einzelnen Zelle entsprechen, ermöglichen. Darüber hinaus sind mikrofluidische Systeme für Langzeitstudien geeignet. Folglich können biologische Informationen zur Verfügung gestellt werden, die durch Methoden, die auf zu einem einzigen Zeitpunkt gemachten Beobachtungen beruhen, wie beispielsweise Durchflusszytometrie, nicht zugänglich sind. Obwohl bereits eine Vielzahl an mikrofluidischen Plattformen, angepasst an die Einzelzellanalyse, präsentiert wurde, bleibt die Entwicklung von Geräten, die ein breites Anwendungsgebiet abdecken, weiterhin eine grosse Herausforderung.

Die in dieser Doktorarbeit präsentierten Resultate diskutieren die Entwicklung von mikrofluidischen Plattformen, die den Anwendungsbereich bestehender Systeme erweitern. Besonderes Augenmerk liegt dabei auf zwei Aspekten. Es wird die genaue Handhabung von einzelnen Mikroben, die durch Volumen im geringen Femtoliterbereich charakterisiert sind, angestrebt. Darüber hinaus werden multifunktionelle Geräteentwürfe, die eine umfassende Analyse einzelner Zellen ermöglichen, fokussiert.

Zuerst wurde ein mikrofluidisches System, das auf bakterielle Zellstudien optimiert war, entwickelt. Das Chip-Design wurde an den gut untersuchten eukaryotischen Modelorganismus *Escherichia coli* (*E. coli*) angepasst. Hauptmerkmal des Geräts war ein Set aus Mikroanalysekammern, ausgestattet mit Zellfallen für das hydrodynamische Einfangen einzelner *E. coli* und ringförmigen Ventilen, die unter Aktivierung das Bakterium in einem Volumen von nur 155 pL einschlossen. Zusätzlich wurde ein Protokoll für die Modifizierung der Oberfläche implementiert, durch das die Analyse von Zelllysaten mittels immunologischer Tests möglich wurde. Die Plattform wurde für die Quantifizierung des Enzyms β -Galaktosidase in einzelnen *E. coli*, welche unter unterschiedlichen Nährstoffbedingungen kultiviert wurden, verwendet. Die Ergebnisse wurden mit Literaturwerten von Ensemble-Messungen verglichen, wobei die erhaltenen Resultate es zusätzlich ermöglichten, die heterogene Genexpression zu erfassen.

Bei einem zweiten Geräteentwurf wurde der Fokus auf multifunktionale Verwendungsmöglichkeiten gelegt. Die Mikrometer grossen Zellfallen wurden auf die Geometrie einzelner *Saccharomyces cerevisiae* (*S. cerevisiae*) Zellen optimiert. Hauptmerkmal war die implementierte Doppel-Ventil-Konfiguration, welche jede Zellfalle umgab. Diese Besonderheit des Designs ermöglichte es innerhalb von Millisekunden zwischen vollständiger und teilweiser Isolation der eingefangenen Zelle zu wechseln. Die Funktionalität der Plattform wurde durch Experimente mit *S. cerevisiae* Zellen demonstriert, welche auf dem Mikrochip unter unterschiedlichen Nährstoffbedingungen kultiviert wurden. Die beobachteten Wachstumsraten waren mit den Werten aus der Fachliteratur vergleichbar. Darüber hinaus ermöglichte unser System die Identifizierung von einzelnen Zellen mit abweichendem Wachstumsverhalten. Zusätzlich wurde ein fluorimetrischer Test durchgeführt um den Co-Faktor NAD(P)H in einzelnen Zellen sowie in Mütter- und Töchterzellen, die zuvor Wasserstoffperoxid ausgesetzt waren, zu quantifizieren. Die erhaltenen Ergebnisse weisen darauf hin, dass unser Gerät verwendet werden kann, um zwischen gesunden und oxidativ-gestressten Zellen zu unterscheiden.

Die dritte Plattform priorisierte die Erforschung der Ursachen von Zell-zu-Zell-Unterschieden. Ziel war es den Einfluss von erblich bedingten stochastischen Effekten zu untersuchen. Damit ist in diesem Zusammenhang das ungleiche Verteilen von zellulären Biomolekülen während der Zellteilung gemeint. Zu diesem Zweck wurde ein Gerät entwickelt, das die Trennung von knospenden Mütterhefezellen von ihren Töchtern ermöglichte. Nach dem Trennungsprozess folgte die chemische Analyse der entsprechenden Einzelzelllysate.

Eine weitere Reihe an Experimenten wurde auf einer bereits bestehenden Plattform für Säugetierzellen durchgeführt. Das Gerät wurde verwendet um den Effekt von verschiedenen Matrices auf die Detektion des Zielanalyten in Immuntests zu messen. In vorherigen Projekten hatte sich die Analyse von Zelllysaten mittels immunologischer Methoden als sehr sensitiv erwiesen und es konnten ausserordentlich tiefe Detektionsgrenzen erreicht werden. Obwohl Immuntests für gewöhnlich eine hohe Spezifität gegenüber dem Zielanalyten aufweisen, stellte sich die Frage ob Matrixeffekte, d.h. Moleküle die im Zelllysate enthalten sind, die Ergebnisse beeinflussen. Erste Hinweise darauf wurden in vergleichenden Experimentserien erhalten, in denen der Analyt β -Galactosidase in unterschiedlichen Matrices untersucht wurde.

Zusammenfassend liegt der Fokus der in dieser Doktorarbeit präsentierten Studien auf der Entwicklung von Strategien für die umfassende Analyse einzelner Mikroben in mikrofluidischen Systemen.

Contents

Abstract	IV
Zusammenfassung.....	VI
Contents	VIII
List of Figures.....	XII
Abbreviations	XIII
1 General introduction.....	- 1 -
1.1 Microfluidics	- 1 -
1.2 Physics of fluids at the microscale.....	- 2 -
1.3 Driving force behind single cell analysis	- 4 -
1.4 Standard methods for single cell analysis	- 6 -
1.5 Microfluidics for single cell analysis	- 10 -
1.5.1 Cell capture.....	- 10 -
1.5.2 Cell isolation	- 12 -
1.5.3 Cell lysis	- 14 -
1.5.4 Analysis.....	- 16 -
1.6 Immunoassays	- 17 -
1.6.1 The past, the present and the future of immunoassays.....	- 17 -
1.6.2 Direct and indirect assays.....	- 19 -
1.6.3 Competitive and non-competitive assays	- 20 -
1.6.4 Antibody-antigen interactions	- 21 -
1.6.5 Different labeling strategies	- 22 -
1.7 <i>Escherichia coli</i> as model organism	- 23 -
1.8 <i>Saccharomyces cerevisiae</i> as model organism	- 25 -
1.9 Open questions and challenges in single cell analysis	- 27 -
1.10 Scope.....	- 29 -
2 Methods.....	- 31 -
2.1 Device fabrication.....	- 31 -
2.1.1 Design development	- 32 -
2.1.2 Preparation of the master molds	- 33 -
2.1.3 Production of the final device	- 35 -
2.2 Operation of the device.....	- 37 -
2.3 Cultivation of <i>E. coli</i>	- 38 -

2.4	Cultivation of <i>S. cerevisiae</i>	- 38 -
3	On-chip enzyme quantification of single <i>Escherichia coli</i>	- 39 -
3.1	Abstract.....	- 40 -
3.2	Introduction	- 40 -
3.3	Materials and Methods	- 43 -
3.3.1	Materials.....	- 43 -
3.3.2	Master mold and device fabrication	- 44 -
3.3.3	Surface modification	- 45 -
3.3.4	Bacteria cultivation and Dil-staining	- 45 -
3.3.5	Immunoassay for β -Galactosidase	- 46 -
3.3.6	Data analysis.....	- 48 -
3.4	Results and discussion	- 50 -
3.4.1	Chip design	- 50 -
3.4.2	Detection assay and increase of sensitivity	- 52 -
3.4.3	Quantification of the enzyme β -galactosidase in individual <i>E. coli</i> cells	- 54 -
3.5	Conclusion	- 56 -
3.6	Acknowledgement.....	- 57 -
4	Cultivation and quantitative single cell analysis of <i>Saccharomyces cerevisiae</i>	- 58 -
4.1	Abstract.....	- 59 -
4.2	Introduction	- 59 -
4.3	Experimental.....	- 61 -
4.3.1	Reagents.....	- 61 -
4.3.2	Device production process	- 62 -
4.3.3	Cell culture.....	- 63 -
4.3.4	Cell cultivation	- 63 -
4.3.5	NAD(P)H assay	- 64 -
4.4	Results and discussion	- 65 -
4.4.1	Chip design	- 65 -
4.4.2	On-chip cell cultivation.....	- 68 -
4.4.3	NAD(P)H assay.....	- 71 -
4.5	Conclusions.....	- 73 -
4.6	Acknowledgements	- 73 -
5	Separation & subsequent biomolecule analysis of single mother-daughter cell pairs	- 74 -
5.1	Abstract.....	- 75 -

5.2	Introduction	- 75 -
5.3	Experimental.....	- 76 -
5.3.1	Reagents.....	- 76 -
5.3.2	Device fabrication.....	- 76 -
5.3.3	Cell culture.....	- 77 -
5.3.4	Mother-daughter cell pair capture and separation	- 77 -
5.3.5	NAD(P)H assay.....	- 79 -
5.4	Results.....	- 80 -
5.4.1	Mother-daughter cell pair separation.....	- 80 -
5.4.2	Biomolecule analysis	- 81 -
5.5	Discussion - Improvement and modification of the existing prototype	- 82 -
5.6	Conclusions.....	- 83 -
5.7	Acknowledgements	- 83 -
6	The influence of matrix effects on the analyte detection in immunoassays	- 84 -
6.1	Abstract.....	- 85 -
6.2	Introduction.....	- 85 -
6.3	Experimental.....	- 87 -
6.3.1	Reagents.....	- 87 -
6.3.2	Device fabrication.....	- 87 -
6.3.3	Bacteria cultivation and lysate preparation	- 88 -
6.3.4	Giant unilamellar vesicle preparation by electroformation.....	- 88 -
6.3.5	Giant unilamellar vesicle preparation by water-oil emulsion transfer	- 89 -
6.3.6	Performance of the immunoassay for β -galactosidase	- 89 -
6.3.7	Performance of the immunoassay with <i>E. coli</i> lysate as matrix component. -	90 -
6.3.8	Performance of the immunoassay with GUVs as matrix component.....	- 90 -
6.3.9	Data analysis.....	- 90 -
6.4	Results.....	- 91 -
6.4.1	Immunoassay performed without additional matrix.....	- 91 -
6.4.2	Immunoassay performed with <i>E. coli</i> lysate as additional matrix	- 92 -
6.4.3	Immunoassay performed with GUVs as additional matrix	- 93 -
6.5	Conclusions.....	- 95 -
6.6	Acknowledgements	- 95 -
7	Conclusion and outlook	- 96 -
8	References	- 98 -

9	Appendix	- 122 -
9.1	Curriculum Vitae	- 122 -
9.2	Publications & conference posters.....	- 124 -

List of Figures

Figure 1: Laminar flow.....	- 3 -
Figure 2: Cellular heterogeneity.	- 4 -
Figure 3: Basic principle of fluorescence microscopy.	- 6 -
Figure 4: TIRF spectroscopy.	- 7 -
Figure 5: Comparison of early generation FACS machines and modern μ FACS devices.....	- 9 -
Figure 6: Common cell capture approaches.....	- 10 -
Figure 7: PDMS-made pneumatic valves.	- 13 -
Figure 8: Direct and indirect sandwich immunoassay formats.....	- 19 -
Figure 9: Competitive and noncompetitive immunoassay formats.....	- 20 -
Figure 10: The influence of the K_D value, the antibody number and the chamber volume on the LOD.	- 21 -
Figure 11: Bright field and fluorescence images of fixed <i>E. coli</i> bacteria.	- 24 -
Figure 12: Wild type (YPH499) budding yeast.	- 26 -
Figure 13: Overview of state-of-the-art single cell analysis methods.....	- 28 -
Figure 14: Overview of the device fabrication workflow.	- 31 -
Figure 15: Reduction of the microanalysis chamber volume.....	- 33 -
Figure 16: SU-8 processing protocol.	- 33 -
Figure 17: Fabrication of the final device by soft lithographic techniques	- 35 -
Figure 18: Photograph that depicts the standard experimental set-up.....	- 37 -
Figure 19: Design and operation of the microfluidic platform.	- 42 -
Figure 20: Control experiments on cell lysis and valve integrity.	- 46 -
Figure 21: Raw data and analysis principle.	- 48 -
Figure 22: Influence of the surface modification on the measurement signal.....	- 49 -
Figure 23: Control experiment related to analyte cross contamination.	- 50 -
Figure 24: Influence of the microchamber volume on detection and quantification.....	- 51 -
Figure 25: β -Galactosidase experiments.....	- 53 -
Figure 26: Quantification of the β -galactosidase levels of individual <i>E. coli</i>	- 54 -
Figure 27: Influence of the carbon source on the β -galactosidase expression.	- 56 -
Figure 28: Design and functionality of the microfluidic device.	- 61 -
Figure 29: Scheme of the fluorimetric NAD(P)H assay.	- 64 -
Figure 30: Construction details of the microfluidic platform.	- 65 -
Figure 31: Influence of the cell trap geometry on the cell load.	- 66 -
Figure 32: Diffusion-based fluid exchange.	- 67 -
Figure 33: On-chip cell cultivation.	- 68 -
Figure 34: Example micrographs of on-chip cell cultivation.	- 69 -
Figure 35: Growth rates.....	- 70 -
Figure 36: Control experiments to ensure single cell analysis and complete lysis.	- 71 -
Figure 37: Fluorimetric NAD(P)H assay.	- 72 -
Figure 38: Design and functionality of the microfluidic device.	- 78 -
Figure 39: Schematic drawing of the fluorometric NAD(P)H assay.....	- 79 -
Figure 40: Scheme of the fluid-based mother-daughter cell pair separation process.....	- 80 -
Figure 41: Biomolecule analysis of separated mother and daughter cells.....	- 81 -
Figure 42: Scheme of potential improvements related to the current device design.	- 82 -
Figure 43: Performance of the β -galactosidase immunoassay without additional matrix.....	- 91 -
Figure 44: On-chip calibration curves illustrating the influence of the <i>E. coli</i> matrix.....	- 92 -
Figure 45: On-chip calibration curve illustrating the influence of the GUV matrix	- 93 -
Figure 46: Immunoassay performed with single GUVs	- 94 -

Abbreviations

AB	Antibody
AC	Alternating current
BSA	Bovine serum albumin
CAD	Computer-aided drafting
cAMP	Cyclic adenosine 3',5'-monophosphate
Dia	Diameter
Dil	1,1'-dioctadecyl-3,3,3,3'-tetramethylindocarbocyanine perchlorate
DNA	Deoxyribonucleic acid
DOPC	1,2-Dioleoyl-sn-glycero-3-phosphocholine
EDTA	Ethylenediaminetetraacetic acid
ELISA	Enzyme-linked immunosorbent assay
EMCCD	Electron-multiplying charge-coupled device
EMIT	Enzyme multiplied immunoassay technique
Fab	Fragment antigen-binding
FACS	Fluorescence-activated cell sorting
Fc	Fragment crystallizable
FDG	Fluorescein di-beta-D-galactopyranoside
GAPDH	Glyceraldehyde 3-phosphate dehydrogenase
GUV	Giant unilamellar vesicles
HEK	Human embryonal kidney cell line
IA	Immunoassay
IPCR	Immuno-polymerase chain reaction
ITO	Indium tin oxide
LB	Lysogeny broth
LC-MS	Liquid chromatography–mass spectrometry
LED	Light-emitting diode
LOD	Limit of detection
LOQ	Limit of quantification
mAB	Monoclonal antibody

MLTC	Murine leydig tumor cells
mRNA	Messenger ribonucleic acid
NADH	Beta-nicotinamide adenine dinucleotide, reduced
NAD ⁺	Beta-nicotinamide adenine dinucleotide, oxidized
NADPH	Beta-nicotinamide adenine dinucleotide phosphate, reduced
NADP ⁺	Beta-nicotinamide adenine dinucleotide phosphate, oxidized
nDEP	Negative dielectrophoresis
OD	Optical density
pAB	Polyclonal antibody
PBS	Phosphate buffered saline
PCN	Plasmid copy number
PCR	Polymerase chain reaction
PDMS	Poly(dimethylsiloxane)
PLL-g-PEG	Poly(l-lysine)-graft-poly(ethylene glycol)
POC	Point of care
RIA	Radioimmunoassay
RNA	Ribonucleic acid
ROS	Reactive oxygen species
RT	Room temperature
POPC	1-palmitoyl-2-oleoyl-sn-glycero-3-phosphocholine
SAV	Surface area to volume ratio
SPE	Solid-phase extraction
TIRFM	Total internal reflection fluorescence microscopy
TRIS	Tris(hydroxymethyl)aminomethan
UV	Ultraviolet
YPD	Yeast extract peptone dextrose

1 General introduction

1.1 Microfluidics

The term microfluidics refers to the science and technology of platforms that handle small fluid volumes in the nano- to picoliter range (1-3). The systems are characterized by internal dimensions at the micrometer scale (4). The origins of this research field can be traced back to molecular analysis, molecular biology and microelectronics (2). First applications were implemented in the analytical sciences in the late 1970s. At that time, the miniaturization of gas and liquid chromatography to the capillary format was presented by Terry et al. (5). In their work they applied classic microfabrication techniques derived from the microelectronic industry, for example photolithography and chemical etching, to produce micrometer-sized channels on silicon wafers. Nevertheless, most research activities back then were directed towards the development of construction elements like micropumps and microvalves (6, 7). It was only at the beginning of the 1990s that application of the concept of miniaturized silicon devices to standard analytical methods such as high-pressure liquid chromatography was reinforced (8). The resulting microanalytical methods which provided enhanced performance in terms of sensitivity and required sample volumes had a great impact on chemical analysis. This success in combination with the rapid growth of genomics in molecular biology acted as driving force for the development of more compact, high-throughput analysis platforms. Contemporarily, the approach of “miniaturized total chemical analysis systems” abbreviated as μ TAS was presented to the scientific community by Manz et al. (9). The idea of μ TAS was to integrate all analytical steps from sample preparation to separation and detection into one device. Later, the concept was generalized to the integration of various laboratory functions into one chip giving rise to the term “Lab on a Chip”. By introduction of soft lithography by Whitesides et al. (10) the microfluidic technology has been made accessible to a much broader community, as this set of methods enabled the inexpensive production of microstructures from elastomeric materials. In addition, clean room facilities were only required for the fabrication of the master molds which, once produced, could be used to generate a large number of replicas.

The use of microfluidic systems has grown in popularity over the last decade and is nowadays widely spread in many different research fields like drug discovery (11, 12), point-of-care-diagnostics (13), cell biology (14), and material sciences (15), to mention just some examples. Despite the great advances achieved so far, not all the expectations that were raised during the early days of microfluidics have yet been fulfilled. Considering the future one main challenge will be to bridge the gap from the proof-of-concept status of a project to its commercialization (16).

1 General introduction

1.2 Physics of fluids at the microscale

In contrast to the fluid physics at the nanoscale, the laws of physics at the microscale do not differ from those at the macroscale to which we are used to from the daily life. However, there are physical phenomena that become more prominent in the nanoliter regime and will be discussed in more detail in the following.

One dominant effect in microfluidics is the occurrence of laminar flow. In laminar flow the fluid particles move in regular layers parallel to the boundary without lateral mixing (17). This is contrasted by the far more frequent turbulent flow characterized with irregular fluctuations and eddies. In this context, an important dimensionless parameter is the Reynolds number (18) that describes the ratio of inertial to viscous forces and is used to predict the flow regime (equation 1) (19-21).

Equation 1: The Reynolds number

$$Re = \frac{\rho * v * l}{\mu}$$

ρ = fluid density | v = flow velocity | l = typical length scale

The Reynolds numbers in water-based microfluidic devices are typically below 1 whereas the critical region in which the transition from laminar to turbulent flow takes place is indicated by much greater values of around 2040 (22) depending on the geometry of the system. As consequence of the absence of turbulences, within a microchannel different fluid streams flow parallel to each other without convective mixing (Figure 1). Nevertheless, laminar flow also exists in the macroscopic world as illustrated, for example, by glacier streams.

Compared to macroscale volumes, diffusion times are significantly shortened in microfluidic systems. This is explained by the fact that the distance a particle has to overcome varies to the square power and, consequently, has great impact on the corresponding characteristic diffusion time (equation 2). Due to the small length scales, diffusion-based mixing on microfluidic devices is a highly efficient and accurate process.

Equation 2: Diffusion time according to the Einstein-Smoluchowski relation

$$\tau_D = \frac{l^2}{2 * D}$$

τ_D = diffusion time | l = traversed distance | D = diffusion coefficient

Another special characteristic of fluid physics in the nanoliter regime is the high surface area to volume ratio (SAV) which leads to the dominance of surface forces over inertial and body forces as described by the scaling laws (11, 23). The implementation of immunoassays on microfluidic chips benefits from the high SAV as the ratio of immobilized antibodies to sample volume is increased and, consequently, also the area at which antibody-antigen interactions can take place.

1 General introduction

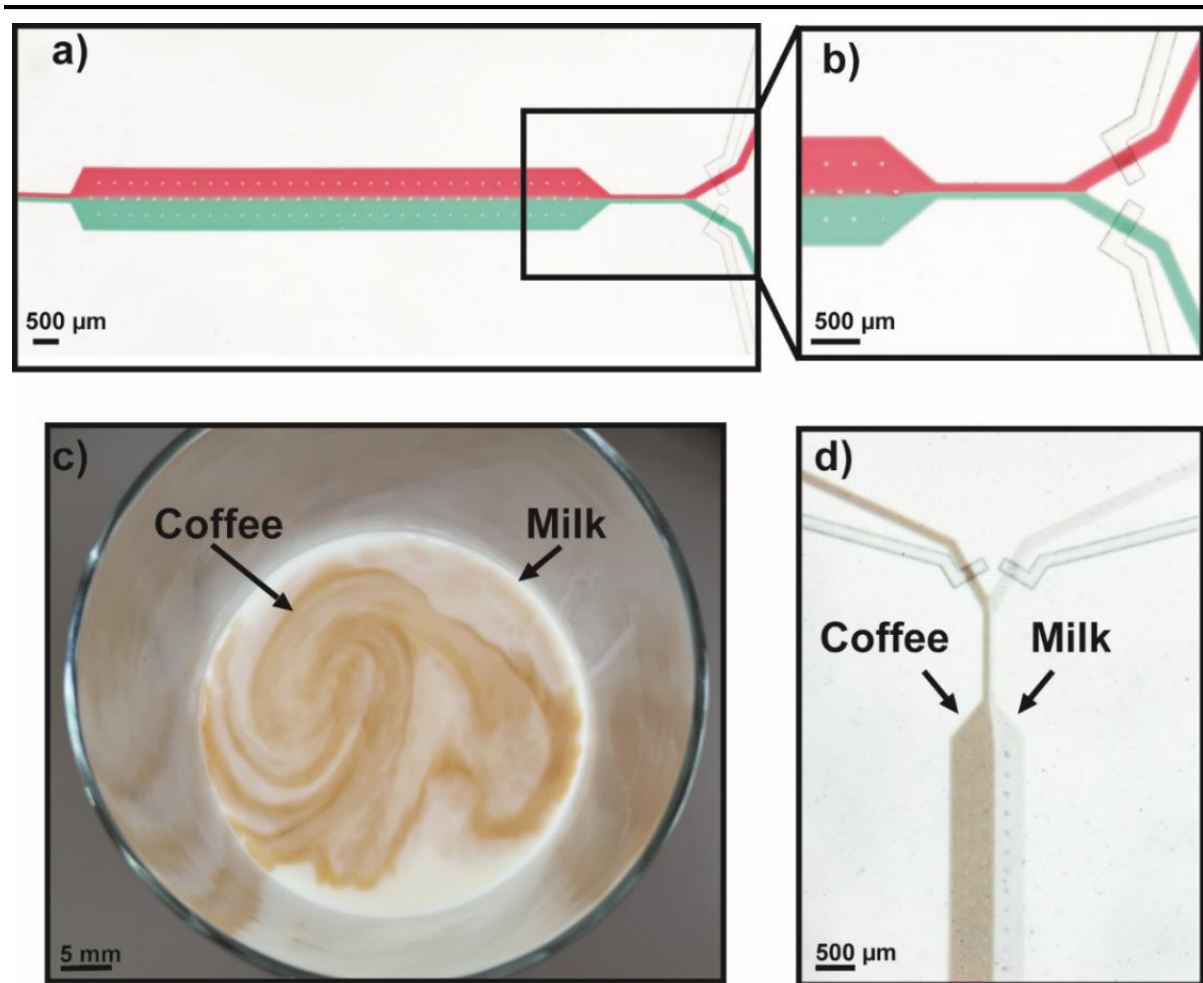


Figure 1: **Laminar flow.** a) Laminar flow profile illustrated by simultaneous introduction of red food dye (top) and green food dye (bottom) into a microfluidic fluid channel. As there are no turbulences, the two fluid streams coexist. b) Magnified micrograph of the laminar flow profile. c) Turbulent flow profile of low-fat milk and coffee in a latte macchiato glass. The picture was taken directly after both fluids were poured into the glass in a parallel manner. d) Laminar flow profile of the same fluids in a microfluidic channel system.

1 General introduction

1.3 Driving force behind single cell analysis

The motivation for the analysis of individual cells is based on the cellular heterogeneity giving rise to significant phenotypic differences even among cells of an isogenic population (24, 25). Bulk measurement methods mask cell-to-cell differences, as only information about the average behavior of a population is provided that may not be representative for all or, in the worst case, for any cell of the population. This can be illustrated by two well-known examples from literature. Firstly, slow-growing persister cells that exhibit multidrug tolerance and exist at small number in some isogenic bacteria populations (26, 27). Under “normal circumstances” persister cells do not fulfill any special function, and the ignorance of these rare cells by bulk analysis would be of minor biological importance. However, under harmful conditions like drug treatment persister cells ensure the survival of the population due to their ability to resist lethal factors. Consequently, an “oversight” of a small subpopulation of rare cells can be of high relevance, for example in case of the treatment of recalcitrant bacterial infections (28). Secondly, populations that consist of two dominant but phenotypically different subpopulations. This bistability is caused by biological feedback loops that create “all-or-nothing” responses, for example during exposure to a stress stimulus (29, 30). In such a case, ensemble-based studies induce misleading results whereas single cell analysis techniques successfully uncover the bistable gene expression pattern (Figure 2).

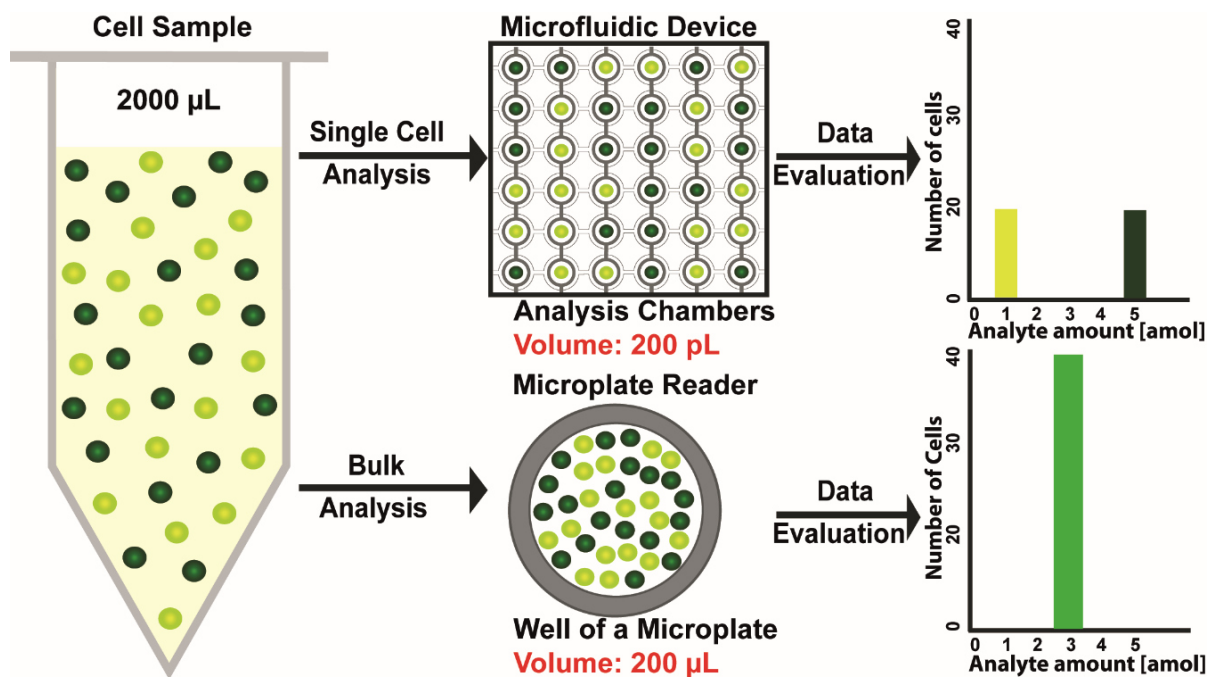


Figure 2: **Cellular heterogeneity.** Bulk measurements (bottom) mask the bistable expression pattern whereas measurements on the single-cell level (top) uncover the two dominant phenotypes of the population.

1 General introduction

Although the large number of studies that was carried out in this field over the last decades clearly demonstrates the heterogeneous nature of cell populations, there is still little known about the sources and control mechanisms, mainly due to the underlying complexity. Cellular heterogeneity can be raised by a great variety of factors of stochastic, programmed, or selection-driven origin. A deeper insight into the regulation processes is of great significance for many different disciplines like cancer research (31, 32), drug screening (33), or evolutionary research to name only a few. Therefore, the development of systems that enable the precise spatio-temporal control and analysis of large numbers of individual cells is required. In this context, microfluidic systems offer some particular advantages, as the accurate manipulation of small fluid volumes in the pico- to femtoliter range matching the dimensions of single cells is ensured. In the following sections, standard single cell analysis methods as well as key steps of on-chip single cell analysis will be discussed in more detail to provide a rough overview of what can be considered as state of the art in this field.

1 General introduction

1.4 Standard methods for single cell analysis

As discussed in the previous section, single cell analysis methods provide information that is not accessible by ensemble measurements. The most common techniques for investigation of individual cells are fluorescence microscopy and flow cytometry. In the following, the basic principle of both methods and recent examples of their use in cell analysis studies will be briefly described.

Since the first microscopic observations of living bacteria from tooth enamel by van Leeuwenhoek in the 17th century (34), our knowledge about cells as well as about microscopy has significantly developed further. Nowadays, frequently used microscopic techniques for single cell studies include wide-field fluorescence microscopy, confocal microscopy (35), and total internal reflection fluorescence microscopy (TIRFM) (36).

The basic principle of wide-field fluorescence microscopy is illustrated in Figure 3. A light source, like for example a xenon arc lamp or a laser, is used to excite a particular fluorophore. The photons of the excitation light are absorbed by the fluorophore molecules that are thereby raised from the electronic ground state to an excited state as depicted in the Jablonski diagram (Figure 3b) (37). The absorbed energy is partly reemitted by non-radiative pathways such as vibrational relaxation or internal conversion and by radiation whose energy is naturally lower than the energy of the original excitation light (38). Consequently, the maximum of the emission spectrum is shifted to longer wavelengths (Figure 3c). This so called Stokes shift named after its discoverer Sir George Gabriel Stoke, enables to separate emission light from excitation light by optical filters. In the example scheme a dichroic mirror is used for this purpose (Figure 3a) (39). Usually an additional optical filter is placed between the objective and the detector to filter stray light and scattered light.

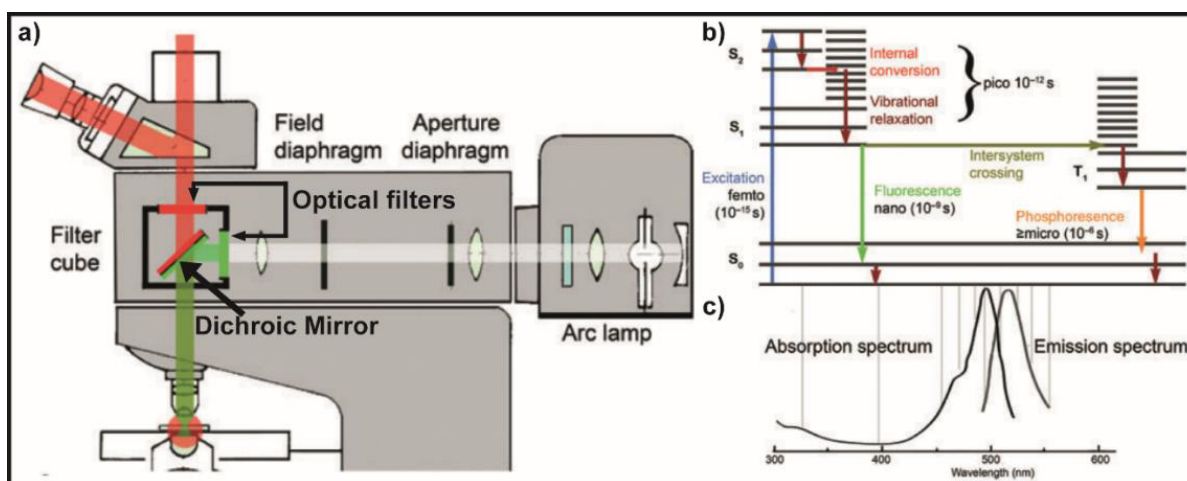


Figure 3: Basic principle of fluorescence microscopy. a) Scheme of the basic construction elements that build up a wide-field fluorescence microscope. b) Scheme of the Jablonski-diagram which depicts the possible electronic states of a molecule and the corresponding transition pathways. c) Scheme that depicts the Stokes shift. Adapted with permission from reference [39]. Copyright (2015) Nature Publishing Group.

1 General introduction

Depending on the numerical aperture of the used objective and the wavelength of the light emitted, wide-field fluorescence microscopy provides a spatial resolution in the xy-plane in the submicrometer range (equation 3). This microscopic technique has been used for manifold single cell studies. For example, the response of individual human cancer cells to the anti-cancer drug camptothecin was analyzed by monitoring the treatment-specific changes in the expression of several hundred different, endogenously tagged proteins (40).

Equation 3: **Rayleigh criterion**

$$R = \frac{0.61 * \lambda}{Na}$$

R = resolution in xy-plane | λ = wavelength of light emitted | Na = numerical aperture

However, wide-field fluorescence microscopy is not the method of choice for imaging thicker three-dimensional specimens, since the maximal achievable resolution in z-direction is significantly lower and only about 1500 nanometer (41). In such cases, confocal fluorescence techniques are preferable, as they allow the discrimination of the background fluorescence signal caused by out-of-focus fluorophores. This is achieved by point illumination in combination with a pinhole positioned in front of the detector and in conjugate to the excitation focal plane. Three-dimensional high resolution images are generated by imaging many thin sections of a specimen which are later reconstructed to one image. This technique was applied, for instance, to quantify not only the global and but also the local concentrations of YFP-labeled signaling proteins in individual fission yeast cells (42). Another common fluorescence spectroscopy technique is total internal reflection (TIRF) microscopy. The general working principle is based on the generation of an evanescent wave by total internal reflection for specimen illumination (Figure 4a). As the evanescent field decays exponentially, the selective excitation of fluorophores in direct adjacency to the coverslip-specimen-interface is feasible (36). The low penetration depth of the excitation light of a few hundred nanometers results in an enhanced signal-to-noise ratio compared to epifluorescence techniques (Figure 4b and 4c). TIRF spectroscopy is frequently applied to investigate dynamic processes which occur at or in close proximity to the cellular plasma membrane. For example, a recent study demonstrated the successful use of TIRF-based spectroscopy for the analysis of single-vesicle motions and exocytosis (43). The performed experiments allowed to monitor in real-time single fusion events of secretory vesicles in human carcinoid BON cells expressing the GFP-tagged neuropeptide Y.

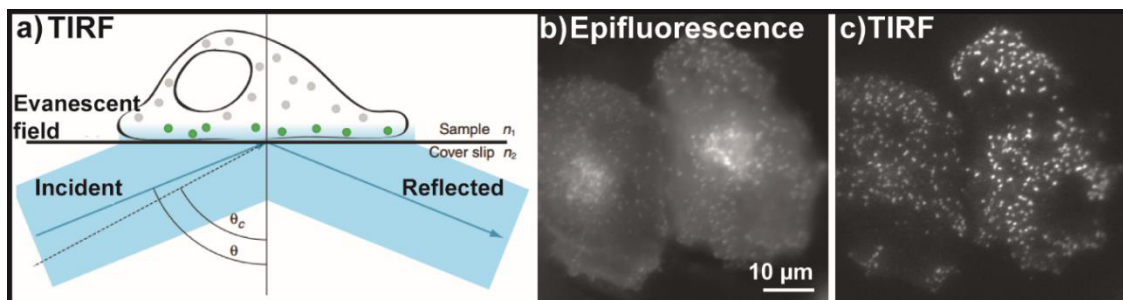


Figure 4: **TIRF spectroscopy.** a) Basic principle of TIRFM. b & c) Epifluorescence and TIRF images of an Clathrin (clathrin light chain–GFP) in HeLa cells. Adapted with permission from reference [36]. Copyright (2015) THE COMPANY OF BIOLOGISTS LTD.

1 General introduction

Another common technique for single cell analysis is flow cytometry which allows to investigate multiple properties of single particles in a fluid stream by the use of laser beams (44). The roots of this method can be traced back to microscopy, blood cell counters and inkjet printing (45). In 1934, the construction plan for a device that enables the counting of single cells flowing through a capillary tube was presented the first time by Moldavan (46). The capillary tube itself was fixed on a microscope stage, and a photodetector connected to the microscope ocular should be used for the detection of the passing cells. This set-up design is considered as the first prototype of a flow cytometer although it is still in dispute if the device had ever been constructed. Inspired by Moldavans design drafts, the Coulter brothers invented in the late 1940s an automated apparatus for counting leukocyte cells (47). The measuring principle is based on the detection of particle size dependent changes in impedance (48). A next important step forward was taken by the development of the first flow sorter by Mack Fulwyler in the mid-1960s (49). Therefore, the Coulter principle for automated cell analysis was combined with the during that time novel ink writing oscillograph technique which enabled to dispose charged ink droplets at clearly defined positions by electrostatic deflection (50). In the newly developed cell sorter machine the cells were first analyzed by the Coulter principle. In a second step, the fluid stream was split into small droplets that were charged and subsequently deposited by deflection into separate containers. Thereby it was possible to isolate individual subpopulations of a cell sample. The next important further development was the implementation of fluorescence-based flow cytometry by Wolfgang Göhde in the late 1960s. The commonly used term fluorescence-activated cell sorting (FACS) is a registered trademark of the technology group Becton, Dickinson and Company that marketed the first commercially available FACS machines. The actual technical invention was realized by their partner Leonard Herzenberg, a Stanford scientist whose research articles (51) disseminated the knowledge about the FACS technology throughout the scientific community. The scheme of Figure 5a depicts one of the first FACS machines and illustrates the basic working principle (52). Fluorescent labeled cells are induced to a fluid stream that is forced to pass a small nozzle. The stream is optimized ensuring sufficient spacing between individual cells. The integrated vibration mechanism lead to droplet formation at a defined distance from the nozzle. Directly after passing the nozzle, the cells are analyzed by irradiation with laser light. Next, droplets are generated which are loaded with single cells. For the subsequent sorting process, the cells are charged according to their characteristics; i.e. cells with different properties are charged differently. Consequently, subpopulations can be sorted by electrostatic deflection. For this purpose, the charged cell droplets pass deflection plates that navigate them according to their charge to different collection vessels.

The early generation of FACS devices was limited with respect to the number of cell parameters that could be investigated. In the beginning, only two dyes, namely fluorescein and rhodamine, were available. In addition, the scattered laser light was detected to determine the cell size.

1 General introduction

Due to significant new developments in the field of multiple laser combinations, fluorophores, and cell sorting capabilities, modern FACS machines make high throughput multi-parameter analysis of single cells feasible. State-of-the-art in the field are 18-color flow cytometers (53). Multi-parameter flow cytometry (MFC) is applied as diagnostic tool for a variety of human diseases. Immunophenotyping, i.e. the analysis of specific antigen expression patterns by the use of fluorophore-labeled antibodies, allows the detection of various tumor markers. For instance, several recent studies reported the successful diagnosis of the myelodysplastic syndromes (MDS) by MFC analysis (54). MDS is a bone marrow disease that a later stage can develop into acute myeloid leukemia. Besides leukemia markers, MFC was also applied for the investigation of breast cancer cells (55) and colorectal cancer stem cells (56).

Regarding the future of flow cytometry, an important trend goes towards the miniaturization of FACS machines (Figure 5b). The focus is thereby on the development of portable, low cost devices that enable the integration of further analysis tools like optics or acoustics (57, 58). The resulting compact and comprehensive analysis platforms are used among others as diagnostic point-of-care devices. In this context, a recently published study of a μ FACS device for the diagnosis of malaria should be mentioned (59).

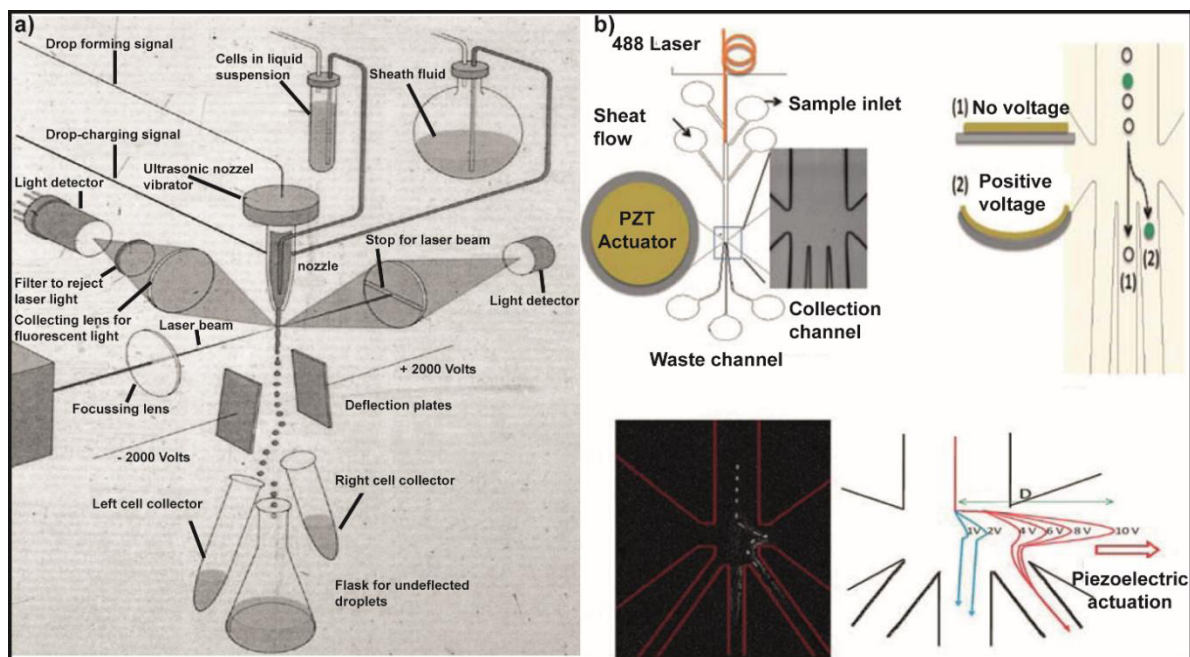


Figure 5: Comparison of early generation FACS machines and modern μ FACS devices. a) Scheme of one of the first FACS machines. Adapted with permission from reference [52]. Copyright (2015) AMERICAN ASSOCIATION FOR CLINICAL CHEMISTRY, INC. b) Scheme of a μ FACS device. Top left: Structure of the microfluidic platform. The main channel (width: 250 μ m) is divided into three side-channels. The channel in the middle is used to collect the waste, and the side channels are used to collect the samples. For excitation (488 nm laser), an optical fiber is used. The excitation light is directed by a Teflon AF coated optofluidic waveguide. In addition, a PZT actuator is implemented on the platform. The marked square depicts the sorting junction of the platform. Top right: If no voltage is applied, the cell is guided towards the main channel for waste collection (1). If voltage is applied to the PZT actuator, the cell is deflected to the side-channels for sample collection (2). Bottom left: Flow profile of a fluorescent bead guided to the side channel. The image consists of superimposing pictures that were taken every 0.3 ms by a high-speed CMOS camera. Bottom right: Bead trajectory plots in dependency of the applied voltage. Adapted with permission from reference [58]. Copyright (2015) Royal Society of Chemistry.

1 General introduction

1.5 Microfluidics for single cell analysis

1.5.1 Cell capture

First step in most single cell analysis procedures is the controlled positioning of individual cells which is particularly important for long-term observation studies. There exists a great variety of different trapping methods that can be divided into two main groups, namely trapping approaches with physical contact and contact-free ones.

Among the first the most widely spread techniques include physical capture by microstructures or cell adhesion by surface functionalization. Many different geometries suitable for physical trapping have been presented ranging from microwells (60, 61) (Figure 6a) and microchambers (62) to lobster-shaped cell trap features (63). One of the most straightforward ways of cell positioning in microchannel systems is based on a rather simple design with a main transport channel connected to side channels whose dimensions correspond to those of the cell. This arrangement enables to capture single cells by suction in case the overall flow is partly aspirated towards the side channels (64) (Figure 6b). In addition, this configuration also allows cell release by flow reversion. A further popular example are hydrodynamic trapping arrays that consist of a large number of micrometer-sized features which serve as barriers and are localized within flow chambers or channels (65) (Figure 6c). The highly parallel manner of the array format can be considered as promising approach towards high throughput measurements.

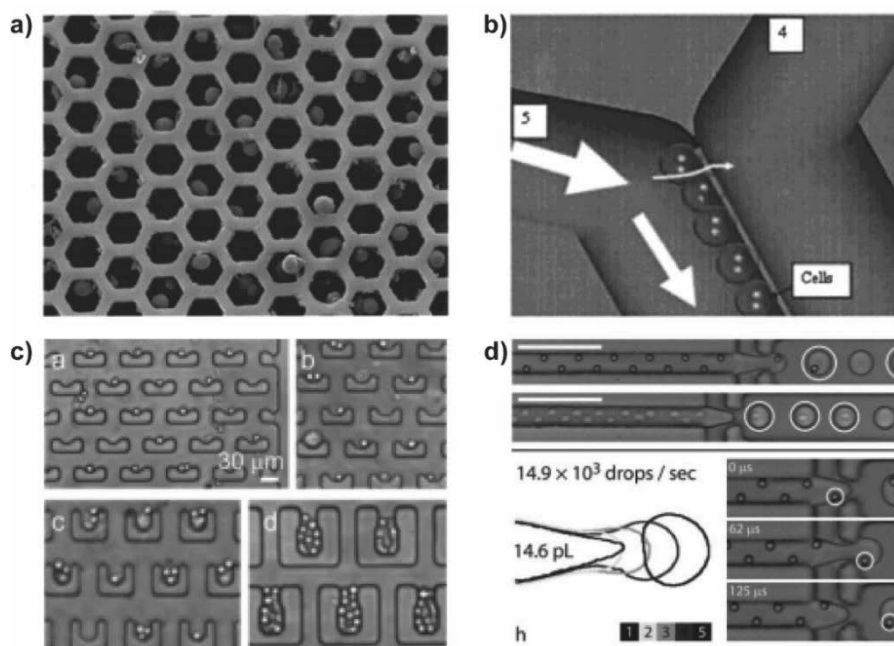


Figure 6: Common cell capture approaches. a) Scanning electron micrograph (SEM) of a microwell array for capture of yeast cells (well diameter of 6 μm). Adapted with permission from reference [61]. Copyright (2015) American Chemical Society. b) Schematic drawing which depicts the cell trapping mechanism in a dam structure device. Adapted with permission from reference [64]. Copyright (2015) American Chemical Society. c) Micrographs of different cell trap geometries for capture of HeLa, Jurkat and 293T cells. Cell trap depth varies from 10 (top left), to 15 (top right), to 30 (bottom left) to 60 (bottom right) μm. Adapted with permission from reference [65]. Copyright (2015) American Chemical Society. d) Micrographs of single-particle droplets (marked by circle) and empty droplets (no mark). Adapted with permission from reference [79]. Copyright (2015) American Chemical Society.

1 General introduction

A further major group of physical cell capture techniques is based on cell adhesion by surface functionalization. The most widespread method is microcontact printing (μ CP) which is a specific type of soft lithography for the generation of self-assembled protein or polymer monolayer patterns on surfaces (66, 67). A recently published work presented a convenient μ CP-based fabrication process for three-color dynamically adhesive substrates (68). The surface of the final platform consisted of three spatially and functionally differing areas. Thereby the defined positioning of different cell types in close contact to each other on the same device was feasible. Another common strategy is the use of hydrogels (69). The wide range of commercially available gels with tailor-made chemical and physical properties provides a great experimental flexibility. A major disadvantage is the difficulty of cell release.

The above mentioned examples illustrate the common advantages of contact-based cell capture techniques that include straightforward production processes, robustness, and simple handling. The suitability of the corresponding methods was demonstrated by the successful trapping of a variety of different cell types ranging from rather large mammalian cells (70) to yeast (71) and bacteria (72). Limitations are related to the physical capture itself, as it is rather difficult to estimate the impact of surface or polymer contact on cellular fitness and physiology.

The second large group are the contact-free cell positioning methods that include magnetic and acoustic forces (73-75), negative dielectrophoresis (nDEP) (76), optical tweezers (77), and droplets (78). Although the underlying working principles of the individual approaches strongly differ, they all require a rather demanding technical equipment resulting in a more sophisticated handling. An obvious advantage of the contact-free techniques is the avoidance of direct physical cell interaction. Nevertheless, cell capture forces can strongly influence the cell physiology as demonstrated by optical tweezer-induced cell lysis. In this context, droplet microfluidics are a good example for contact-free techniques that do not apply additional holding forces (79) (Figure 6d).

1 General introduction

1.5.2 Cell isolation

Depending on the type of the later performed analysis, defined spatial isolation of the cell may be required. This is virtually always the case for the analysis of cell lysates due to the risk of analyte loss or cross-contamination. In the last years, several convenient cell compartmentalization methods have been established. The most popular ones include cell isolation by means of microwells (80, 81), droplets (82), and microchambers (83). Each of the above mentioned techniques has its specific advantages and limitations which will be discussed in more detail in the following.

In this context, the most straightforward approach is the use of microwells that benefit from simple fabrication processes and user-friendly handling. In addition, they can be produced from many different biocompatible materials and design geometries. In several studies the successful application of microwells as single cell microenvironments for embryonic stem cells was reported. The focus was thereby on self-renewal and differentiation behavior analysis (84, 85). Although microwells provide defined microenvironments with single-cell resolution, which makes them interesting alternatives to standard cell culture systems, some major drawbacks have to be overcome. Due to their static properties controlled manipulation of the cell or its direct surrounding, for example medium exchange or exposure to a stress stimulus, is rather difficult. Therefore, they can be considered as bridging technology between standard 96-well plates and complex microfluidic cell culture systems.

Another common strategy for cell isolation is the use of aqueous droplets based on water-oil emulsions (86-88). Thereby, the encapsulation of single cells in small fluid volumes in the nano- to picoliter range is feasible (87). Compared to other techniques, a major benefit is the generation of several thousand droplets per second that enables high throughput single cell analysis. As droplets can be easily merged and fused, reagent delivery towards the cell, e.g. fresh cell culture medium, enzyme substrates, or stimulating substances can be realized easily. In addition, droplet incubation- and storage over a period of several days, for example in narrow channels or syringes, enables the performance of long-term experiments (89). Droplet-based systems have been used for numerous single cell analysis studies with focus on DNA (90, 91) and RNA amplification, protein expression (92), and growth rates (93) to mention just a few. A drawback is related to the difficulty to remove reagents and fluids selectively from the droplet.

1 General introduction

A further concept is the use of microchambers based on PDMS-made pneumatic microvalves which are also commonly called “Quake valves” as firstly presented by Stephen Quake and coworkers (94). The microchambers can be designed in variable sizes and configurations (Figure 7). In numerous works the successful isolation of single cells in volumes down to the low picoliter range has been presented whereas the small analysis volumes resulted in high analyte concentrations after cell lysis and, consequently, low detection limits (95, 96). A major advantage over the above mentioned techniques is that the valve mechanism allows precise and fast exchange of the enclosed fluids (97). Therefore, also complex assay protocols including multiple reagent and washing steps can be carried out in a reliable manner. A limiting factor are the connectors required for valve control, since a large number of connectors complicates the up-scaling of the systems to highly parallel single cell analysis formats.

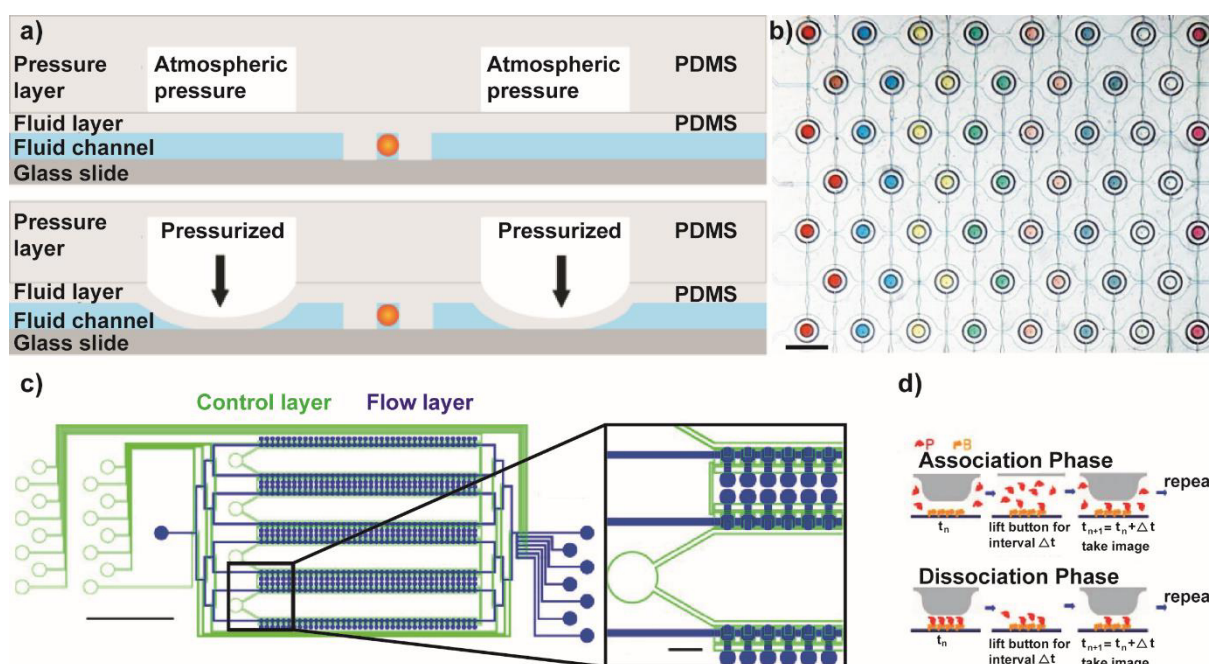


Figure 7: PDMS-made pneumatic valves. a) Scheme which illustrates the basic working principle of single cell isolation in microanalysis chambers by pneumatic PDMS microvalves. The scheme depicts the cross sectional view of a microanalysis chamber design used in various projects of this thesis. The single cell (orange sphere) is captured between two PDMS piles serving as physical cell trap. By pressurization of the ring-shaped valve, the cell is completely isolated from the surrounding. b) Micrograph of a microanalysis chamber array. For visual support, the microanalysis chambers are loaded with different food dyes. Chambers that are connected to the same pressure line enclose identical food dyes; i.e. each chamber within a row can be operated individually. Adapted with permission from reference [70]. Copy right (2015) American Chemical Society. c) Scheme illustrating the design of a microfluidic device for studying in a highly parallelized format the kinetics of biomolecular interactions. d) Scheme depicting the actual experimental procedure of an on-chip performed kinetics study. Bound proteins B (yellow components) interact with proteins in solution P (red components). Adapted with permission from reference [97]. Copyright (2015) AIP Publishing LLC.

1 General introduction

1.5.3 Cell lysis

To gain quantitative information about the genomic, transcriptomic, proteomic, or metabolomic state of a single cell at defined point in time, cell lysis is required in some cases. This can be achieved by chemical, optical, electrical, or mechanical means (98). The choice of method depends strongly on the overall experimental set-up and the properties of the target analyte. The chosen lysis conditions may not affect the analyte itself, and the lysis process should be faster than the cellular kinetics related to the analyte synthesis as otherwise the results can be falsified by signal cascade events. Consequently, the requirements for proteome analysis differ significantly from those for metabolome analysis. In the first case, mild lysis conditions should be prioritized to prevent analyte denaturation, whereas in the latter, time is an extremely critical factor giving preference to rather harsh but efficient methods. In the following section, common lysis strategies frequently implemented on microfluidic devices will be discussed.

The most popular lysis technique is chemical lysis which is based on the use of hypoosmolar buffer solutions. Thereby, a concentration gradient of solutes is generated by the cell surrounding hypertonic buffer resulting in an increased diffusion of water molecules into the cell. Consequently, the cell swells until the expansion leads to membrane rupture (99, 100). The process can be accelerated by the addition of detergents that incorporate into the cellular lipid bilayer and cause the solubilization of proteins and lipids that are part of the membrane. Frequently used detergents are Triton X-100, proteinase K, and sodium dodecyl sulfate (101). The latter enables cell lysis within milliseconds but also causes protein denaturation. As previously mentioned, the lysis conditions have to be adapted to the analyte properties. Another related and important issue is the cell type. For example, lysis of mammalian cell membranes can be induced by much milder conditions than in case of bacteria or yeast that additionally contain a cell wall. The digestion of this rigid layer which is mainly composed of peptidoglycans, polysaccharides, and glycoproteins requires enzymes like lysozyme or lyticase resulting in a more complex buffer composition. The widespread use of chemical lysis is based on the large range of commercially available buffer compositions and the simple implementation that requires only basic laboratory equipment.

A further common technique is electrical lysis. Numerous studies presented the convenient on-chip implementation of microelectrodes (102, 103). By application of electrical fields membrane pores are generated that lead to subsequent membrane rupture (104). The required field strengths depend on the cell type and size but are usually between 1 to 10 KV/cm (105). Electrical lysis occurs within milliseconds and is therefore suitable for the study of fast cellular kinetics. As the technical equipment and the on-chip implementation are demanding, the method is normally applied in combination with electrical cell trapping, as in this case the technical features are already integrated in the set-up.

1 General introduction

Optical lysis is related to high technical demands and costs and therefore not as widespread as chemical lysis. This lysis strategy relies on laser pulses that are focused on a defined spot in close proximity to the cell. The laser pulses generate mechanical shock waves that lead to cell lysis within microseconds (106-108). Therefore, this method is also suited for the observation of highly dynamical cellular processes. Disadvantages are possible bubble formation, heating effects, and the limited number of cell types that can be analyzed, as the method is mainly applicable for adherent cells. Another optical cell lysis possibility is the use of “ μ -hotplates” (109). For this approach, micrometer-sized patterns of gold or carbon strongly absorbing infrared light are applied to the surface. Exposure of the microstructures to IR radiation generates a local temperature increase which induces cell death, if cells are in close proximity. This method enables the defined optical heating of small volumes without requiring direct contact to a temperature control instrument.

Further methods include thermal or mechanical lysis. Thermal lysis is the method of choice for DNA or RNA amplification by PCR, as a heating system is required per se (110). Due to the risk of denaturation, this method cannot be applied for proteins or other heat sensitive analytes. Mechanical lysis can be carried out by bead-beating systems or sharp microstructures as presented in a work of Di Carlo et al. (111). Normally this is not the first choice, as the lysis efficiency is not as good as for other methods. A common drawback is, for example, incomplete cell lysis caused by vesicle formation.

1 General introduction

1.5.4 Analysis

Quantitative biomolecule analysis on the single-cell level is linked to some major challenges. Although the intracellular concentration of most analytes is in the millimolar range, the absolute amounts are extremely small due to the low volume of a single cell of a few pico- to femtoliter. A further main difficulty is the wide dynamic range of analyte concentrations. Some molecules occur at few others at several thousand copies. Moreover, there exists a great variety of different but structural resembling biomolecules. Consequently, the analysis method has to provide high sensitivity and selectivity.

Single cell analysis techniques can be grouped into non-invasive and invasive approaches. The first are mostly based on optical methods like fluorescence spectroscopy (112). Common applications include the long-term observation of living cells incorporating fluorophore-labeled target molecules. A drawback though is the limited number of targets that can be observed simultaneously. Furthermore, fluorescence-based flow cytometry methods are frequently applied in clinical diagnostics, especially in the fields of immunology and hematology. Otherwise Raman spectroscopy (113, 114) or impedance measurements (115) could be used as label-free alternatives.

Invasive methods like chemical analysis of cell lysates are commonly used for quantitative biomolecule analysis. In this context, an important factor is the analysis volume which should be as low as possible to prevent dilution of the cell lysate and, consequently, of the target molecules. Convenient concepts include lysate encapsulation within small droplets or microchambers based on flexible pneumatic valves. Apart from the analysis volume, signal amplification is a further crucial aspect. For instance, quantitative single cell DNA and RNA analysis in microfluidic devices was driven forward, among other things, by the signal amplification power of the polymerase chain reaction (PCR) (116). For other biomolecules not accessible to PCR the situation is more difficult. Recently, several studies reported the successful use of immunoassay-based techniques that can be applied to a much broader range of analytes from small messenger molecules to large proteins. Fascinating limits of detection have been achieved for assays that used enzyme labels (70) or DNA-labels (117, 118).

Mass spectrometry is another analytical method suitable for single cell analysis (119). For example, a recent study demonstrated the successful quantification of metabolites in single yeast cells by MALDI-MS (120). Key component of the utilized set-up was the microarrays for mass spectrometry platform (MAMS) that allowed the positioning of single cells at well-defined spots. Another interesting study reported the MS-based investigation of single human bone marrow cells (121). The cells were labeled by different antibodies coupled to transition element isotopes and analyzed individually by atomic mass spectrometry measurements. This approach allowed the parallel analysis of 34 different parameters and provided a comprehensive insight into immunological cell signaling processes.

A further interesting approach is the combination of microfluidics with mass spectrometry (122). In this context, a recent work of a droplet microfluidic sample injection system for the use in an inductively coupled plasma mass spectrometer should be mentioned (122). The microfluidic interface enabled to eject sample volumes of only 1 μL as liquid jet. Functionality of the system was proven by elemental analysis of individual red blood cells from bovines.

1 General introduction

1.6 Immunoassays

The general operation principle of immunoassays is based on the highly specific interaction of an antibody to its antigen. For analyte quantification it is additionally necessary that one of the immunoanalytical reagents is coupled to a signal-generating label. The high specificity and sensitivity of the immunoassay technology is founded on exactly these two basic requirements. There is a great variety of different assay types and labels available. The choice of the method strongly depends on the analyte, the sample matrix, and the required sensitivity. In the following sections, the most common assay formats and labels are discussed in more detail.

1.6.1 The past, the present and the future of immunoassays

The early generation of assays were radioimmunoassays (RIA) that were presented to the scientific community for the first time in 1959 by Yalow and Berson (123). They developed a competitive assay format for the detection of native insulin from blood samples. Thereby, the unlabeled native insulin of the sample competed for antibody binding sites with insulin that was labeled by gamma-radioactive isotopes of iodine. The subsequent evaluation was carried out by radioactivity measurements with a scintillation counter. For their work, they were awarded the Nobel Prize in Medicine in 1977. A further milestone in the immunoassay development was achieved by the enzyme-multiplied immunoassay technique (EMIT) in the early 1970s. The first assay reported by Rubenstein et al. (124) enabled the detection of morphine. Key component was a morphine-lysozyme conjugate that served as labeled antigen in a competitive assay format. By the binding of morphine to the antibody, lysozyme was sterically hindered and thereby inhibited. In an actual assay, the amount of unlabeled morphine of the sample was quantified by measuring the enzyme activity of the unbound morphine-lysozyme conjugate. For this purpose, the bacterium *Micrococcus luteus* was added to the reaction mixture and the decrease in turbidity after bacteria lysis by active lysozyme was monitored. This technique has two main advantages over standard RIAs. First, it is a homogeneous assay format. Therefore, it is not necessary to separate free labeled antigens from bound ones. In RIAs this is a crucial step as the radioactivity measurement is unable to distinguish between free or bound radioactive antigens. Second, enzyme labels are more convenient to handle than radioactive labels that require special laboratory safety standards and trained experts. The EMIT format led to the development of further alternatives to radioisotope labeling, such as fluorescence polarization (125) and chemiluminescence. The latter is of particular importance due to its high sensitivity and its routine use in present automated immunoassay analyzers (126).

1 General introduction

A next important step forward was taken by the development of the hybridoma technology by Kohler and Milstein in 1975 (127). Until then, assays were performed with purified polyclonal antibodies originating from human or animal sources and therefore only available at low quantities. In addition, the low specificity of the polyclonal antibody mixtures was another issue. Both drawbacks could be overcome by the hybridoma technology that enabled the large scale production of monoclonal antibodies. The basic principle includes the fusion of immortal myeloma cells with antibody forming B-cell lymphocytes isolated from the spleen of immunized animals. The created hybridoma cells are immortal and produce homogeneous immunoglobulins with high specificity towards the target antigen. For their work, Kohler and Milstein received the Nobel Prize in Medicine in 1984.

The enhanced availability of antibodies led to the development of sandwich assays which are state-of-the-art in programmed assay formats. Further technological progress enabled the integration of formerly manual performed assay protocols into automated systems. Present clinical chemistry analyzers can handle a large number of samples simultaneously and are operated in a stand-alone mode.

Regarding the future of immunoassays, main research foci are on multiplexing and on enhanced analytical sensitivity. The driving force behind is the development of improved platforms that make new applications accessible. A good example of this are multi-analyte-immunoassays that enable the simultaneous detection of a set of clinically related target molecules. This could be realized, for instance, by the Luminex technology (128, 129). This special type of bead-based flow cytometry uses specific capture antibodies which are immobilized on differently colored beads. Thereby, identical capture antibodies are linked to beads of the same color. In a next step, the bead-labeled capture antibody mixture is incubated with the analyte mixture and fluorescent labeled detection antibodies. The resulting immunocomplex-sandwiches consist of the capture antibody that is linked to a specifically colored bead, the analyte, and the second antibody that is linked to a fluorescent reporter dye. The subsequent analysis is carried out with a multicolor flow cytometer. One channel is used to identify the analyte by bead color while a second channel enables the analyte quantification by detection of the reporter dye fluorescence.

Another important aim of ongoing research activities is the improvement of assay sensitivity for the detection of new biomarkers. One main focus thereby is on early screening and diagnosis of cancer and cardiovascular diseases. In this context, DNA labels as applied in barcode assays or Immuno-PCR (IPCR) are a convenient approach (130-132). The basic principle is to combine the specificity of antibody-antigen interactions with the signal amplification power of PCR. Compared to the ELISA format, the detection limits of IPCR are improved by about a factor of 1000, depending on the assay and the target analyte. In addition, up to 150 biomolecules can be analyzed simultaneously.

1 General introduction

1.6.2 Direct and indirect assays

In a direct assay the primary antibody that binds to the analyte is directly coupled to the signal-generating label (133) (scheme on the left-hand side of Figure 8). Consequently, there is no need for a secondary detection antibody. This approach has one main benefit. The risk of unspecific binding and therefore of high background signals is reduced as less incubation steps are required than in an indirect assay format.

In contrast, an indirect assay requires two different antibodies (134) (scheme on the right-hand side of Figure 8). A monoclonal primary antibody that binds to the target analyte and a detection antibody that binds to the Fc part of the primary antibody. Thereby, the secondary antibody is coupled to the signal-generating label. An obvious drawback is the complex assay protocol. An advantage is the better signal amplification, as several labeled secondary antibodies can bind to one primary antibody. In addition, the same labeled detection antibody can be used in different assays in case the specific primary antibodies originate from the same species. Therefore, indirect formats are mostly given preference over direct ones if multiple assays have to be performed. In such cases, the labeling of each monoclonal primary antibody would be very expensive. Consequently, a further advantage of the indirect assay format is the cost reduction.

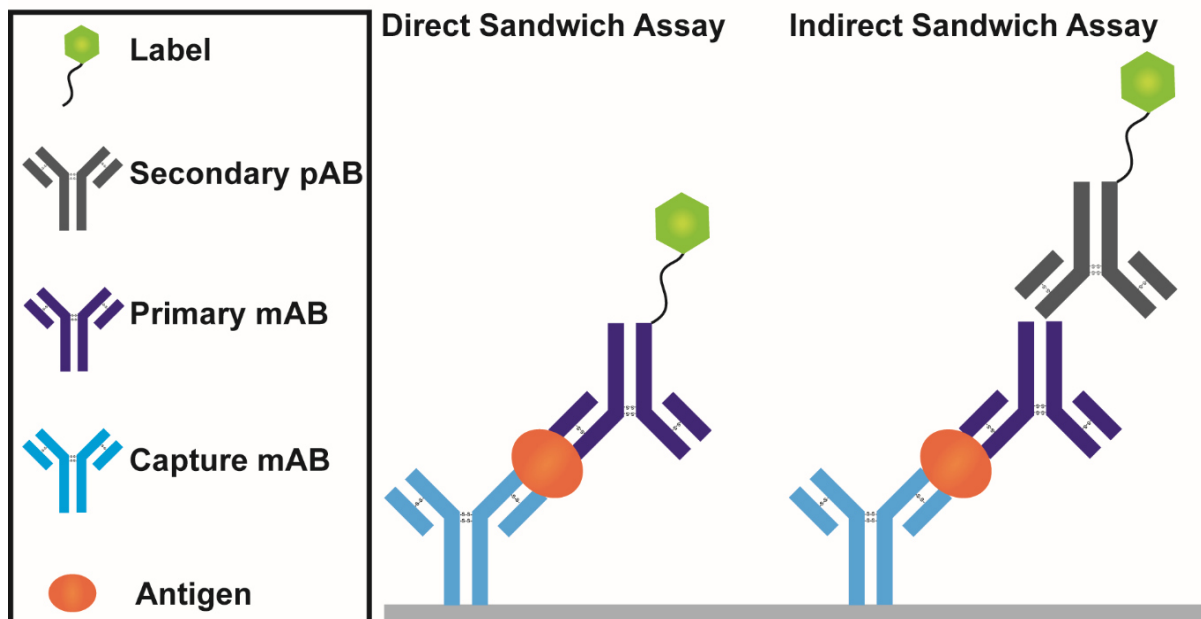


Figure 8: Direct and indirect sandwich immunoassay formats. Left: Schematic drawing of a direct assay. The label is directly coupled to the primary antibody binding to the antigen of interest. Right: Schematic drawing of an indirect assay. The label is coupled to a secondary antibody that binds to the primary antibody.

1 General introduction

1.6.3 Competitive and non-competitive assays

In a competitive assay unlabeled analyte molecules of the sample compete with a known amount of labeled analyte molecules of the immunoassay for a limited number of antibody binding sites (135). If there is no analyte present, all antibody binding sites are occupied by labeled analyte molecules, and the signal is maximal. If the analyte concentration in the sample increases, less labeled analytes can bind to the available capture antibodies. As a consequence, the detected signal decreases. Hence, the signal is inversely proportional to the amount of analyte that was present in the sample (136). As no secondary antibody is required, this is the method of choice for low molecular weight analytes. A drawback is the often lower sensitivity compared to a non-competitive assay (137). The assay sensitivity is based on a slight excess of labeled analyte molecules over available antibody binding sites. Consequently, the limit of detection of the assay also strongly depends on the careful optimization of the labeled analyte concentration.

The most common type of non-competitive assay is the sandwich format (Figure 8 and schematic drawing on the right-hand side of Figure 9). Thereby, the analyte is embedded by two antibodies, namely the capture antibody and the detection antibody. This approach is only accessible to large macromolecules, as the target analyte has to provide two different antigenic epitopes that can be bound simultaneously. Commonly the antigen is “sandwiched” between a monoclonal high affinity antibody serving as capture antibody and a labeled (direct assay) or unlabeled (indirect assay) primary antibody. The detected signal is directly proportional to the amount of analyte present in the sample (138). The main benefit is the provided high assay sensitivity.

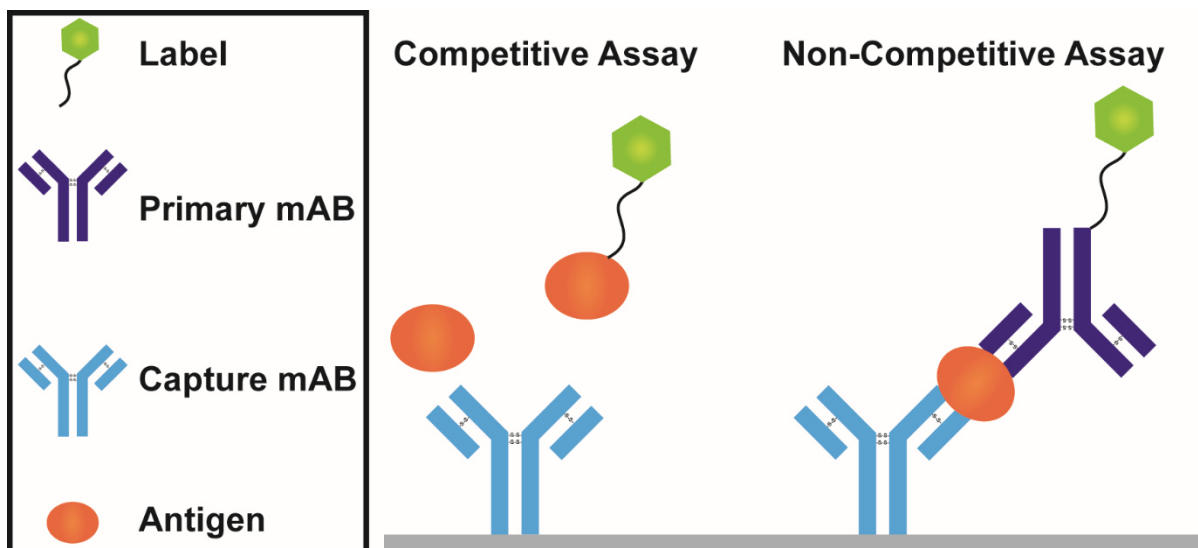


Figure 9: Competitive and noncompetitive immunoassay formats. Left: Schematic drawing of a competitive immunoassay. Unlabeled antigens of the test sample compete with a known amount of labeled antigen of the assay for antibody binding sites. The detected signal is inversely proportional to the antigen concentration of the test sample. Right: Schematic drawing of a non-competitive sandwich assay. The detected signal is directly proportional to the antigen concentration of the test sample.

1 General introduction

1.6.4 Antibody-antigen interactions

The antibody-antigen binding is based on a dynamic equilibrium and can be described by the law of mass action (equation 4). The reversible and non-covalent interactions leading to the complex formation are mainly attributed to electrostatic and hydrophobic forces, hydrogen bonds, and van der Waals forces (139). The strength of the interactions is defined as affinity and is inversely proportional to the equilibrium dissociation constant (140). If multiple epitopes and paratopes are involved, reference is made to the functional affinity, the so-called avidity (141).

Equation 4: Determination of the eq. dissociation constant by application of the law of mass action

$$K_D = \frac{K_d}{K_a} = \frac{[Ag][Ab]}{[AgAb]}$$

K_D = eq. dissociation constant | K_d = dissociation rate constant | K_a = association rate constant
[Ag] = free antigen | [Ab] = free antibody | [AgAb] = antigen-antibody-complex

The affinity of an antibody to its antigen is an important assay parameter, as it impacts the minimal number of antigens that can be detected. This can be further clarified by rearranging equation 4 and replacing the equilibrium dissociation constant (K_D) by the equilibrium affinity constant (K_A) which is the reciprocal of K_D and directly proportional to the affinity.

Equation 5: The influence of the equilibrium affinity constant K_A on the ratio of bound to free antigen

$$\frac{[AgAb]}{[Ag]} = K_A * [Ab]$$

K_A = eq. affinity constant | [Ab] = available antibody binding sites

Besides the affinity constant, the analysis volume and the number of available antibodies are further important factors that influence the limit of detection of immunoassays performed on microfluidic devices. This was demonstrated in a recent study carried out on microfluidic antibody capture (MAC) chips (Figure 10) (142). The reduction of the analysis volume resulted in higher effective antigen concentrations pushing the equilibrium towards the bound complex. In addition, the volume reduction accelerated the establishment of the equilibrium state. The reduction of the spot size led to a lower amount of available antibodies. The consequential lower fraction of bound antigen (Figure 10b) could be compensated by either parallel reduction of the analysis volume (Figure 10c) or use of an antibody with higher affinity.

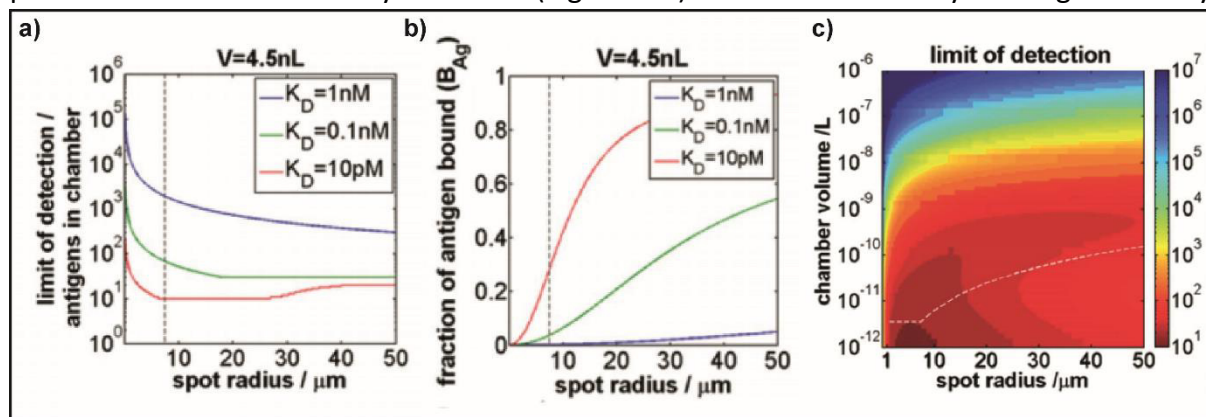


Figure 10: The influence of the K_D value, the antibody number and the chamber volume on the LOD. Adapted with permission from reference [142]. Copyright (2015) Royal Society of Chemistry.

1 General introduction

1.6.5 Different labeling strategies

Frequently used labels in immunoassays are enzymes (*143, 144*), fluorophores (*145*), DNA conjugates (*146*), acridinium- and isoluminol derivatives for chemiluminescence (*147*), and radioactive isotopes (*148*). The latter were utilized in the first immunoassays and are still in use today despite the special safety precautions, as they provide an extremely high sensitivity. Commonly used are radioactive isotopes of iodine (γ -emitter) due to the relatively long half-life of around 8 days and the emission of low energy photons. The labeling itself is based on covalent linkage to the tyrosine residues of the antibody or the antigen.

Another labeling strategy includes the use of acridinium esters for chemiluminescence measurements. The main benefits are high quantum yields and low background signals (*149*). The achieved assay sensitivities are comparable to or even better than those of radioimmunoassays. Moreover, coupling of the label to the antibody can be realized easily by activated esters or imidates (*150*).

Another option is to use fluorophores that are directly coupled to the antibody. A main advantage is the straightforward labeling process as there is a great variety of different cross-linkers commercially available. A major drawback is the relatively low sensitivity which is mainly due to two factors. First, there is no further signal amplification as it is the case for enzyme- or DNA labels that lead to a signal increase over time. Second, most fluorophores are hydrophobic. This can influence the binding properties of the coupled antibody negatively resulting in an increased non-specific binding and high background signals.

One of the most popular labeling approaches includes the use of enzymes. The enzymes can be coupled directly or indirectly to the antibody. The direct strategies are in general related to demanding techniques and purification steps of the final conjugate. Commonly the enzyme label is linked covalently to the antibody. Frequently applied linkage techniques use heterobifunctional cross linker reagents that enable the reaction to two different functional groups (*151*). In most cases, amino groups, thiol groups or cis-hydroxyl-groups are involved in the covalent bond formation (*151, 152*). Indirect strategies are either based on the avidin-biotin-system (*153*) or bacterial protein A or G (*154*). In the former case, a biotinylated antibody is used to bind the avidin-coupled enzyme. In the latter case, the enzyme is coupled to bacterial protein G or A binding to the FC part of the antibody. Enzyme labels provide a high sensitivity, as the signal is amplified over time by an increase of the colored product molecules.

A rather recent method is the universal immuno-polymerase chain reaction (IPCR) which is based on the use of DNA conjugates. Thereby, a biotinylated antibody is coupled via streptavidin to a biotinylated DNA label to form the final antibody-DNA-conjugate (*155*). The main benefits are related to the enhanced sensitivity and multiplexing.

Digital assay formats based on single molecule arrays (SiMoA) (*156, 157*) enable the performance of highly sensitive single molecule ELISAs. The key concept relies on the isolation and detection of single enzyme-linked immunocomplexes immobilized on beads which are placed individually in wells enclosing volumes in the femtoliter range (*158*). Signal read-out is performed by time-lapsed fluorescent imaging. Digital ELISA formats were used, for example, for the detection of prostate-specific antigen (PSA) at sub-femtomolar concentrations (*159*).

1 General introduction

1.7 *Escherichia coli* as model organism

Escherichia coli (*E. coli*) is a rod-shaped, gram-negative bacterium (Figure 11) that was discovered in 1885 by the medical scientist and bacteriologist Theodor Escherich, who investigated the causes of infant diarrhea and gastroenteritis (160). Since then, *E. coli* was widely used in research laboratories around the world and is therefore frequently referred to as the best studied prokaryotic organism. Due to its simple and inexpensive cultivation, *E. coli* already served as model in important studies of bacterial physiology and growth in the 1940s. A good example is the work on bacterial conjugation (161, 162) which was awarded the Nobel Prize in 1958. The short doubling time of approximately 20 minutes makes *E. coli* a favorable organism to study the causes of adaptive diversification and evolutionary dynamics. In this context, particular reference should be made to the *E. coli* long-term evolution experiment headed by Richard Lenski (163, 164). In this study, mutations in the genome of twelve initially isogenic populations have been monitored since 1988. The daily passaged bacteria are cultured in minimal medium with limited glucose access. Therefore, bacteria exhibiting a more efficient glucose utilization than others have a benefit in evolution. As expected, an enhanced fitness was observed over the course of generations (165). The cells of more recent populations are larger and proliferate faster. Interestingly, the twelve starting populations adapted differently to identical conditions. For instance, the cell size increased for all populations but varies by a third according to the population (166).

Furthermore, *E. coli* is also an important organism in the field of biological engineering. In 1973, the construction of the first recombinant DNA containing organism was reported by Stanley Cohen and Herbert Boyer (167). In the experiment, genes from two different drug-resistant *E. coli* strains were recombined. One gene provided resistance to tetracycline and the other one to kanamycin. The plasmid DNA carrying the corresponding genes was isolated, and short, single-stranded DNA sequences, so called “sticky ends”, were generated by the use of the restriction enzyme EcoR1. The complementary EcoR1 ends of the cut plasmid fragments were then fused by DNA ligase. The resulting recombinant plasmid molecule was inserted into *E. coli* resulting in a genetically modified organism which was resistant to tetracycline and kanamycin. The presented concept of DNA recombinant engineering was a milestone in biotechnology and had a great impact on the pharmaceutical- and agriculture industry. Common biopharmaceutical products based on this technology include virus vaccines, monoclonal antibodies (168), and therapeutic proteins such as insulin (169). In this context, *E. coli* is one of the most popular “cell factories” for the expression of recombinant proteins (170). The main benefits of *E. coli* as a host cell are the fast growth kinetics, the inexpensive cultivation, the feasible high cell culture densities, the profoundly studied genetics, and, most important, the well-established transformation with exogenous DNA.

1 General introduction

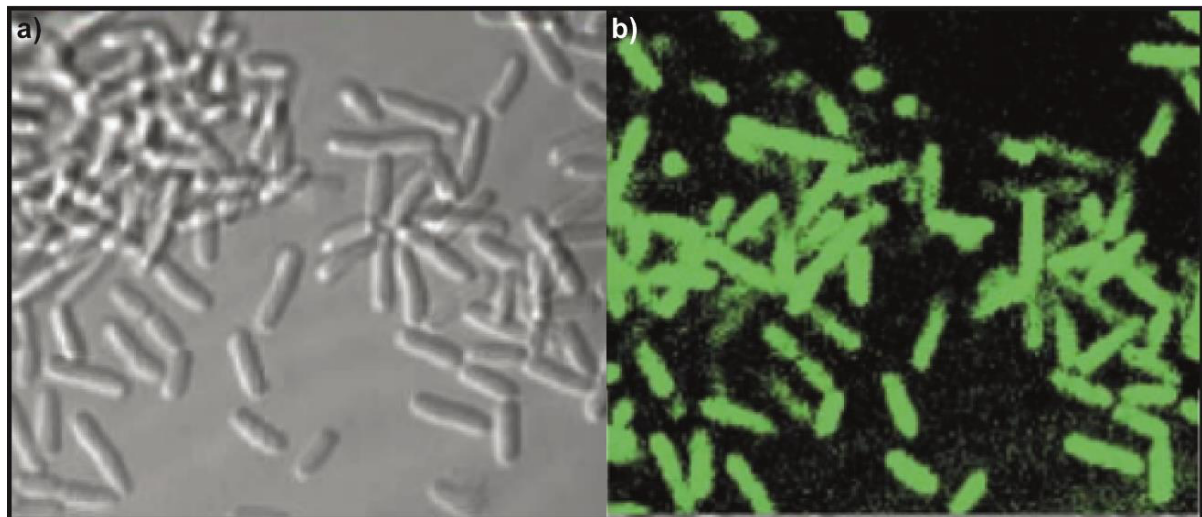


Figure 11: Bright field and fluorescence images of fixed *E. coli* bacteria. a) Bright field micrograph of *E. coli*. b) Confocal fluorescence image of the same bacteria. The images depict the rod-shaped structure of the bacteria which are around 2 μm in length and 1 μm in diameter. Adapted with permission from “Locked TASC probes for homogeneous sensing of nucleic acids and imaging of fixed *E. coli* cells”, S. Sando, A. Narita, T. Sasaki and Y. Aoyama, *Organic and Biomolecular Chemistry*, 2005, 3, 1002–1007. Copyright (2015) Royal Society of Chemistry.

In a nutshell, *E.coli* is the best-studied representative of the world of bacteria and therefore in general a convenient model for bacteria related research issues. In addition, it is an ideal organism to carry out research studies on evolutionary biology and bioengineering due to the properties illustrated above.

1 General introduction

1.8 *Saccharomyces cerevisiae* as model organism

Saccharomyces cerevisiae (*S. cerevisiae*) is a single-cell eukaryote (Figure 12) (171) that has been used since ancient times for brewing and baking (172, 173). It is one of the best investigated eukaryotic systems or, to put it in another way, it is the *E. coli* of the eukaryotic world. This is mainly due to, on the one hand, the simple and inexpensive cultivation of yeast and the profound knowledge gained during thousands of years of usage, and on the other, its function as a simple model for significantly more complex eukaryotes. The latter is the reason for the important role of yeast in functional genomics and systems biology, as discussed in the following.

The sequencing of the *S. cerevisiae* genome was completed in 1997 and was therefore the first entirely sequenced eukaryotic DNA (174). As it was known before, that several genes present in yeast and in humans encode similar proteins (175), it was natural to attempt the use of yeast genome sequences for the interpretation of human DNA sequences. Studying yeast genes to gain important information about their human analogs is also advantageous, as gene manipulation in yeast is much cheaper and easier than in mammalian systems. Shortly after publication of the *S. cerevisiae* DNA sequence, a nearly complete library of depletion mutants was constructed (176, 177). Therefore, each gene in the genome was deleted and replaced by a drug resistance gene and a label. Thereby a specific sequence of several nucleotides served as molecular barcode. This strategy enables to trace individual mutants and to investigate the biological impact of a loss of gene function on the phenotype in a systematic manner. Functional profiling, which is defined as the gene-protein-function association by analysis of mutants, is of special interest for the discovery of disease-related genes in humans. In this context, a good example is the Werner syndrome, which is caused by an autosomal recessive mutation of the WRN gene, resulting in premature aging and other symptoms related to the high mutation rates associated with the disease (178). The corresponding human gene sequence is highly similar to the SGS1 gene in yeast. Yeast cells with mutation in the SGS1 gene also exhibit shorter average life-spans and a greater nucleolar enlargement and fragmentation (179). Similar effects of mutations in related human and yeast genes have also been reported for hereditary nonpolyposis colon cancer (180), several mitochondrial dysfunction diseases (181), and Parkinson's disease (182).

1 General introduction

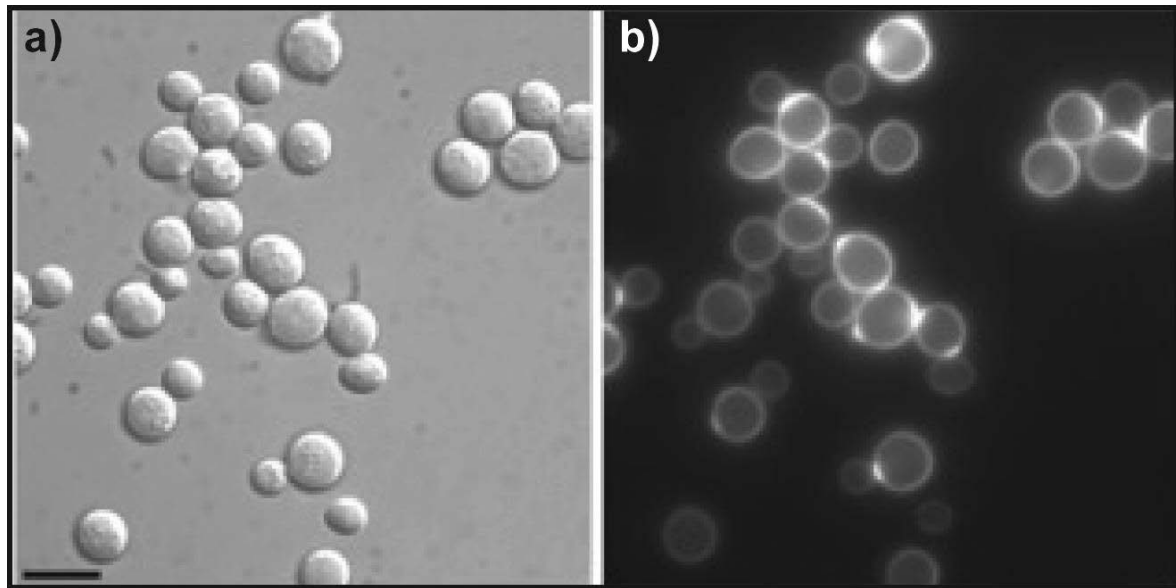


Figure 12: **Wild type (YPH499) budding yeast.** a) Bright field image. b) Fluorescence image of the same yeast cells stained with calcofluor white (CFW). The images depict the characteristic globular shape and bud formation of this yeast type. Adapted with permission from reference [171]. Copyright (2015) Company of Biologists Ltd.

Another related research field frequently using yeast as model organism is systems biology. The primary aim is to provide a holistic view of complex biological processes by the use of computational models (183). Compared to more complex eukaryotes, studies in yeast can be carried out rapidly and cost-efficiently. Thereby, the development of concepts for the quantitative description of biological networks and the corresponding computational analysis tools is facilitated. In addition, many well-established high-throughput genomics methods were originally designed for yeast. Possible applications focus on biomedical research and the chemical industry. For instance, the use of mathematical cell models could simplify drug target screening processes (184) or the identification of convenient organisms for the production of biofuels (185) or fine chemicals (186).

Briefly summarized, *S. cerevisiae* has been a commonly used organism for thousands of years and due to the characteristics illustrated above, it will continue to play an important role in a great variety of different research fields.

1.9 Open questions and challenges in single cell analysis

One of the main challenges of single cell analysis is related to the low absolute amount of analytes present in a cell. For this reason, most studies that have been carried out so far in this research field used either sophisticated single molecule detection methods (38) or signal amplification techniques based on PCR (116) as illustrated in Figure 13a by the microchip developed in the research group of Stephen Quake. The former are difficult to reconcile with automation concepts and high throughput measurements. The latter have the disadvantage of being limited in terms of the type of analyte since PCR is only accessible to DNA and RNA. The difficulty of low copy number analyte detection is further exacerbated in the case of the analysis of small microbes with volumes in the low femtoliter range. For this reason, devices suitable for the quantitative analysis of single yeast cells or bacteria are still rare. In this context, a recent publication demonstrating the successful MS-based quantification of metabolites from the glycolytic pathway in single yeast cells should be mentioned (120). The general workflow is depicted in Figure 13b. Limits of detection in the range of 100 amol to 10 fmol were achieved matching the concentration levels of most metabolites in single yeast cells (120). However, the cell load status of the reservoirs was based on a Poisson distribution leading to empty or multiple occupied reservoirs. This issue also concerns most droplet-based microfluidic systems representing another frequently used single cell analysis method (Figure 13c). In addition, droplet-based analysis approaches suffer from the difficulty to selectively remove substances that were once added to the droplet. Thereby the performance of washing steps, that are substantial part of most bioassay protocols, is hindered.

To sum it up, current state-of-the-art single cell analysis methods are limited with regard to the analyzable cell- and analyte type. To be precise, the majority of the systems is optimized towards the analysis of large mammalian cells and can be used to detect essential genes or gene products that are normally present at rather high levels. Moreover, the precise and automated manipulation and control of a single cell and its environment remains a difficult task. Regarding the future the following major challenges have to be overcome. First, methods capable of analyzing a great variety of different cell types and analytes should be developed. Thereby the flexibility with regard to the biological questions that can be addressed with the same platform would be significantly increased. For instance, not only essential but also rare analytes could be detected. Second, label-free detection techniques should be implemented. This would allow, in contrast to the frequently utilized chromosomally tagged fluorophore-fusion libraries, the analysis of non-genetically modified wild type cells. Third, strategies should be implemented to replace the sophisticated single molecule detection techniques by standard microscopic procedures. In the following section, it will be discussed in detail how the analysis approaches of this thesis aim to overcome the above-mentioned challenges.

1 General introduction

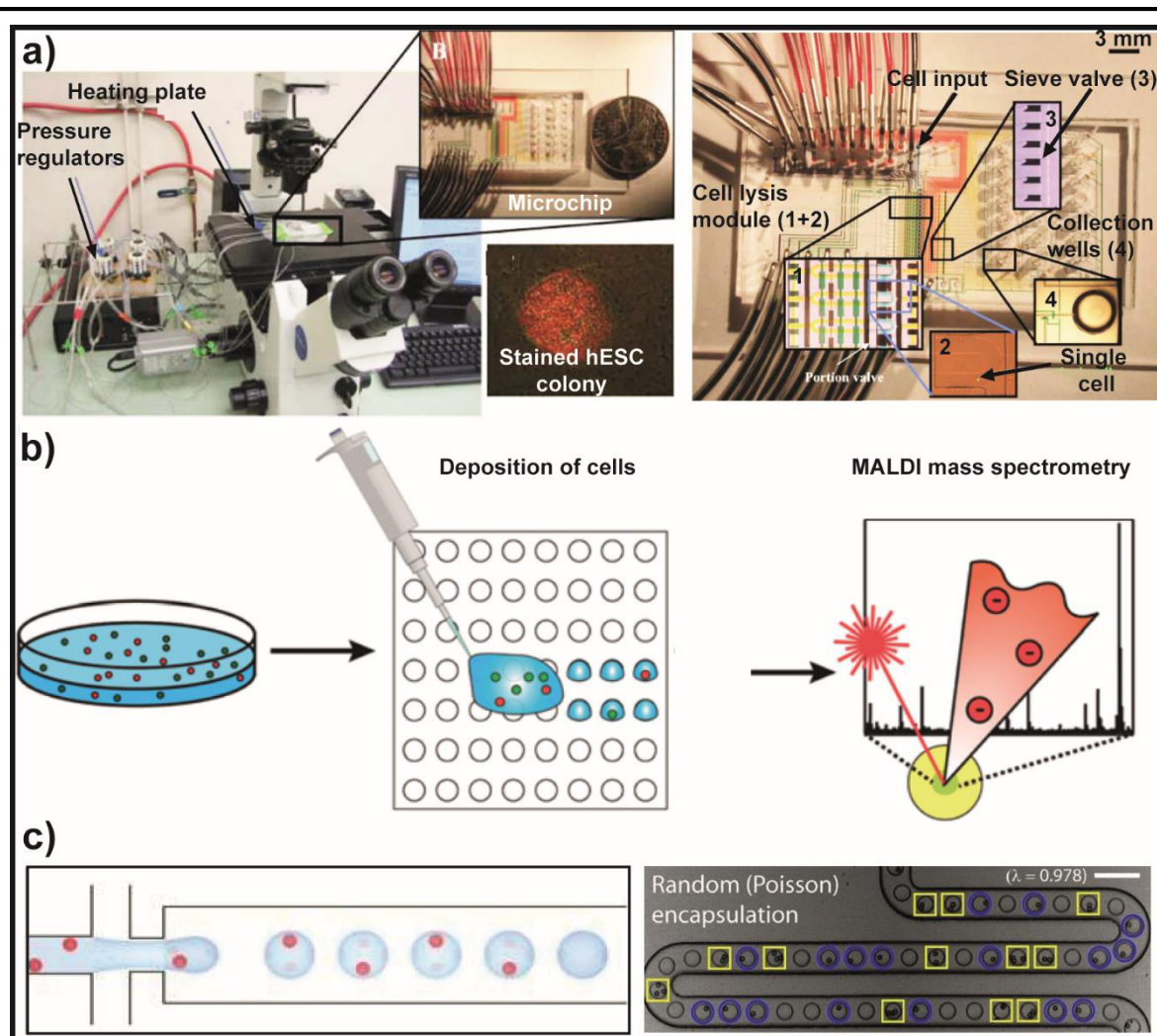


Figure 13: Overview of state-of-the-art single cell analysis methods. a) Left: Photograph of the experimental set-up required for the mRNA extraction and cDNA synthesis of individual human embryonic stem cells. The system includes a microscope, a heating stage and a computer to regulate the air pressure required for the valve control. Right: Magnified picture of the microfluidic chip depicting the crucial subunits of the device which enabled the gene expression profiling of individual human embryonic stem cells (hESC). Adapted with permission from "A microfluidic processor for gene expression profiling of single human embryonic stem cells", J. F. Zhong, Y. Chen, J. S. Marcus, A. Scherer, S. R. Quake, C. R. Taylor and L. P. Weiner, *Lab on a Chip*, 2008, 8, 68-74. Copyright (2015) Royal Society of Chemistry. b) Schematic drawing of the workflow of a single cell analysis experiment by MALDI-MS. Individual cells are positioned at defined spots by the use of the microarrays for mass spectrometry (MAMS) platform. After covering the single cells with an adequate matrix, the MALDI-MS experiment is performed to study, for instance, the metabolite levels of single algal cells. Adapted with permission from "Analysis of single algal cells by combining mass spectrometry with Raman and fluorescence mapping", S. R. Fagerer, T. Schmid, A. J. Ibanez, M. Pabst, R. Steinhoff, K. Jefimovs, P. L. Urban and R. Zenobi, *The Analyst*, 2013, 8, 68-74. Copyright (2015) Royal Society of Chemistry. c) Left: Schematic drawing of cell encapsulation within droplets. Right: Illustration of the cell encapsulation process following a Poisson distribution. Adapted with permission from Reference [79]. Copyright (2015) American Chemical Society.

1 General introduction

1.10 Scope

Individual cells of an isogenic population can display significantly different phenotypes (187). The great variety of factors contributing to this cellular heterogeneity make the investigation of the underlying mechanisms to a challenging task (188). In this context, single cell analysis methods are of particular importance, as they unravel the biological complexity of cell heterogeneity studies to some extent. As discussed in previous sections of this introduction, measurements on individual cells provide biological information that is not accessible by population measurements. Important related research issues concern the interplay between intrinsic cellular processes and extrinsic stimuli or the influence of rare cells on the emergence of drug resistances. However, the implementation of single cell analysis techniques remains difficult. Most state-of-the-art techniques such as fluorescence-activated cell sorting (FACS) (51) provide only physiological snapshots of single cells. The study of complex biological research questions as those mentioned above requires long-term observation of individual cells. Consequently, advanced techniques that enable the accurate spatio-temporal control of individual cells over several cell cycles have to be applied. The use of microfluidic systems is thereby a promising approach, as the precise control of small fluid volumes matching those of single cells is feasible. So far, several convenient microfluidic devices for single cell studies have been presented. However, most of them were limited with respect to the scope of application. The majority of available platforms is optimized for the analysis of large mammalian cells and for one particular purpose of use.

Aim of this thesis is the development of microfluidic devices that overcome the limitations of existing systems. Three key aspects are prioritized. First, reliable manipulation and control of single microbes significantly smaller than typical mammalian cells should be feasible. Second, multifunctional device designs are targeted that enable the comprehensive characterization of individual cells. Third, the quantification of metabolites or proteins as analytes of interest is aimed.

The first presented microfluidic system is optimized for bacterial cell studies. The device consists of a set of microchambers equipped with micrometer sized features for hydrodynamic capture of single *E. coli*. Each cell trap is surrounded by a ring-shaped valve which, when actuated, isolates the single bacterium in a volume in the low picoliter range. In addition, a surface modification protocol is presented that allows immunoassay-based analysis of the single-cell lysate. Detailed information about the challenges of bioanalyte quantification in bacteria enclosing volumes in the femtoliter range is provided in chapter 3.

The second platform focuses on multifunctional use. The cell trapping features are adapted to the geometry of single *S. cerevisiae* cells. Key characteristic of the design is a convenient double valve configuration that enables to switch between complete and partial isolation of the captured cell. In a first application on-chip cell culture studies are combined with chemical analysis of the corresponding cell lysates, as described in more detail in chapter 4.

1 General introduction

The third system is aimed to investigate a specific source of cellular heterogeneity, the so called inheritance noise. The term describes the uneven distribution of cellular components, especially of messenger RNA, during the cell division process. Therefore, a device design is presented that enables the on-chip separation of budding *S. cerevisiae* mother cells from the corresponding daughters and subsequent analysis of the cell lysates. Details are discussed in chapter 5.

A further project is performed on an already existing device for mammalian cells and evaluates the effect of different sample matrices on analyte detection in immunoassays, as described in chapter 6.

In a nutshell, the studies of this thesis place emphasis on comprehensive cell analysis with focus on biomolecule quantification in single microbes on microfluidic devices.

2 Methods

2.1 Device fabrication

The device fabrication can be subdivided into three main steps: (1) Development of the device design according to the application requirements, (2) Preparation of the master molds by photolithography, (3) Production of the final device by soft lithography. The entire workflow of the fabrication process is illustrated in Figure 14. A detailed description of the main steps is provided in the following sections.

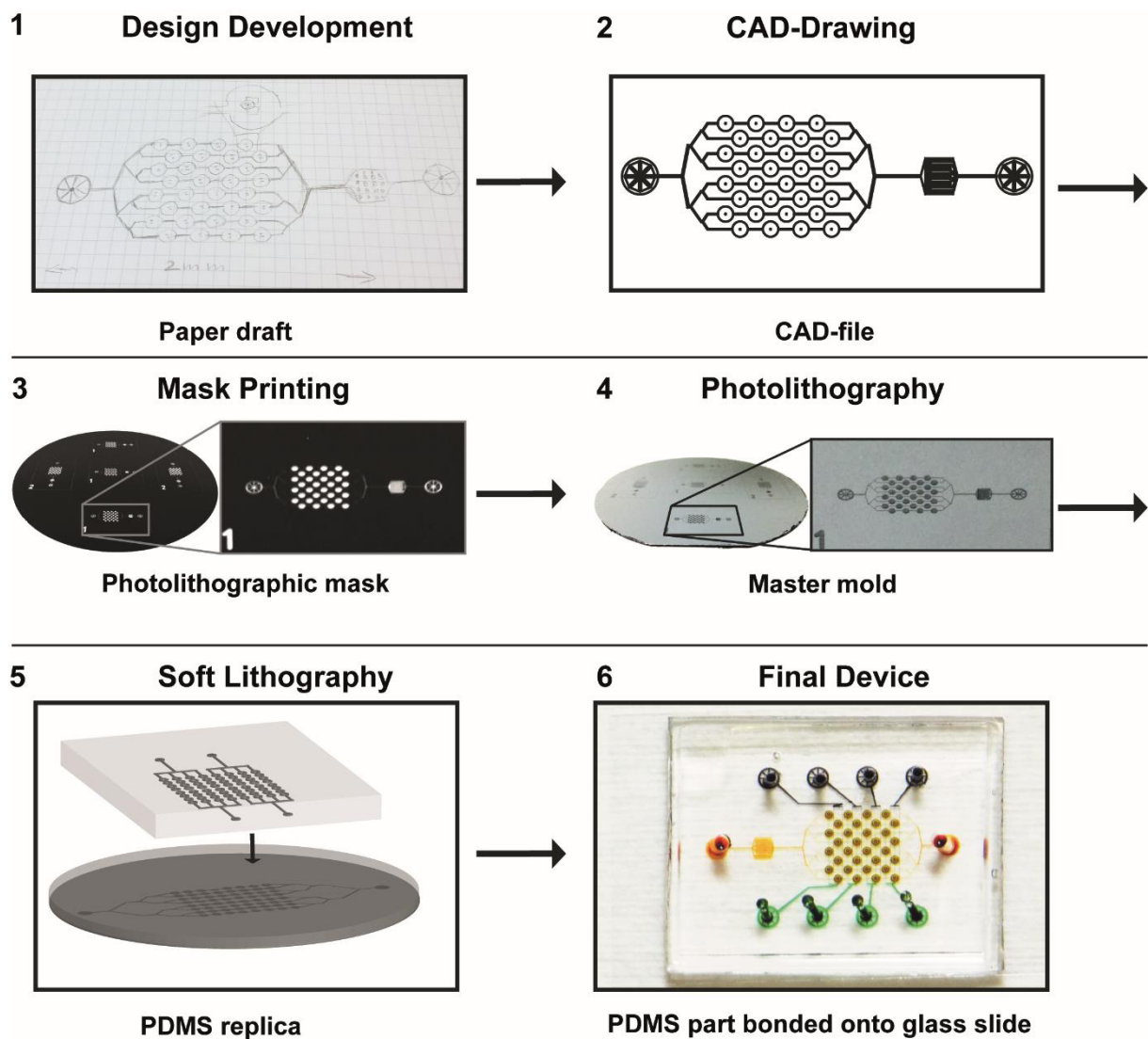


Figure 14: Overview of the device fabrication workflow. First, new design ideas are collected and are implemented in an initial paper draft. Next, a technical drawing of the paper draft is created. The design of the generated CAD-file is transferred to a photolithographic mask that is subsequently utilized for master mold fabrication by photolithography. The silicon master mold is used to generate PDMS replica of the design by soft lithographic techniques. Bonding of the assembled PDMS building block to a glass slide leads to the final device.

2 Methods

2.1.1 Design development

The new chip designs presented in this work base on a previously published device which consists of an array of microchambers equipped with cell traps for mammalian cells. The further development of the precursor design focused on the expansion of the application range. One important enhancement concerns the cell trapping features that were optimized for the capture of significantly smaller microbes like *E. coli*. Consequently, the strategy of using micrometer-sized features for physical cell capture can now be applied to a broad range of different cell types. A further crucial advancement concerns the reduction of the chip dimensions. Down-sizing of the channel heights and valves resulted in microanalysis chamber volumes in the low picoliter range. The related high analyte concentrations after cell lysis had a beneficial impact on the detection limits of the performed assays. Another important methodical progress was achieved by the construction of a double-valve-configuration. The multifunctional microanalysis chambers enabled to combine cell cultivation with chemical analysis studies. An overview of all performed design developments is provided in Table 1.

Table 1. Size parameters

Parameter	Size	Functionality
<i>Channel height [μm]</i> (Constant valve radius of 70 μm)	15	Fully
	12	Fully
	10	Fully
	5	Partially*
<i>Valve radius [μm]</i> (Double-valve-configuration) (Constant channel height of 10 μm)	Outer radius: 250 Inner radius: 100	Fully
	Outer radius: 250 Inner radius: 70	Fully
<i>Valve radius [μm]</i> (Single-valve-configuration) (Constant channel height of 10 μm)	90	Fully
	80	Fully
	70	Fully
	60	Partially**
	50	Partially**
	40	Partially**
	30	Partially**
	20	Inoperable
<i>Gap size of the cell trap [μm]</i>	4.0	Fully
	3.5	Fully
	3.0	Fully
	2.0	Fully
	1.5	Fully
	1.0	Fully
	0.8	Fully
	0.5	Inoperable

*The fluid channel was stable in case of open valves but collapsed during valve actuation.

**Individual valves were still functional but proper manual alignment of the valve array to the fluid layer was not possible anymore.

2 Methods

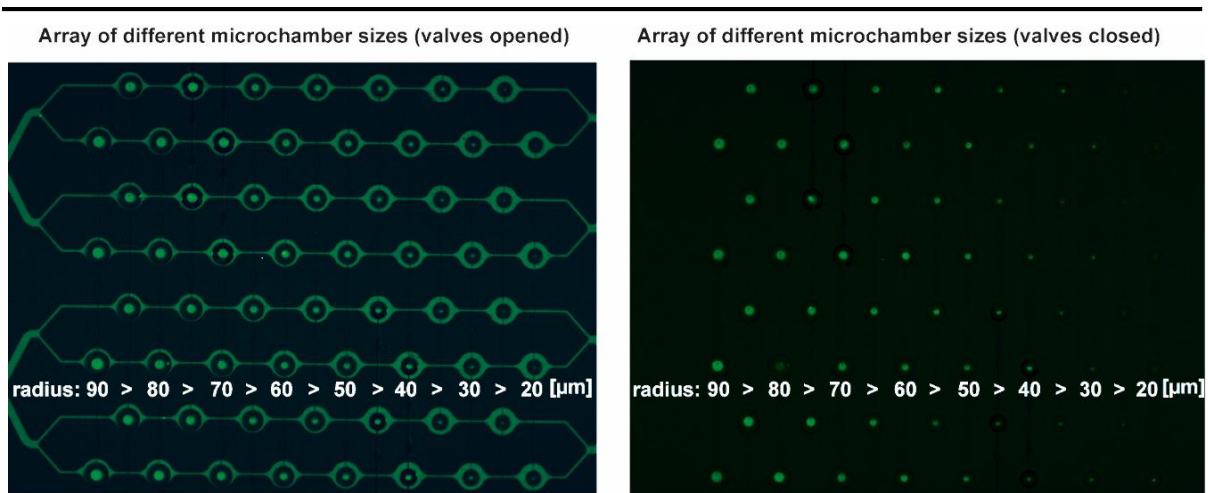


Figure 15: Reduction of the microanalysis chamber volume by down-scaling of the valve inner radius. Fluorescent micrographs of a device stability experiment. The inner radii of the ring-shaped valves were reduced stepwise by $10\ \mu\text{m}$ within a row of the array. Left: The device was flushed with fluorescent solution (fluorescein in dest. water, $50\ \text{nM}$) while the valves were still opened. Right: The valves were actuated and the surrounding fluorescein solution was exchanged by non-fluorescent buffer solution. Only fully functional valves still incorporated the fluorescent dye. This was the case for all tested inner radii except for the smallest test case under investigation ($20\ \mu\text{m}$). Nevertheless, manual alignment was not feasible in a reliable manner for inner radii smaller than $70\ \mu\text{m}$.

2.1.2 Preparation of the master molds

All master molds used in this work were fabricated by photolithography in a clean room facility. Photolithography is a microfabrication technique that enables to transfer geometric patterns of a photomask to a photoresist-covered substrate by the use of optical radiation. The overall workflow is depicted in Figure 16.

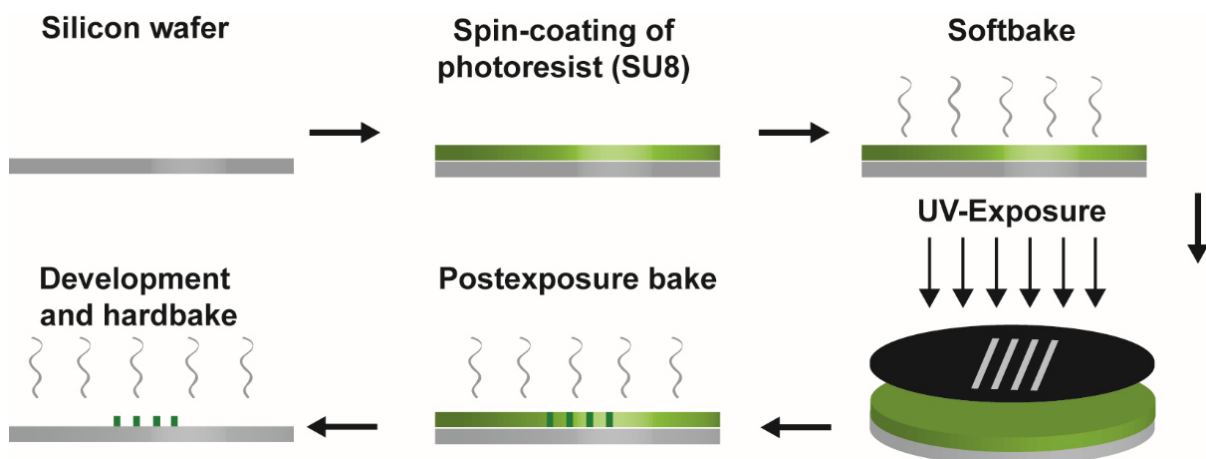


Figure 16: SU-8 processing protocol. Schematic drawing of the photolithographic master mold fabrication process. First, photoresist is spin-coated onto a $100\ \text{mm}$ silicon wafer. The subsequent soft-bake step is carried out to evaporate the solvent and to densify the coating. Next, the chip design is transferred from the photomask to the substrate by exposure to UV light. After a post-exposure bake to finalize the initiated polymerization, the photoresist is developed and hard-baked.

2 Methods

The master molds utilized in all projects were prepared according to the following protocol. The specified process parameters refer to the production criteria of the *E. coli* analysis device. The corresponding parameters of the other utilized devices are depicted in Table 2.

In a first step, a 100 mm silicon wafer was dehydrated at 200 °C for 10 min. After cooling down, the photoresist was spin coated onto it to a final height of 10 µm. The applied spinning protocol included three steps. The first two guaranteed an equal distribution of the resist on the wafer (100 rpm for 20 s, 500 rpm for 10 s) whereas the last one defined the resulting height (SU8-2010, 2500 rpm for 30 s). Next, the wafer was soft baked at 95 °C for 180 s and subsequently exposed to UV light (130 mJ/cm², measured at 365 nm) in a mask aligner (MA-6 mask aligner, Karl Süss, Germany) through a transparency photomask. After a post exposure bake (95 °C, 240 s), the photoresist was developed for 3 min (mr-DEV600 developer). Next, the wafer was cleaned with clean-room grade isopropanol and dried in a stream of nitrogen. The wafer was hard baked for 3 h at 200 °C, and the final heights of the SU-8 features were confirmed with a step profiler (Dektax XT advanced, Bruker). For silanization, the master form was stored overnight in a desiccator with 50 µL 1*H*,1*H*,2*H*,2*H*-perfluorodecyltrichlorosilane at a pressure of 100 mbar. After silanization, the completed master molds were stored in a dust-free environment until usage.

Table 2: *SU-8 processing parameters*

Project	<i>E. coli</i> Analysis	Yeast Analysis	Mother- Daughter-Cell Separation	Matrix Effects
<i>Channel height [µm]</i>	10	15	15	20
<i>Photoresist</i>	SU-8 2010	SU-8 2015	SU-8 2015	SU-8 2015
<i>Spin speed [rpm]</i>	2500	2750	2750	1750
<i>Soft bake time [s]</i>	180	210	210	240
<i>Exposure [mJ/cm²]</i>	130	130	130	150
<i>Post exposure bake time [s]</i>	240	270	270	300
<i>Develop time [s]</i>	180	210	210	240

2 Methods

2.1.3 Production of the final device

The projects of this thesis were realized using double-layer devices made from PDMS. Therefore, so-called soft lithography was applied. Soft lithographic processes are based on replica molding. Thereby, the non-cured precursor of an elastomer is casted from a master mold exhibiting the relief pattern of the target design. After curing of the polymer, the generated elastomer replica is removed from the corresponding master mold and is ready for use or for further processing. The basic workflow is illustrated in Figure 17.

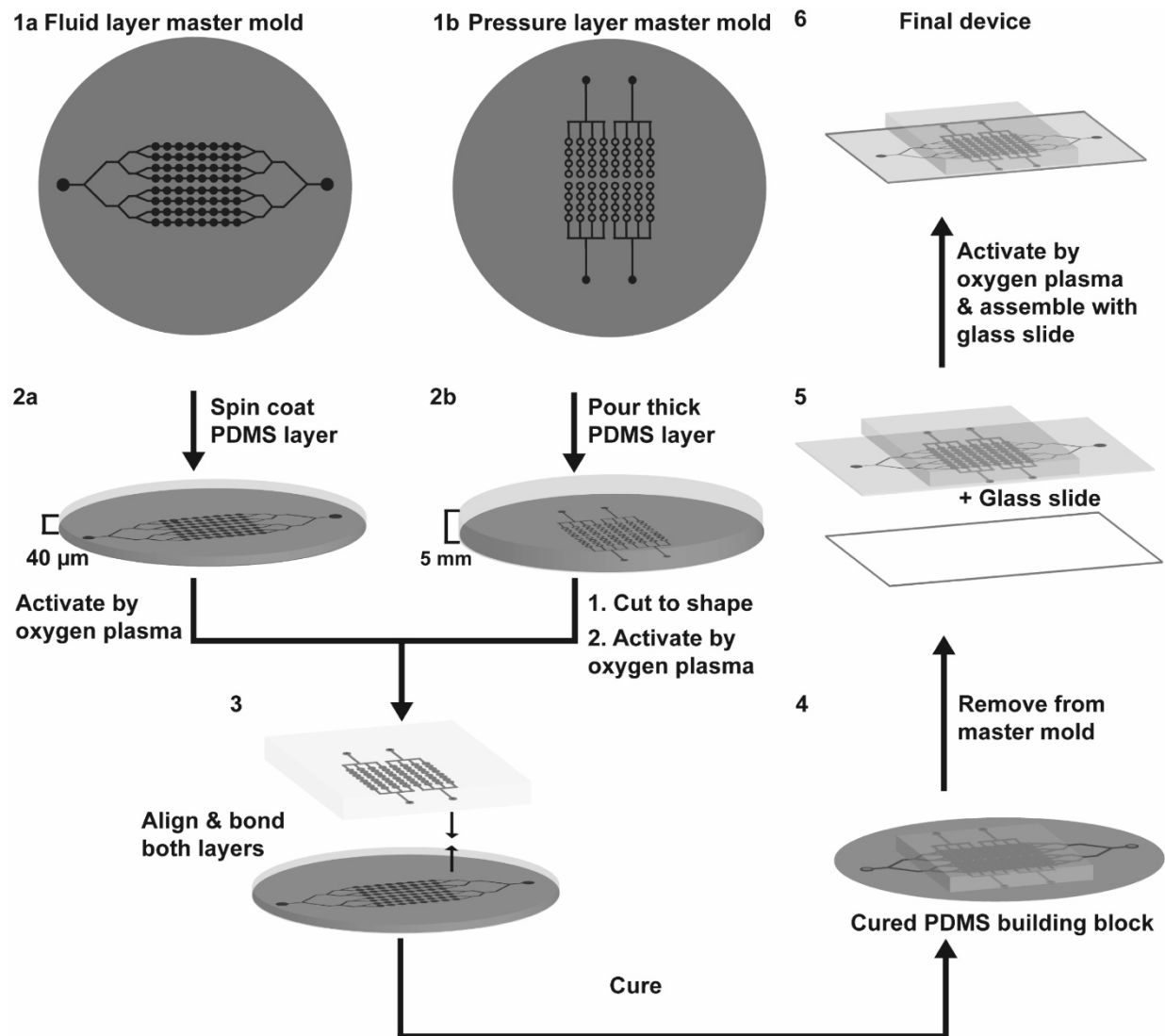


Figure 17: Fabrication of the final device by soft lithographic techniques. In a first step, a 10:1 mixture of PDMS oligomer and curing agent is prepared. The mixture is spin-coated onto the fluid layer master mold and poured onto the pressure layer master mold, respectively. After curing, the PDMS pressure layer is removed from the master mold and cut to shape. In addition, holes for the pressure connectors are generated by a biopsy puncher (1 mm diameter). Next, the PDMS coated fluid layer master mold and the processed pressure layer are activated by oxygen plasma and aligned under a microscope. After a further curing step, the assembled PDMS building block is removed from the wafer. Holes for the fluid inlet and outlet are generated by a biopsy puncher (1.5 mm diameter). The PDMS unit and a glass slide are activated by oxygen plasma, assembled and placed on a hot plate to finalize the bonding process. The completed device is stored in a dust-free environment until usage.

2 Methods

A detailed description of the applied fabrication steps is provided in the following protocol. In a first step, PDMS monomer and curing agent were mixed at a ratio of 10:1 and degassed at a pressure of 50 mbar for 20 min. For production of the pressure layer, a 5 mm thick layer of PDMS mixture was poured onto the corresponding master mold, once again degassed under the above mentioned conditions and subsequently cured at 80 °C for 3 h. For production of the fluid layer, the PDMS mixture was spin-coated on the corresponding master mold to the desired final height (Table 2) and cured at 80 °C for 1 h. Next, the elastomer replica of the pressure layer was removed from the master mold and cut to shape by a razor blade. Access holes for the pressure valve connectors were punched by a biopsy puncher (1 mm diameter). The tailored top part and the fluid layer were activated by oxygen plasma (0.75 mbar, 18 W, 45 s) and aligned under a microscope. PDMS was poured around the composed device to facilitate the later peel off process. The completed PDMS part was hardened at 80 °C for 1 h. Next, the composed PDMS part was cut to shape with scissors and fluid inlet- and outlet holes were generated by a biopsy puncher (1.5 mm diameter). To close the fluid channels, the PDMS part was bonded to a glass cover slide. Therefore, the glass slide and the PDMS part were activated by oxygen plasma (0.75 mbar, 18 W, 45 s), assembled and placed on a hot plate to complete the bonding process. The final device was stored in a dust-free environment until usage.

2 Methods

2.2 Operation of the device

Although the presented microfluidic devices vary in their design due to the different application requirements, they all share one basic characteristic. They all contain integrated pneumatic valves for precise spatio-temporal isolation of single cells. Consequently, proper valve operation was an essential precondition for the performance of all experiments. Key element thereby was a home-made pressure control system with nitrogen gas supply which was connected to the device by custom-made metal connectors and silicon tubing (Figure 18). Before the experiment the pressure lines of the top layer were loaded with PBS by centrifugation. For valve actuation, a pressure of 3 bar was applied ensuring complete microchamber closure under the operated flow-rates of 1-30 $\mu\text{L}/\text{min}$. To guarantee precise opening times in the range of milliseconds, the pressure valves were operated by a LabVIEW program.

All reagents and buffer solutions were introduced into the device by pumping. Therefore, the corresponding solutions were filled into plastic syringes connected to Teflon tubing and loaded into the device by the use of a syringe pump (NanoJet, CHEMYX, Stafford, USA). For all platforms stability tests were carried out. Thereby, device stability was confirmed for flow-rates of 1-30 $\mu\text{L}/\text{min}$. For cell capture experiments, flow rates greater or equal to 5 $\mu\text{L}/\text{min}$ were applied, as trapping efficiency was higher at high flow-rates.

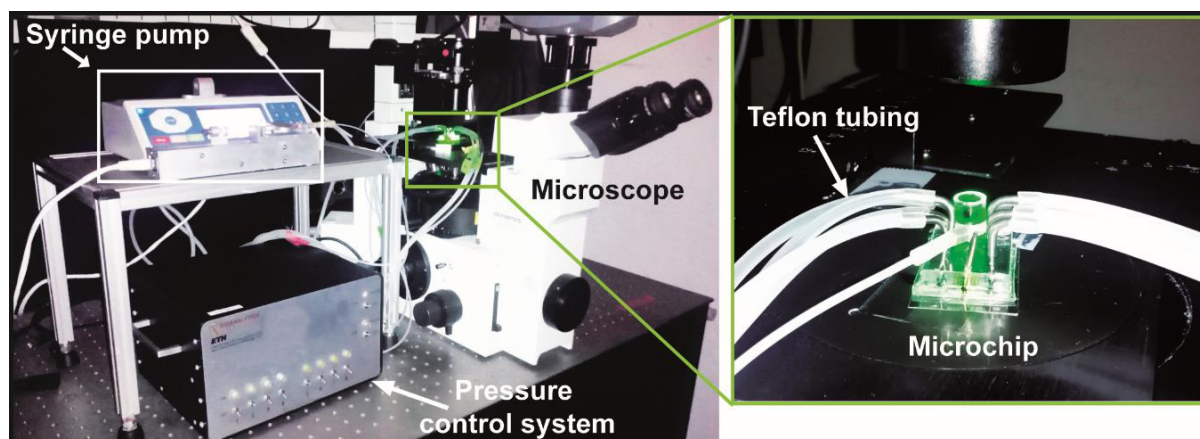


Figure 18: Photograph that depicts the standard experimental set-up. Left: The entire set-up including the pressure control system, the syringe pump and the microchip placed on the microscope. Right: Photograph of the microchip.

2 Methods

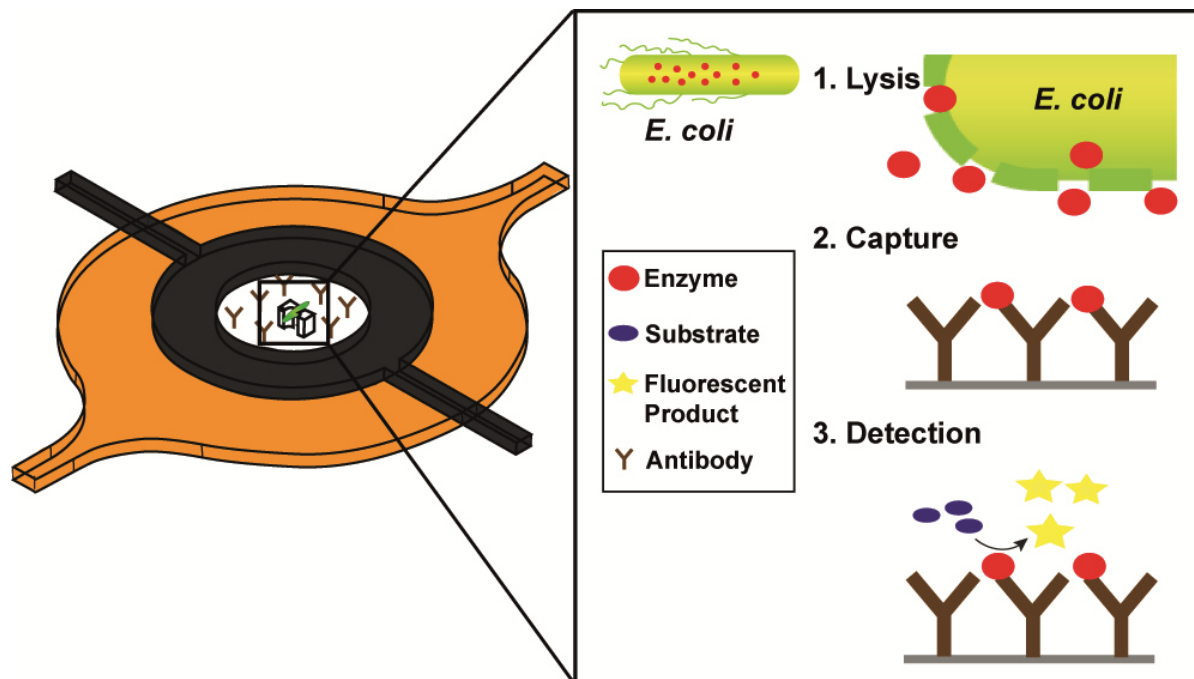
2.3 Cultivation of *E. coli*

For strain maintenance bacterial glycerol stocks were prepared. Therefore, 900 μL of an overnight LB culture of *E. coli* of the strain K-12 MG1655 and 900 μL of 50 % glycerol in distilled water were added to a 2 mL cryovial, gently mixed and stored at $-80\text{ }^{\circ}\text{C}$. For short-term maintenance and use, *E. coli* were streaked out on dry LB agar plates and incubated at $37\text{ }^{\circ}\text{C}$ for 24 h. The culture plates were sealed with parafilm and stored at $4\text{ }^{\circ}\text{C}$ for a maximum of 4 weeks. For preculture preparation a 15 mL falcon tube containing 3 mL of LB Broth (Lennox with additional 20 mM glucose) was inoculated with a single *E. coli* colony of the previously prepared LB agar plates. The following incubation was performed at $37\text{ }^{\circ}\text{C}$ with constant shaking at 220 rpm until an OD600 of approximately 1 was reached. The preculture was inoculated into a 15 mL falcon tube containing 3 mL M9 minimal medium at a dilution of 1 to 200. Depending on the later on performed experiment, the culture medium was completed either with 20 mM glucose or 20 mM lactose in case induction of β -galactosidase expression was required. Subsequent cell sample preparation steps were performed according to the requirements of the specific experiment.

2.4 Cultivation of *S. cerevisiae*

For long-term maintenance, glycerol stocks were prepared. Therefore, 900 μL of an overnight YPD culture of *S. cerevisiae* of the strain YSBN6 and 900 μL of 30 % glycerol in distilled water were added to a 2 mL cryovial, gently mixed and stored at $-80\text{ }^{\circ}\text{C}$. For short-term maintenance and use, *S. cerevisiae* were streaked out on dry YPD agar plates and incubated at $30\text{ }^{\circ}\text{C}$ for 36 h. The culture plates were sealed with parafilm and stored at $4\text{ }^{\circ}\text{C}$ for a maximum of 4 weeks. For preculture preparation, a 15 mL falcon tube containing 3 mL YPD (1 % yeast extract, 2 % bacteriological peptone, 2 % D-glucose) was inoculated with a single *S. cerevisiae* colony of the YPD agar plate. The subsequent incubation was carried out at $30\text{ }^{\circ}\text{C}$ with shaking at 200 rpm (KS 4000 i control, IKA, Staufen, Germany) until late log-phase growth was reached. Next, the preculture was inoculated in a 15 mL falcon tube containing 3 mL YPD medium at a dilution of 1 to 100. The following incubation was performed at $30\text{ }^{\circ}\text{C}$ with shaking at 200 rpm until early log-phase growth was reached. Subsequent cell sample preparation steps were performed according to the requirements of the specific experiment.

3 On-chip enzyme quantification of single *Escherichia coli* bacteria by immunoassay-based analysis



The content of this chapter is adapted with permission from the following research article: On-Chip Enzyme Quantification of Single *Escherichia coli* Bacteria by Immunoassay-based Analysis, Simone Stratz, Klaus Eyer, Felix Kurth, and Petra S. Dittrich, *Analytical Chemistry* 86 (2014), 12375-12381.

DOI: 10.1021/ac503766d.

Copyright (2015) American Chemical Society.

Modifications made to the original publication

The figure numbering, the table numbering, and the reference numbering were changed. In addition, the supporting information was integrated into the text of the main publication. Therefore, a few connecting sentences, which were not included in the original publication, were added to simplify the reading flow. For a larger view, the size and the position of some figures were changed.

Contributions of the individual authors

Simone Stratz: Designed the research, planned and performed all experiments, analyzed the data, and wrote the publication.

Klaus Eyer: Provided advice on the development of the assay protocol and on the purchase of the assay reagents. In addition, he proofread the publication.

Felix Kurth: Provided advice on the *E. coli* cultivation and on the performance of the bacteria experiments. In addition, he proofread the publication.

Petra Dittrich: Designed the research and wrote the publication.

3.1 Abstract

Individual bacteria of an isogenic population can differ significantly in their phenotypic characteristics. This cellular heterogeneity is thought to increase the adaptivity to environmental changes on a population level. Analytical methods for single-bacteria analyses are essential to reveal the different factors that may contribute to this cellular heterogeneity, among them the stochastic gene expression, cell cycle stages and cell ageing. Although promising concepts for the analysis of single mammalian cells based on microsystems technology were recently developed, platforms suitable for proteomic analyses of microbial cells are by far more challenging. Here, we present a microfluidic device optimized for the analysis of single *Escherichia coli* bacteria. Individual bacteria are captured in a trap and isolated in a volume of only 155 pL. In combination with an immunoassay-based analysis of the cell lysate, the platform allowed the selective and sensitive analysis of intracellular enzymes. The limit of detection of the developed protocol was found to be 200 enzymes. Using this platform, we could investigate the levels of β -galactosidase in cells grown under different nutrient conditions. We successfully determined the enzyme copy numbers in cells cultured in defined medium (3517 ± 1579) and in complex medium (4710 ± 2643), and verified the down-regulation of expression in medium that contained only glucose as carbon source. The strong variations we found for individual bacteria confirm the phenotype heterogeneity. The capability to quantify proteins and other molecules in single bacterial lysates is encouraging to use the new analysis platform in future proteomics studies of isogenic bacteria populations.

3.2 Introduction

In recent years, numerous single-cell proteomic studies revealed the occurrence of phenotypic heterogeneity within populations of the same cell type (189-192). Significant cell-to-cell differences were found for the concentration of various metabolites (193), second messengers (194), proteins (195-197) and co-factors (62, 65). The stochastic nature of gene transcription and translation processes is considered to be essential for cellular adaptation and evolution, and plays an important role for the fitness of a cell population (187, 198, 199). Moreover, strong genotypic diversity within a population is associated with the emergence of various diseases like cancer (200-203). Therefore, investigation of the underlying mechanisms controlling the noise level in gene expression is of high pharmacological and biological interest.

Microbial cells such as *Escherichia coli* are of particular interest for studies of cell heterogeneity, as they have short doubling times of approximately 20 min. Hence, the adaptation to an environmental change, e.g., supplied stress factors or altered growth conditions, can be conveniently monitored over several populations within a reasonable time. One well-investigated example in this context is the emergence of antibiotic-resistant cells. Here, the study of the mechanisms is important to develop new or improve current antibiotics (204-207).

3 On-chip enzyme quantification of single *Escherichia coli*

Heterogeneity studies require measurement methods and systems that enable analysis on the single-cell level. Microfluidic platforms are particularly suitable for this purpose, as they allow precise manipulation of fluid volumes in the pico- and nanoliter range and facilitate accurate transport and positioning of cells. Due to these advantages, various microfluidic platforms optimized for single-cell measurements were developed in the past few years. Several studies reported the successful analysis of DNA and RNA by the use of polymerase chain reaction (PCR) (208-210). The enzymatic nucleic acid amplification guarantees high selectivity and sensitivity whereby the two main challenges of single-cell analyte detection (low analyte copy numbers and great variety of different but structural-resembling biomolecules) are overcome. Nevertheless, PCR is only applicable to DNA and RNA. The analysis of other cellular biomolecules requires very sensitive detection methods or amplification techniques which are accessible to a broader scope of analytes, for example, immunoassay-based methods.

Previously, we reported a microfluidic platform suitable for single-cell stimulation and subsequent analysis of proteins and secondary messengers produced by single mammalian cells (62). Furthermore, we implemented the concept of enzyme-linked immunosorbent assays (ELISA) on this chip design (70). The used high affinity capture and detection antibodies provided a great selectivity while the enzymatic conversion of a substrate to a fluorescent product generated efficient signal amplification. We successfully quantified the housekeeping protein GAPDH in U937 cells and HEK293 cells, as well as the secondary messenger cAMP in MLT cells.

The above-mentioned studies demonstrate the great potential of microsystem technology for single-cell analysis but are nevertheless only accessible to mammalian cells. Systems suitable for the investigation of significantly smaller microorganisms are still rarely found because the capture and the analysis are more challenging due to their smaller size (72, 211, 212). This reduction in intracellular volume results in a drastically lower analyte number in bacteria ranging from a few hundred to thousand per protein compared to mammalian cells, in which analyte numbers are increased by a hundred-fold (213, 214). To meet the demands of low copy number analyte detection in single bacteria, we developed our recent concept of capturing and isolating single cells in tiny chambers significantly further. This required substantial downscaling of the existing device for mammalian cells and improvement of the assay sensitivity.

3 On-chip enzyme quantification of single Escherichia coli

The here-introduced microfluidic platform is adapted to the specific requirements of single *E. coli* bacteria analysis. We initially reduced the size of all features that are needed for spatial capture and isolation of single bacteria (Figure 19).

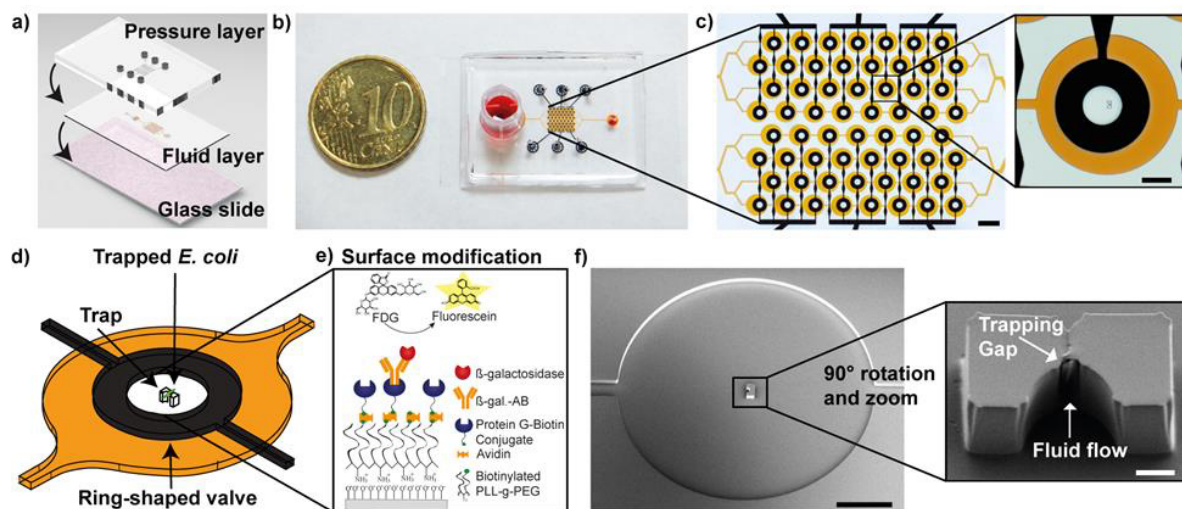


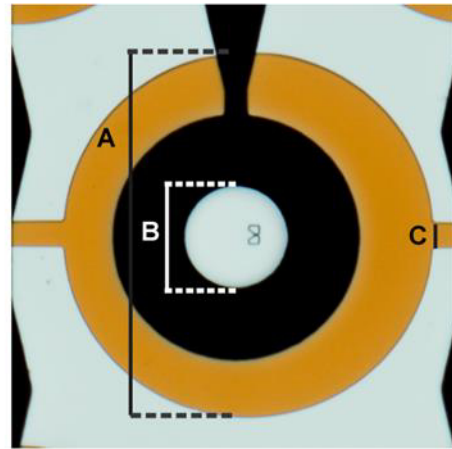
Figure 19: Design and operation of the microfluidic platform. a) The schematic drawing depicts the different layers required for the microfluidic platform. The pressure layer (PDMS) is bonded onto the fluid layer (PDMS), and this assembly is finally bonded onto a glass slide. b) Photograph of the entire device. c) Micrographs of the chamber array (scale bar 450 μm) and one chamber (scale bar 100 μm). For visualization, the fluid channels are filled with orange food dye, the control layer is filled with black ink and the closed microchambers are filled with a colorless buffer solution. d) Schematic drawing of a single microchamber. Fluid flow is used to capture a single bacterium in the cell trap (gap size 1 μm). The ring shaped valve allows spatial isolation of the bacterium from the surrounding medium. e) Schematic drawing of the immunoassay for the detection of β -galactosidase. β -Galactosidase binding antibodies are immobilized on the surface via avidin linkers and PLL-g-PEG biotin. After surface modification, single *E. coli* bacteria expressing β -galactosidase are trapped, isolated and finally lysed. After lysis, the formerly intracellular enzyme binds to the immobilized antibodies. After a washing step, the amount of bound enzyme is detected by adding the β -galactosidase substrate FDG that is converted into galactose and highly fluorescent fluorescein. f) Scanning electron micrographs of a cell trap made of PDMS (Scale bars, left: 100 μm , right: 2 μm).

Cell traps with an extremely small gap size of around 1 μm allowed mechanical trapping of individual *E. coli* in the center of each microchamber (Figure 19d and 19f). Due to the microchamber volume reduction from formerly 625 pL (70) to only 155 pL (Figure 19c and Table 3), much higher analyte concentrations are achieved with the same amount of analyte released from the cells. Therefore, it was possible to quantify low copy number analytes that occur at levels of a few hundred molecules per bacterium. To demonstrate the operational capability of the device, an immunoassay for the detection of the enzyme β -galactosidase in single *E. coli* bacteria was performed. β -Galactosidase was chosen as the target analyte as its expression in *E. coli* is regulated by the thoroughly investigated lac operon (215, 216), which is turned on and off depending on the available carbon source in the culture medium. In an actual experiment, the influence of the carbon source on the β -galactosidase expression was investigated by analyzing bacteria samples cultured with either glucose or lactose. The enzyme levels obtained from our on-chip studies could be validated by literature values of comprehensive bulk measurements as well as single-cell measurements (217-219).

3 On-chip enzyme quantification of single Escherichia coli

Table 3: **Size parameters of the microfluidic device.** Comparison of the size parameters of the new microfluidic device for single bacteria analysis and the formerly used microfluidic device for single mammalian cell analysis.

Parameter	Old Design	New Design
Channel height	20 μm	10 μm
Chamber dia. [A]	600 μm	460 μm
Chamber dia. [B]	200 μm	140 μm
Channel width [C]	40 μm	30 μm
Chamber volume	625 μL	155 μL
Trap gap size	5 μm	1 μm



3.3 Materials and Methods

3.3.1 Materials

Silicon wafers were obtained from Si-Mat (Kaufering, Germany). Photoresist SU-8 2010 was obtained from Microchem (Newton, MA, USA). 1H,1H,2H,2H-perfluorodecyltrichlorosilane was supplied by ABCR (Karlsruhe, Germany). Sylgard® 184 silicone elastomer kit was purchased from Dow Corning (Midland, MI, USA). Lactose monohydrate and D-(+)-glucose were obtained from Thermo Fisher Scientific (Geel, Belgium). LB agar powder, LB broth (Lennox) powder microbial growth medium, disodium hydrogen phosphate heptahydrate, magnesium sulphate heptahydrate, calcium dichloride dihydrate, potassium dihydrogen phosphate, protein G-biotin conjugate, ethylenedinitrilotetraacetic acid disodium salt dihydrate (EDTA), lysozyme from chicken egg white and fluorescein di- β -D-galactopyranoside (FDG) were supplied by Sigma-Aldrich (Buchs, Switzerland). Phosphate buffered saline (PBS) and 1,1'-dioctadecyl-3,3,3'-tetramethylindocarbocyanine perchlorate (DiI) were purchased from Life Technologies Europe (Zug, Switzerland). Biotin-derivatized poly(l-lysine)-grafted poly(ethylene glycol) (PLL-g-PEG-biotin) and poly(l-lysine)-grafted poly(ethylene glycol) (PLL-g-PEG) were obtained from SuSoS AG (Dübendorf, Switzerland). Avidin was obtained from AppliChem (Gatersleben, Germany). Monoclonal anti- β -galactosidase antibody (mAB) was supplied by Santa Cruz Biotechnology (Dallas, TX, USA). Tris(hydroxymethyl)aminomethane hydrochloride (TRIS-HCl) was purchased from Bio-Rad (Richmond, CA, USA).

3 On-chip enzyme quantification of single Escherichia coli

3.3.2 Master mold and device fabrication

Briefly, the device is composed of two layers hereinafter referred to as fluid layer and control layer, both made of PDMS. The fluid and control layer were separately fabricated by casting PDMS from the corresponding master forms. Alignment, assembly, and bonding of both layers resulted in the final PDMS device, which was afterwards bonded to a glass slide to close the fluid channels. Due to the smaller design of the features, a chrome-glass mask (Compugraphics Jena GmbH, Jena, Germany) was used instead of a film mask for the photolithography process. The fabrication principle was reported previously (62, 70, 220). The following protocol describes in detail the adaptations that have been made to the fabrication protocols of the precursor devices.

For preparation of the master molds the photoresist SU-8 2010 was spin coated on two silicon wafers to a final height of 10 μm at 2500 rpm for 30 seconds, soft baked at 95 °C for 240 seconds and exposed with UV light (130 mJ/cm²) in a MA 6 mask aligner (Süss MicroTec, Germany) through a transparency photomask (Micro Lithography Services, UK). After a post exposure bake, the photoresist was developed for 3 minutes (mr-DEV600 developer). The wafers were hard baked for 3 hours at 200 °C and the heights were confirmed with a step profiler (Dektax XT advanced, Bruker). For silanization the wafers were stored overnight in a desiccator with 50 μL of 1*H*,1*H*,2*H*,2*H*-perfluorodecyltrichlorosilane (ABCR, Karlsruhe, Germany) under low atmospheric pressure (100 mbar).

For fabrication of the fluid layer, PDMS monomer and curing agent (Sylgard® 184 silicone elastomer kit, Dow Corning) were mixed at a ratio of 10:1, degassed under low atmospheric pressure (50 mbar) for 20 minutes, spin coated on the corresponding master mold at 2600 rpm (Spin Coater WS-400-6NPP/LITE, Laurell technologies Corporation, North Wales) for 60 seconds to build a 30 μm high PDMS coating and then stored for 1 hour at 80 °C for curing. To build the control layer, a 5 mm thick layer of PDMS and curing agent (10:1 mixture) was poured on the corresponding master mold and stored for 3 hours at 80 °C for curing. Afterwards, the control layer was cut to shape and holes for the pressure valves were generated with a biopsy puncher (1mm diameter, Miltex, York, PA). For assembling, both layers were activated by oxygen plasma (0.75 mbar, 18 W, custom-made plasma cleaner) for 60 seconds and aligned under a microscope (Multizoom AZ100 M, Nikon Corporation, Japan). The bonding process of the two layers was completed by a 1 hour curing-step at 80 °C. After the assembled PDMS chip was removed from the master mold, access holes for the fluid inlet and outlet were punched using a biopsy puncher (1.5 mm diameter, Miltex, York, PA). The completed PDMS part and a glass cover slip (Menzel Gläser # 1, Germany) were activated by oxygen plasma (0.75 mbar, 18 W, Harrick Plasma Cleaner PDC-32G) for 45 seconds, assembled and placed on a hot plate at 50 °C for 5 minutes to finalize the bonding process.

Immediately afterwards, a 1:1 mixture of PLL-g-PEG-biotin/PLL-g-PEG (0.05 % (w/v) in PBS) was centrifuged into the device (800g, 5 min). This part of the surface modification protocol is time-critical, as PLL-g-PEG-biotin can only bind to the plasma-activated surface. This activation remains for about 10 minutes to guarantee consistent PLL-g-PEG-biotin binding.

3 On-chip enzyme quantification of single *Escherichia coli*

3.3.3 Surface modification

Directly after bonding, a 1:1 mixture of PLL-g-PEG-biotin/PLL-g-PEG (0.05 % (w/v) in PBS) was centrifuged into the device (800g, 5 min) to generate avidin binding sites on the surface. After 1 h of incubation time, the device was flushed with PBS (10 μ L/min, 5 min) and the remaining reagent solutions (Table 4) were loaded into the device by using a syringe pump (NanoJet, CHEMYX, Stafford, USA). Every reagent immobilization step was completed by a 5 min flow-free reagent incubation time and a 5 min washing step (PBS). For reagent immobilization steps, a flow-rate of 5 μ L/min was used; for washing steps, the flow-rate was set at 10 μ L/min (Table 4).

Table 4: Surface modification protocol.

Reagent	Concentration [%, w/v]	Time [min]	Flow rate [μ L/min]	Flow-free incubation time [min]
PLL-g-PEG/PLL-g-PEG biotin	0.05	10	5	5
PBS	-	5	10	-
Avidin	0.05	10	5	5
PBS	-	5	10	-
Protein G, biotin	0.0025	10	5	5
PBS	-	5	10	-
Anti- β -gal. antibody	0.0005	10	5	5
PBS	-	5	10	-

3.3.4 Bacteria cultivation and Dil-staining

LB agar and LB broth were prepared according to the suppliers specifications. *E.coli* MG1655 (containing the lac operon) were streaked out on LB agar plates, incubated at 37 °C for 24 h, and then stored at 4 °C until usage. For analysis of bacteria samples cultured in complex medium, a preculture was prepared by inoculating 3 mL LB medium completed with 20 mM lactose with a single *E. coli* colony of the LB agar plate. Subsequent incubation was carried out in a 15 mL falcon tube at 37 °C with constant shaking at 220 rpm (KS 4000 i control, IKA, Staufen, Germany) until the optical density measured at 600 nm (OD600) was approximately 1. For analysis of bacteria samples cultured in defined medium, 3 mL M9 minimal medium completed with 20 mM lactose was inoculated with a preculture grown in complex medium (OD600 of 1) at a dilution of 1 to 200. Subsequent incubation was carried out at 37 °C with constant shaking at 220 rpm until the OD600 was approximately 1. For fluorescent staining of the bacterial membrane, Dil (stock concentration 100 μ M in methanol) was added to the *E. coli* culture to a final concentration of 650 nM and incubated for 5 min at 37 °C while shaking. Afterwards, the bacteria sample was washed twice with PBS by centrifugation (MiniSpin plus, Eppendorf, 14100g, 4 min) to remove nonincorporated dye. Before introduction into the device, the sample was diluted 1:1000 with PBS and filtered (Partec CellTrics® 10 μ m, LabForce AG, Switzerland) to remove larger particles that could block microfluidic channels and cell traps.

3 On-chip enzyme quantification of single *Escherichia coli*

3.3.5 Immunoassay for β -Galactosidase

The microfluidic device was placed on an inverted microscope (Olympus IX70) and loaded with the previously Dil-stained *E. coli* sample using a syringe pump (NanoJet, CHEMYX, Stafford, USA) at a flow rate of 5 $\mu\text{L}/\text{min}$ for 5 min. Single *E. coli* bacteria were trapped inside the hurdles, and isolated by closing the microchambers after sufficient bacterial cells were trapped. To ensure the analysis of single cell lysates, fluorescence images were taken of every microchamber (Figure 20) using an EMCCD camera (iXon Ultra, Andor Technologies, Ireland) in combination with a 60X water immersion objective and the internal zoom of the microscope (1.5X).

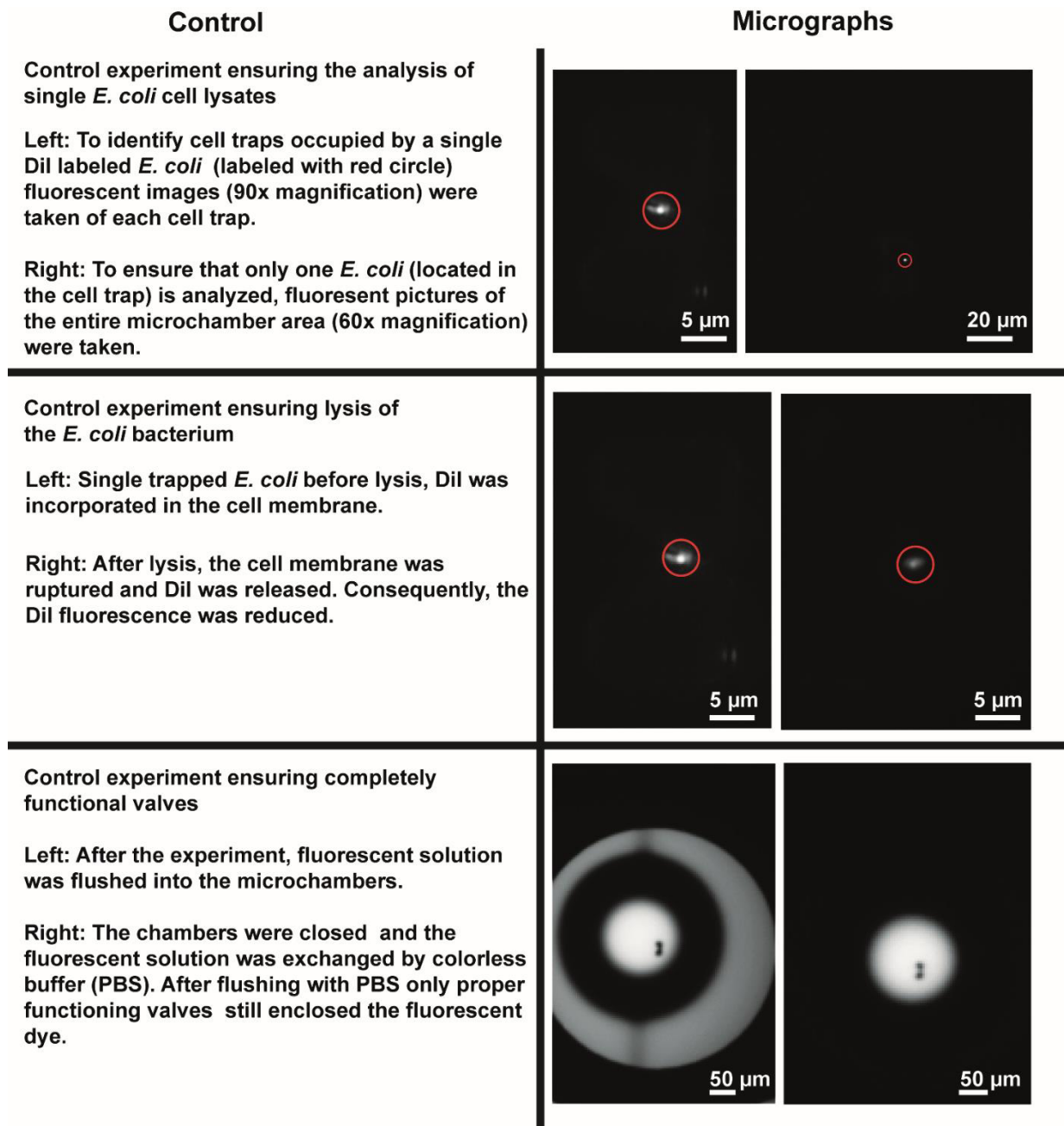


Figure 20: **Control experiments on cell lysis and valve integrity.** Control experiments, which were performed on each microfluidic device. Left column: Explanations. Right column: Example micrographs from an actual experiment.

3 On-chip enzyme quantification of single *Escherichia coli*

The Dil fluorescence was detected by the use of a metal halid lamp (X-Cite 120 PC, Olympus) and an appropriate filter set (excitation: 546/12 and emission: 607/80, AHF Tübingen, Germany). Images were taken at 200 ms exposure time. Afterwards, lysis buffer (10 mM Tris-HCl completed with 1 mM EDTA, 0.1 mM NaCl and 10 mg/mL lysozyme, pH 8.0) was supplied to the microfluidic chip while the chambers were kept closed. To introduce the lysis buffer to the trapped cells, the chambers were quickly opened (700 ms opening time), thereby exchanging the cell-surrounding fluid. The lysis buffer was incubated for 30 min and at same time the analytes were allowed to bind to the functionalized surface. After a subsequent 10 min washing step of the device with PBS (flow rate of 5 μ L/min, closed microchambers), the freshly prepared substrate solution (250 nM fluorescein di- β -D-galactopyranoside (FDG) in PBS, 5 μ L/min) was introduced into the device and subsequently to the microchambers (700 ms opening time, 5 s delay time between opening different chambers). Data acquisition was started immediately after substrate addition. Fluorescent images were taken every 30 min of every microchamber for a period of 3 h (4X objective, exposure time 300 ms, gain X100, excitation filter: 470/40, and emission filter: 525/50). For the calibration curve, the immunoassay was performed with known β -galactosidase concentrations instead of bacteria (Figure 25). To prevent accumulation of the enzyme on the surface, the chambers were closed during introduction of the enzyme solution, and only quickly opened (700 ms opening time) to guarantee precise enzyme concentrations inside the chambers. The subsequent assay performance and data acquisition was carried out under identical conditions, as in case of an experiment with *E. coli* bacteria. To investigate if the chamber position within the image area influences the detected fluorescence signal, each β -galactosidase concentration was immobilized in multiple chambers of the same device.

In addition, the assay was performed for each β -galactosidase concentration on two different devices to test for chip-to-chip variations. As no significant deviations in the detected fluorescence signals were observed, a significant influence of the chamber position or the device on the measurement can be excluded.

3 On-chip enzyme quantification of single Escherichia coli

3.3.6 Data analysis

The acquired fluorescence images were analyzed using the image processing software ImageJ (221). The fluorescence intensity over the whole chamber area was measured (I_{chamber}). To compensate for minor intensity deviations of the fluorescent signal within the image and potential chip-to-chip variations, a circular area of the same pixel size in the microstructure-free PDMS region directly above the microchamber of interest was analyzed (I_{outside} , Figure 21). The obtained fluorescence intensity value was subtracted from the measuring value of the inner microchamber as shown in Equation 6.

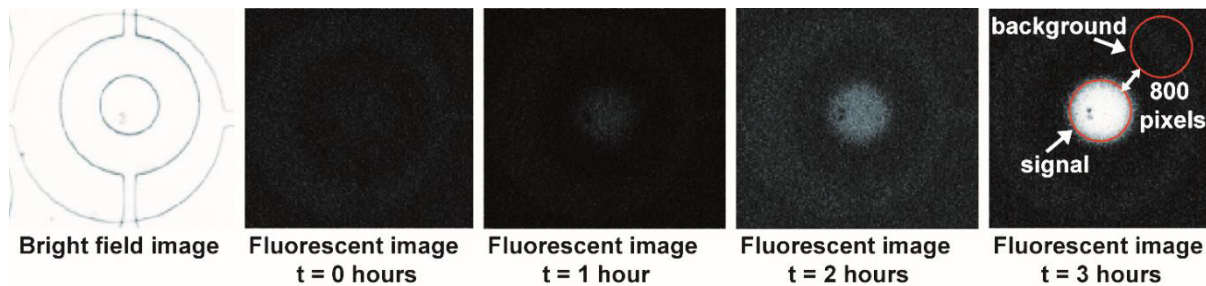


Figure 21: Raw data and analysis principle. Bright field and fluorescent images of the same microchamber containing the lysate of a single *E. coli* bacterium. The starting time ($t = 0$ hours) is specified as the point in time when the substrate FDG is introduced to the microchamber. The fluorescent signal within the microchamber increases over time since the amount of fluorescent product of the enzymatic reaction increases. For background correction an image section directly next to the closed microchamber of identical pixel size is subtracted from the detected fluorescent data within the microchamber.

Equation 6: Correction of the fluorescence intensity values.

$$I_{\text{corr}} = I_{\text{chamber}} - I_{\text{outside}}$$

In case the immunoassay was performed in the absence of the analyte β -galactosidase (i.e., empty, bacteria-free chambers), there was still a slight background fluorescence signal detectable due to the small amount of substrate molecules that self-hydrolyze in aqueous medium (I_{bg}). To account for the self-hydrolysis, the fluorescence intensity values obtained from a control experiment performed without the analyte β -galactosidase (Figure 22) were subtracted from the measuring values of the inner microchamber as shown in Equation 7.

Equation 7: Background correction.

$$I_{\text{bgcorr}} = I_{\text{corr}} - I_{\text{bg}}$$

The corrected fluorescence values (I_{bgcorr}) were plotted as a function of time. Due to the rate limitation of the enzyme, substrate conversion is considered to be maximal in the beginning, and the resulting fluorescence over time plot exhibits therefore linear behavior. The slope was determined by linear fitting. Only data of microchambers occupied by a single bacterium and equipped with completely operational sealing valves were used. Microchambers meeting these requirements were identified by functional checks (Figure 20). A data set was only used if the correlation coefficient (R^2) of the linear fit was ≥ 0.95 .

3 On-chip enzyme quantification of single Escherichia coli

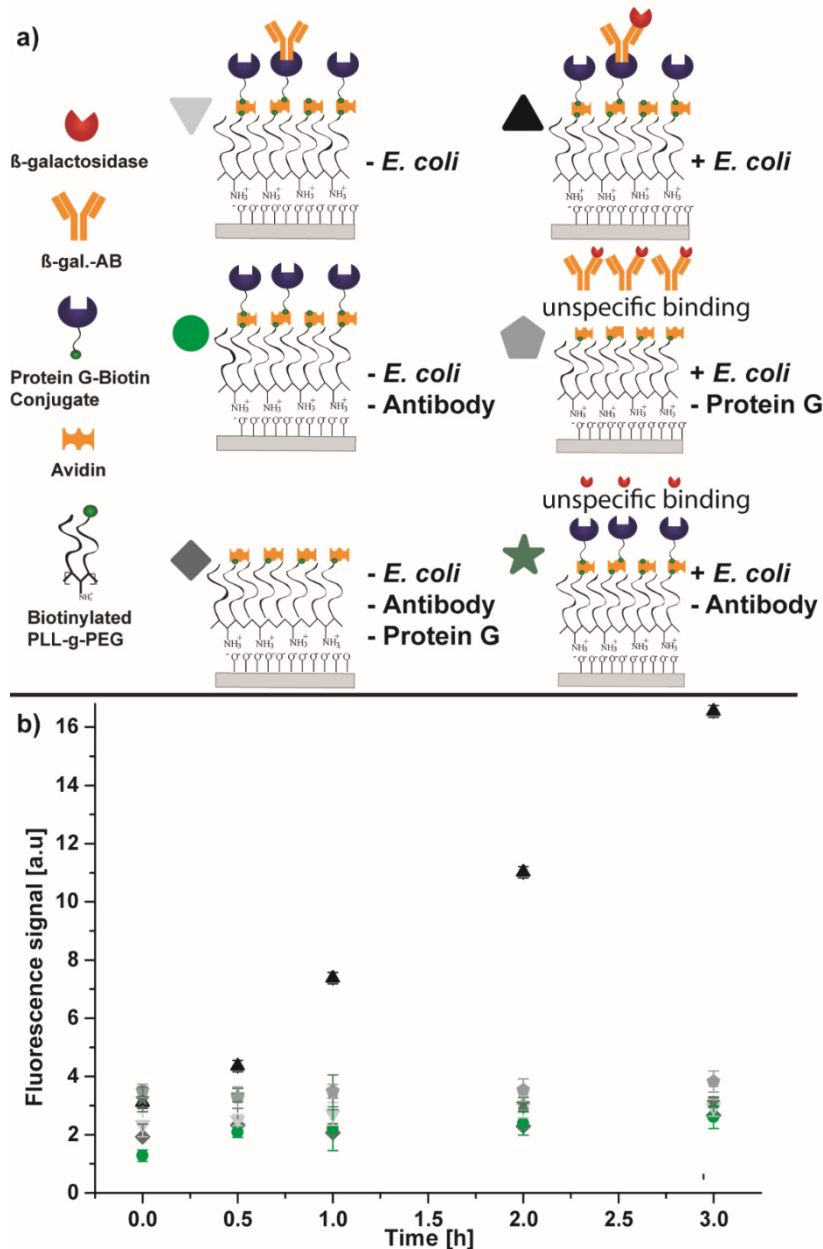


Figure 22: Influence of the surface modification on the measurement signal. Control experiments to investigate the influence of the surface modification on the background signal in terms of unspecific binding and basic background variations originating from the surface modification itself. a) Left: Caption of the schematic drawing. Right: Schematic drawings of the six different test cases under investigation. b) Fluorescent signal curves from the actual experiments after introduction of FDG. Data taken from a regular experiment with microchambers enclosing the lysate of a single bacterium (▲) is compared to control experiments each lacking one or more essential building blocks of the complete surface modification and *E. coli* lysate, respectively. To test for unspecific binding of the analyte β-galactosidase (★, no AB) or the antibody (●, no protein G) to the surface, the device was flushed with *E. coli* lysate before the substrate FDG was added. To evaluate the influence of further incomplete surface modification configurations, no *E. coli* lysate was flushed into the device before the substrate FDG was introduced (▽, ●, ◆). Thereby it was tested if the surface modification itself had an influence on the background signal change over time any influence of potential surface modifications can be excluded as well as significant unspecific binding. The low measured fluorescence signal in the absence of *E. coli* bacteria is mainly caused by self-hydrolysis of the substrate FDG.

3 On-chip enzyme quantification of single Escherichia coli

3.4 Results and discussion

3.4.1 Chip design

The microfluidic platform meets the specific requirements of bacteria capture and analysis (Figure 19 and Table 3, for size parameters). The device provides 60 analysis microchambers in total, which are arranged in 8 rows of alternating 7 or 8 chambers per row connected by microchannels (channel height of 10 μm) (Figure 19c). A key feature of the analysis microchambers is the centrally placed micrometer sized structure for the hydrodynamic trapping of a single bacterium (Figure 19d and 19f). To enable trapping of a single *E. coli* bacterium with a longitudinal diameter of around 1 μm , the distance of the two PDMS piles, which act as mechanical cell catch, was downscaled to only 1 μm (Figure 19f). The microchambers can be tightly sealed by a round-shaped valve, thereby isolating a volume of only 155 pL. In principle, we could design the microchip so that every valve is separately addressable. To reduce the numbers of connections for actuating the valves, we here combined subsets of three valves per row. To prevent that β -galactosidase molecules immobilized in upstream microchambers contaminate the subsequent microchambers, the valves were opened time-delayed during FDG introduction (Figure 23).

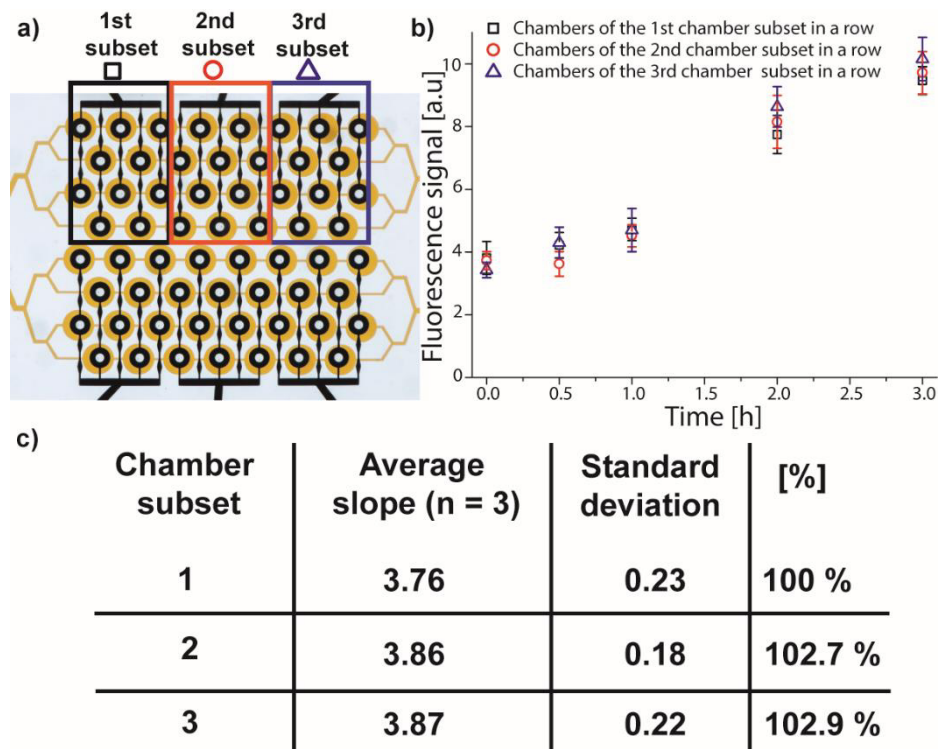


Figure 23: **Control experiment related to analyte cross contamination.** The ring-shaped valves are actuated in subsets to decrease the number of control lines. b) Control experiments were performed to investigate if β -galactosidase molecules immobilized in upstream microchambers contaminate the subsequent microchambers, when the valves are opened to introduce the substrate FDG. In these experiments the same β -galactosidase concentration of 1000 enzyme copies per microchamber was immobilized on the entire microfluidic device. Afterwards the immunoassay was performed as in an actual experiment with *E. coli* bacteria. The substrate FDG was introduced by opening the three individually controllable chamber subsets consecutively with a time delay of 5 seconds, and the fluorescence signals were recorded. c) Determination of the slope revealed no significant deviations for chambers of different subsets. In addition, chambers of the same subset had a low standard deviation, demonstrating the high precision of the results.

3 On-chip enzyme quantification of single Escherichia coli

Reduction of the microchamber volume from formerly 625 pL (70) to only 155 pL (Figure 19c) allowed to achieve much higher analyte concentrations with the same amount of released enzyme. This fact improved the limit of quantification of the directly measured analyte fluorescein by the factor of 2.5 (Figure 24) because less product needs to be converted to achieve a threshold concentration. As illustrated by the calibration curve (Figure 25a), we reliably quantified enzyme copies down to a limit of quantification of 400 enzymes per microchamber (concentration: ~ 4 pM). Distinguishing the β -galactosidase induced signal from the background signal was possible until the enzyme number was below 200 copies per microchamber, i.e., per bacteria, in the later measurements.

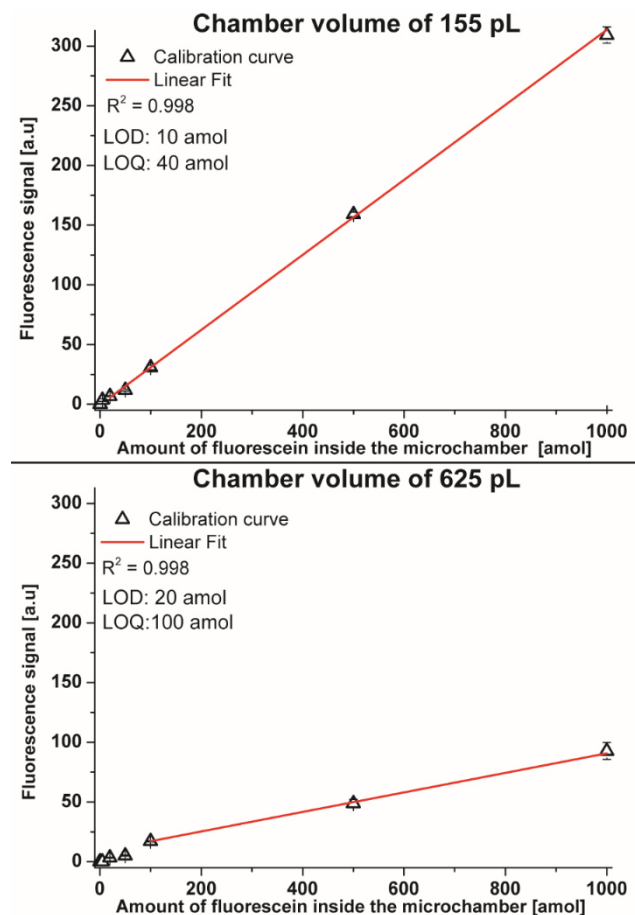


Figure 24: Influence of the microchamber volume on detection and quantification. To investigate the influence of the chamber volume on the limit of detection of the performed immunoassay, different amounts of fluorescein (fluorescent product of the hydrolysis of FDG by β -galactosidase, and therefore the directly detected analyte) were flushed into the new device with a small chamber volume (upper graph, 155 pL) and into the previously used device with a larger chamber volume (lower graph, 625 pL). The microscope settings were exactly the same as for the β -galactosidase immunoassay (4x objective, exposure time 300 ms, gain x100, excitation at 470 ± 20 nm and emission at 525 ± 25 nm). Due to the significantly smaller chamber volume, the same absolute amount of analyte (fluorescein in attomole) per chamber resulted in higher concentrations in the 155 pL microchambers compared to the 625 pL microchambers. This chamber volume reduction improved the limit of quantification by the factor of 2.5 (see diagram above). In case of the 625 pL microchambers, only the measurement values of the three highest analyte amounts could be used for the linear fit, as a linear correlation between fluorescent signal and fluorescein amount no longer existed for the lower analyte amounts. LOD: Limit of detection; LOQ: Limit of quantification.

3.4.2 Detection assay and increase of sensitivity

Our target analyte was the enzyme β -galactosidase that catalyzes the hydrolysis of fluorescein di- β -D galactopyranoside (FDG). The expression of this enzyme in *E. coli* is regulated by the lac operon (215, 216), which is turned on in case lactose is metabolized, thus up-regulating the expression of β -galactosidase. The enzyme is captured by surface-immobilized antibodies present in the chamber (Figure 19e). After addition of FDG, the captured enzyme converts the substrate FDG into fluorescein. Due to the absence of other limiting factors in the beginning of the reaction, the slope of the fluorescence signal over time corresponds to the number of captured enzymes. Despite the signal amplification provided in this assay, the following aspects contributed to the final high sensitivity: (1) the quality of the antibody and (2) the surface modification.

Thus, (1, antibody characterization) to investigate the affinity of the utilized monoclonal antibody for the enzyme β -galactosidase, the dissociation constant (K_D) value was determined by surface plasmon resonance (SPR) measurements. The obtained K_D of 12 nM ensured a high affinity. The thereby provided high measurement sensitivity enabled a clear distinction between the fluorescence signal over time curve of a microchamber occupied by a single bacterium from the background curve of a bacteria-free microchamber (for example curves, see Figure 25b).

(2, Surface modification) PLL-g-PEG was chosen as surface coating instead of the formerly used bovine serum albumin (BSA) (70), as it prevents non-specific protein adsorption even more effectively (222, 223). Due to this exchange, the background signal was very low (Figure 22). The slight, but negligible increase of fluorescence intensity in the negative controls can be attributed to the self-hydrolysis of FDG in aqueous medium. In previous studies, PLL-g-PEG was identified to reduce biofilm formation of bacteria (224, 225). In an actual experiment, we compared the adhesion behavior of *E. coli* bacteria to the surface for three differently coated microfluidic devices (no coating, BSA-coating and PLL-g-PEG-coating). It revealed that the PLL-g-PEG coating reduced adhesion by 98 % (compared to an uncoated device) and by 70 % (compared to a BSA-coated device), respectively. We assume that the comb-like polymer architecture of PLL-g-PEG made adhesion to the glass or PDMS surface less favorable for *E. coli*, as bacteria adherence beyond the cell trap was prevented in most cases. Nevertheless, sticking of bacteria outside of the gap was frequently observed due to small irregularities in the surface of the PDMS-based cell trap, e.g., corrugations at the corners of the trap piles in the nanometer size range (Figure 19f). Therefore, some of the traps were occupied by multiple bacteria. Microchambers, which were occupied coincidentally by two bacteria were analyzed and the obtained average enzyme values were approximately twice as high as the corresponding average enzyme values of microchambers occupied by a single bacterium (Figure 26).

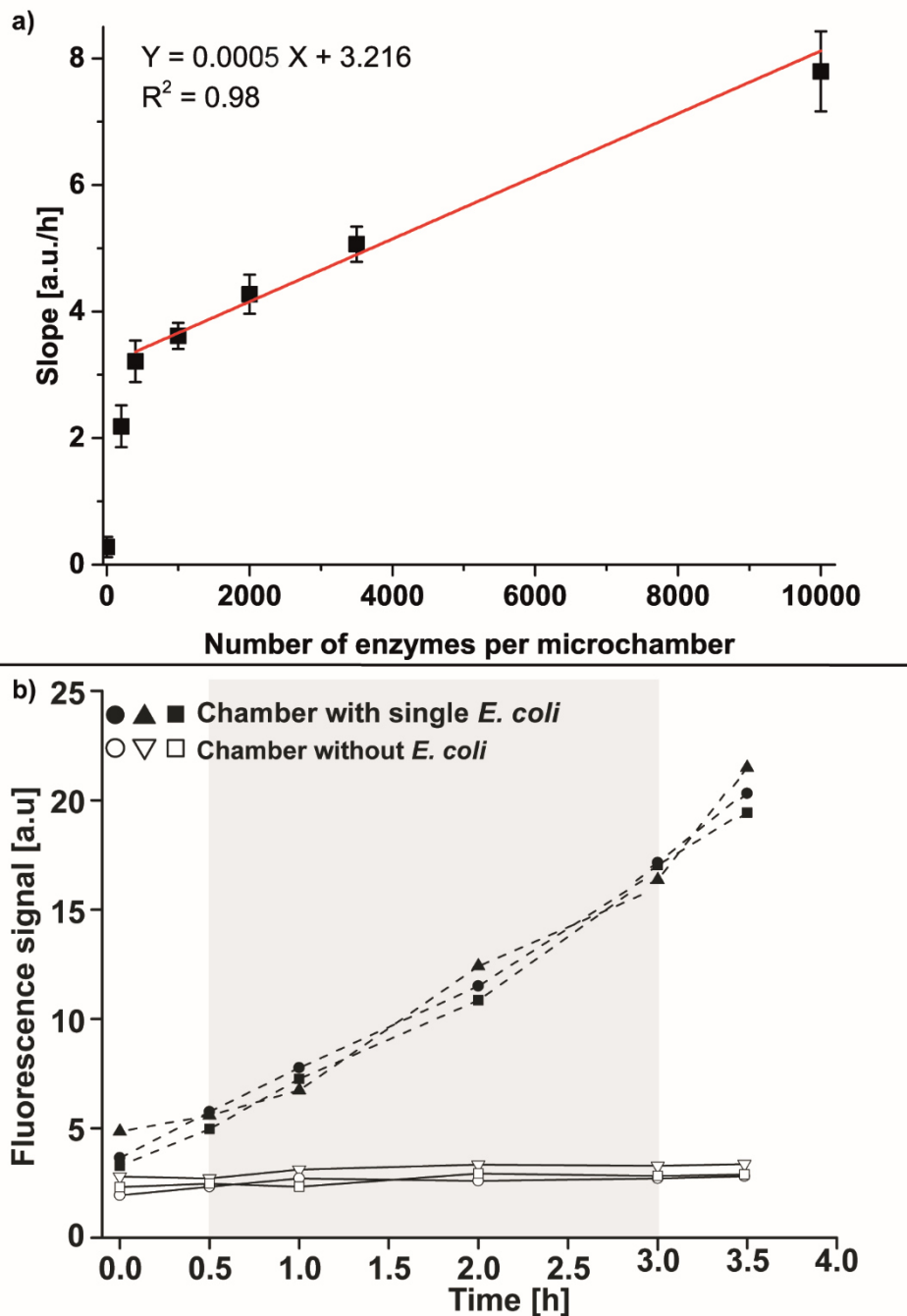


Figure 25: **β -Galactosidase experiments.** a) On-chip calibration curve. For generation of the calibration curve, six different known β -galactosidase concentrations were immobilized on different microfluidic devices ($n = 3$). Afterward, the fluorescent signal increase over time was detected. The slopes of the six different curves exhibit a linear correlation to the amount of added enzymes. The limit of quantification was found to be 400 enzymes per microchamber, whereas the limit of detection was 200 enzymes per microchamber. b) Fluorescent signal over time inside microchambers that enclosed the lysate of single trapped *E. coli* bacterium, and signal in empty chambers (background signal). The area shaded in grey indicates the linear part of the curve. The slope derived from this part was used to quantify the amount of enzymes present in a single *E. coli* bacterium.

3 On-chip enzyme quantification of single *Escherichia coli*

3.4.3 Quantification of the enzyme β -galactosidase in individual *E. coli* cells

Next, we determined the β -galactosidase content of individual *E. coli* MG1655 bacteria. Single Dil-labeled *E. coli* bacteria were trapped and lysed. To ensure that only one bacterium was present in a microchamber, fluorescent pictures were taken from the cell trap and the entire microchamber. Complete cell lysis was verified by taking fluorescence pictures of the trapped bacterium before and after lysis (Figure 20). As the cell membrane is disintegrated during the lysis process, it is no longer possible to accumulate the Dil molecules and therefore the fluorescent signal of a lysed bacterium decreases significantly while the signal of an intact bacterium remains constant (226). Next, the β -galactosidase substrate FDG was introduced. The conversion of FDG to highly fluorescent fluorescein was monitored over a time period of 3 h. From these measurements, fluorescent signal over time curves were generated (Figure 25b) and the concentrations were determined using the calibration curve (Figure 25a). *E. coli* samples grown in either defined or complex medium were analyzed to evaluate the influence of the composition of culture medium on the β -galactosidase expression (Figure 26). The carbon source was lactose in both cases (final concentration of 1 wt %). Data analysis revealed that single bacteria cultured in defined medium contained on average 3517 ± 1578 enzymes (i.e., concentration of $6 \mu\text{M}$ in a single bacterial cell), while single bacteria cultured in complex medium contained on average 4710 ± 2643 enzymes.

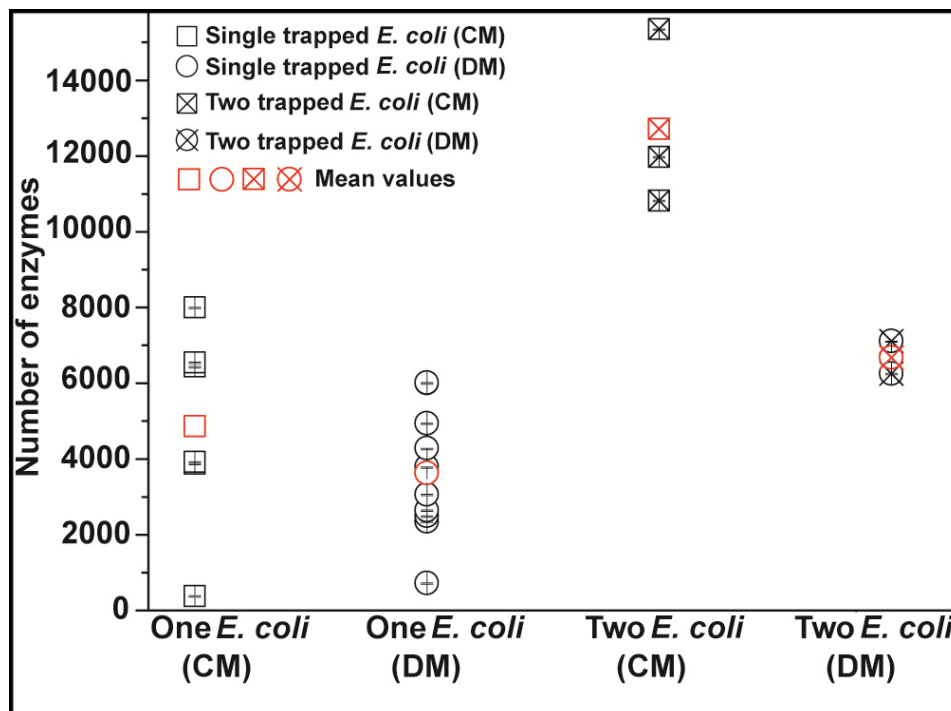


Figure 26: **Quantification of the β -galactosidase levels of individual *E. coli*.** Analysis of single *E. coli* bacteria ($n=25$ cells). Bacteria were either grown in defined medium (DM) or complex medium (CM), with lactose as carbon source (10 g/L). The average amount of enzyme was slightly higher for bacteria grown in CM (open black squares, 4710 ± 2643 enzymes per bacterium) than for bacteria grown in DM (open black circles, 3517 ± 1578 enzymes per bacterium). The average enzyme values of microchambers coincidentally occupied by two bacteria (open black squares with cross (CM), 12321 ± 2279 enzymes for two bacteria) respectively open black circles with cross (DM, 6481 ± 587 enzymes for two bacteria)) were approximately twice as high as the corresponding average values of microchambers occupied by a single bacterium. The error bars of the single *E. coli* data points indicate the 95 % confidence interval based on the calibration curve.

3 On-chip enzyme quantification of single *Escherichia coli*

We assume that the slightly higher expression levels of *E. coli* cultured in complex medium is mainly due to the fact that complex medium provides more preformed nutrients, such as amino acids, than defined medium, that could lead to a higher protein expression in general. The obtained enzyme numbers are in good agreement with previously reported values from bulk measurements (213). Interestingly, the variations are large, in particular for the complex medium, which is in accordance with the general noisy gene expression in *E. coli* bacteria (227).

We could further quantify the influence of the carbon source, here glucose or lactose, on the expression of β -galactosidase. In the presence of an energetically more favorable carbon source than lactose, for example glucose, the operon is turned off and, as a consequence, the β -galactosidase expression is strongly down regulated. As soon as the available glucose is depleted, the lac operon is turned on to enable the metabolization of lactose. In an actual experiment, single bacteria cultured in complex medium with glucose as carbon source (final concentration of 1 wt %) were analyzed and the fluorescence signal over time curves were compared with the curves of bacteria cultured under the same conditions but with lactose as carbon source (Figure 27). The measurements revealed that it was not possible to distinguish the fluorescence over time curve from the background signal of a bacteria free microchamber. Therefore, it can be concluded that the enzyme number was below the limit of detection of 200 enzyme copies, which confirms previous results that indicated 0 to 5 copies per bacterium in case of glucose as carbon source (219). Compared to these former studies, it should be emphasized here, that we are not using sophisticated single-molecule detection methods and, in addition, are not limited to enzymes as target analytes. The applied method is more general, as it also facilitates the implementation of other immunoassays, e.g., enzyme-linked immunosorbent assays (ELISAs) including competitive ELISAs. Consequently, a wide range of different biomolecules can be targeted, provided that appropriate antibodies are available.

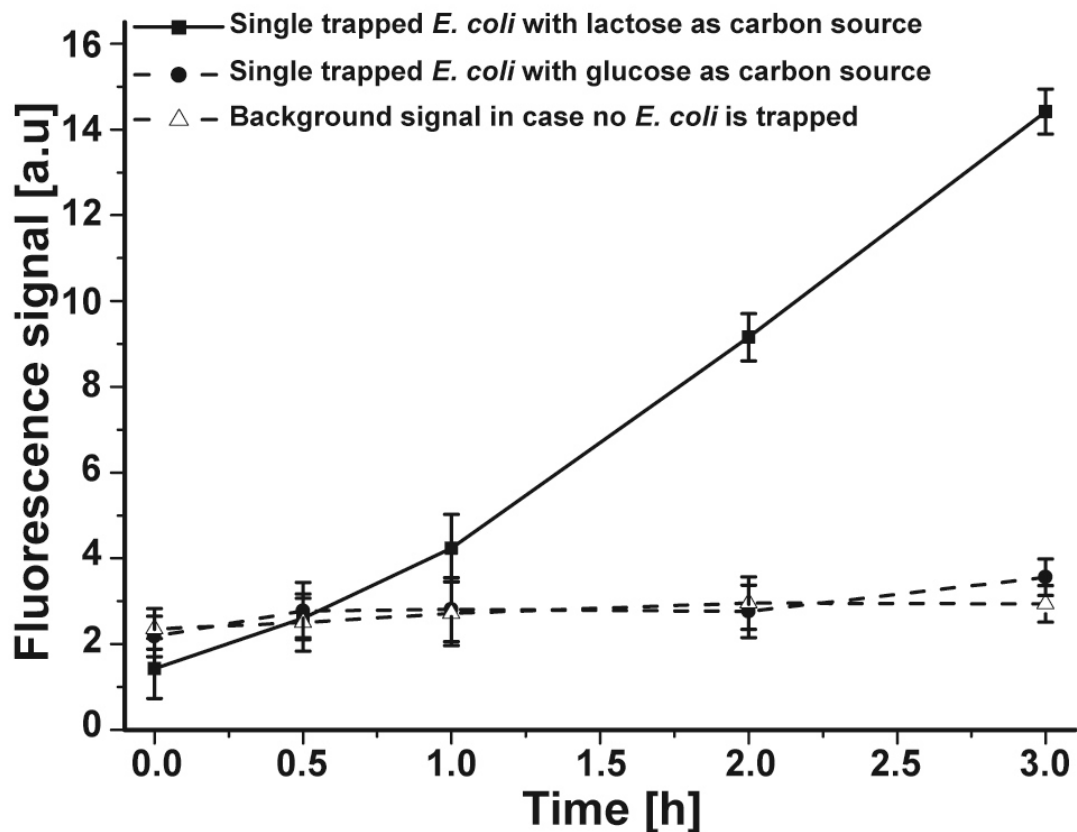


Figure 27: **Influence of the carbon source on the β -galactosidase expression.** Fluorescence signal for lysates of single bacteria cultured with lactose as carbon source (filled squares) or with glucose as carbon source (filled circles). In case of the bacteria cultured with glucose, the fluorescence signal could not be distinguished from the background signal of an empty, bacteria-free microchamber (open triangles).

3.5 Conclusion

We successfully developed a microfluidic device, which enables the analysis of single *E. coli* bacteria by immunological assays. A key feature of the device is a set of microchambers equipped with bacteria cell traps and capable of isolating volumes in the low picoliter range. Combining the low analysis volume (155 pL) with the high selectivity and sensitivity of immunological assays made it possible to quantify intracellular analytes occurring at levels of a few hundred copies per bacterium without employing sophisticated single-molecule detection techniques. For β -galactosidase, the limit of detection was 200 enzymes and the limit of quantification was 400 enzymes. As the cell lysate analysis and the analyte detection are performed in situ in the sealed microchamber, sample contamination or loss of compounds is avoided effectively. In addition, the analysis method is accessible to a broad scope of analytes ranging from second messengers to small peptides to proteins, and the detection of multiple compounds is possible as well. The only requirement is a set of specific antibodies. Future work focuses on the up-scaling of the method by increasing the number of microchambers and automation of the detection by use of a scanning microscope and automated readers. Therefore, the herein presented platform holds the potential for high throughput proteomic analysis of single bacteria.

3.6 Acknowledgement

The authors gratefully acknowledge P. E. Verboket and B. Sebastian for fabrication of the master molds and for taking SEM pictures of the device. We also would like to thank C. Bärtschi and H. Benz for the construction of the custom-built pressure control system and the clean room facility FIRST at ETH Zurich. Furthermore, we would like to acknowledge Prof. Dr. P. Kast who generously provided *E. coli* MG1655 as well as M. Weber and Prof. Dr. D. Neri for their time and help with the Biacore measurements. The work was funded by the European Research Council (ERC Starting Grant, Project No. 203428, n μ LIPIDs).

4 Cultivation and quantitative single cell analysis of *Saccharomyces cerevisiae* on a multifunctional microfluidic device

The content of this chapter is submitted in the following research article: Cultivation and quantitative single cell analysis of *Saccharomyces cerevisiae* on a multifunctional microfluidic device, Simone Stratz, Pascal Emilio Verboket, Karina Hasler, and Petra S. Dittrich (2015).

Modifications made to the original publication

The figure numbering, the table numbering, and the reference numbering were changed. In addition, the supporting information was integrated into the text of the main publication. Therefore, a few connecting sentences, which were not included in the original publication, were added to simplify the reading flow. For a larger view, the size and the position of some figures were changed.

Contributions of the individual authors

Simone Stratz: Designed the research, planned and performed experiments, analyzed the data, and wrote the publication.

Pascal Emilio Verboket: Provided advice on the development of the device design and fabricated the master molds in the clean room. In addition, he proofread the publication.

Karina Hasler: Planned and performed experiments on yeast growth and analyzed the corresponding data.

Petra Dittrich: Designed the research and wrote the publication.

4 Cultivation and quantitative single cell analysis of *Saccharomyces cerevisiae*

4.1 Abstract

Here, we present a multifunctional microfluidic device whose integrative design enables to combine cell culture studies and quantitative single cell biomolecule analysis. The platform consists of 32 analysis units, which are interconnected by microchannels and equipped with two key features; first, a micrometer-sized trap for hydrodynamic capture of a single *Saccharomyces cerevisiae* yeast cell; second, a convenient double-valve configuration surrounding the trap. Actuation of the inner ring-shaped valve isolates the trapped cell completely in a small analysis volume of 230 pL. Actuating of the outer valve with integrated opening results in a partial isolation, i.e. the cell surrounding fluid can be exchanged diffusion-based without causing shear stress or cell loss. Functionality of the device was proven by cultivation of *Saccharomyces cerevisiae* under varying conditions. The observed on-chip cell division rates are in good agreement with those of conventional shake flask cultures, whereby our platform also enabled to identify individual cells with growth characteristics that differ from those of the main population. This system feature was taken advantage of in oxidative cell stress studies. Therefore, individual cells were exposed to hydrogen peroxide and the influence of the stress factor on the cell growth was monitored. In addition, we successfully quantified the cofactor NAD(P)H in single and few cells facing the mentioned differing microenvironments. Consequently, the new double-valve feature enables to analyze the influence of an external stress factor on the cellular fitness in a more comprehensive way as cell growth and intracellular biomolecule levels can be investigated.

4.2 Introduction

The stochastic nature of gene expression processes, e.g. transcriptional bursting (228-230), and unequal partitioning of bioactive compounds during cell division (231, 232) can lead to a great phenotypic heterogeneity within an isogenic cell population. This variety in phenotypes was recently confirmed by multiple single cell studies. Large cell-to-cell fluctuations in concentration of intracellular analytes were observed for a variety of different biomolecules ranging from small metabolites (193, 233) and cofactors (62) to rather large proteins (70, 118, 197) and enzymes (234, 235). This random cellular noise and the resulting phenotypic heterogeneity are thought to be essential for a population's adaptability to environmental changes (236-238).

Taking into account the important role of microorganisms in the biotechnology sector (239, 240), it becomes evident that a better understanding of phenotypic diversity and the underlying control mechanisms is not only important from the perspective of evolutionary research. Prominent examples in the case of the yeast *Saccharomyces cerevisiae* are the wine making (241, 242), brewing (243, 244), and baking industry (245-247) that use strains with phenotypes perfectly adapted to the specific conditions of the production process. Besides industrial applications, yeast is of particular interest for cellular noise studies, as it is an ideal model organism for more complex eukaryotic systems (248, 249). For instance, around one fifth of human disease genes have close matches in the yeast genome and therefore make it an appropriate living test system for new drug candidates against human diseases (250-252).

4 Cultivation and quantitative single cell analysis of *Saccharomyces cerevisiae*

Furthermore, yeast is also used to study basic processes in eukaryotic cells such as DNA repair (253), aging (254), or lipid metabolism (255). Measurement methods capable of analyzing individual cells facilitate the investigation of these fundamental research questions. In this context, microfluidic systems offer some particular advantages, as they match the dimension range of single cells, i.e. precise transport and isolation of small fluid volumes down to the range of a few pico- to femtoliter is feasible (256, 257). So far, several studies on single yeast cell analysis successfully operated on microfluidic platforms have been reported. For example, a microfluidic dissection device for monitoring the complete replicative lifespan of single budding yeast cells was presented by Heinemann and co-workers (258). Other studies demonstrated the on-chip analysis of secreted or intracellular biomolecules (112, 259). However, quantification of analytes in single yeast cells remains difficult (120). Recently, we introduced a platform suitable for protein analysis of single *E. coli* bacteria (234). Key feature of this device was a small ring-shaped valve that isolated the bacterium in a volume in the low picoliter range. Consequently, analyte dilution after cell lysis was prevented which led to a low detection limit of a few hundred enzymes.

Here, we developed this microfluidic device significantly further to couple growth analysis and quantification of intracellular metabolites. In the advanced design the former single ring-shaped valve was replaced by a double-valve configuration (Figure 28c). The double-valve configuration centrally surrounding the cell trap consists of a small inner ring-shaped valve and a larger outer ring-shaped valve with a gap. Actuation of the inner valve lead to a complete encapsulation of the captured cell in a small volume of 230 pL (Figure 28f) while actuation of the outer valve lead to a partial encapsulation within the volume of 3 nL (Figure 28e) whereby the cell ambient fluid can be replaced in a shear-stress free manner by diffusion (Figure 32). To proof the operational capability of the device, single *S. cerevisiae* cells were captured and grown on-chip for 6 h under varying cultivation conditions including optimal nutrient supply, no nutrient supply, and nutrient supply combined with oxidative stress inducing reagents. Furthermore, we performed a fluorimetric assay (Figure 29) to quantify the NAD(P)H levels in individual healthy and oxidatively stressed yeast cells. As one important function of NAD(P)H is to maintain the intracellular redox state, the concentration of the reduced form decreases in case the cell is exposed to reactive oxygen species (ROS) (260, 261). Therefore, low intracellular NAD(P)H levels can be considered as indicator for oxidative cell stress (262, 263).

4 Cultivation and quantitative single cell analysis of *Saccharomyces cerevisiae*

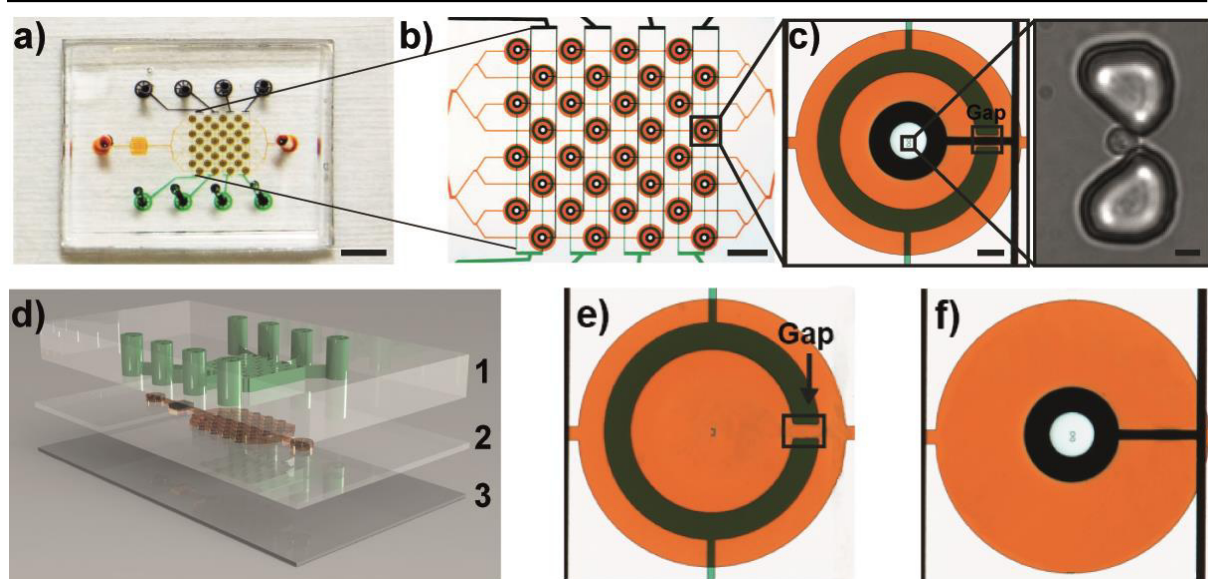


Figure 28: Design and functionality of the microfluidic device. a) Photograph of the platform (scale bar 5 mm). b) Micrographs of the entire set of analysis chambers (scale bar 1mm). c) Left: Micrograph of one analysis chamber (scale bar 100 μ m). For visual support the fluid channels are loaded with orange food dye, the outer valves are loaded with green food dye, the inner valves are loaded with black ink and the closed analysis chambers are loaded with colorless buffer solution. Right: Micrograph of a cell trap that is occupied by a single *Saccharomyces cerevisiae* cell (scale bar 5 μ m). d) Scheme of the different layers required for the microfluidic device. e) Scheme of the partial isolation arrangement for cell cultivation; i.e. only the outer valve with gap is actuated. f) Scheme of the complete isolation arrangement for cell analysis; i.e. only the inner ring-shaped valve is actuated.

4.3 Experimental

4.3.1 Reagents

All reagents were used as received. All solutions were prepared with ultrapurified water (Milli-Q system, Millipore®) if not mentioned otherwise. Silicon wafers were obtained from Si-Mat (Kaufering, Germany). Photoresist SU-8 2010 was obtained from Microchem (Newton, MA, USA). 1H,1H,2H,2H-perfluorodecyltrichlorosilane was supplied by ABCR (Karlsruhe, Germany). Sylgard® 184 silicone elastomer kit was purchased from Dow Corning (Midland, MI, USA). D(+)-glucose was obtained from Thermo Fisher Scientific (Geel, Belgium). YPD agar powder, YPD Broth powder microbial growth medium, lyticase lyophilized powder from *Arthrobacter luteus*, lysozyme powder from chicken egg white, resazurin sodium salt, diaphorase extracted from *Clostridium kluyveri*, magnesium chloride hexahydrate, potassium chloride, Atto 565-Biotin, hydrogen peroxide solution 30 % (w/w) in H₂O and β -nicotinamide adenine dinucleotide phosphate tetra(cyclo-hexylammonium) salt (NADPH, reduced) were supplied by Sigma-Aldrich (Buchs, Switzerland). Phosphate buffered saline (PBS) and 1,1'-dioctadecyl-3,3,3'-tetramethylindocarbocyanine perchlorate (DiI) were purchased from Life Technologies Europe (Zug, Switzerland).

4 Cultivation and quantitative single cell analysis of *Saccharomyces cerevisiae*

4.3.2 Device production process

Briefly, the used platform is made of two polydimethylsiloxane (PDMS) layers, which are bonded to a glass slide. The PDMS layers, i.e. a so-called fluid layer and a control layer, were produced independently by casting the polymer from master molds, which were fabricated by standard microfabrication techniques. After plasma activation of the individual parts, the two PDMS layers were bonded. Subsequently, the completed PDMS part and the glass slide were bonded to obtain the final device (Figure 28a). The general production principle was described in previous publications (62, 70, 220). Minor changes were implemented in the manufacturing protocol due to the new developed double-valve configuration and the size reduction of channels and cell capture features. The following protocol describes in detail the adaptations that have been made to the fabrication protocols of the precursor devices.

The master molds were fabricated by spin coating the photoresist SU-8 2015 on two silicon wafers (2750 rpm, 30 s) to a layer height of 15 μm . After a soft bake (95 $^{\circ}\text{C}$, 210 s) the resist was exposed to UV light (130 mJ/cm^2) through a printed photomask (Micro Lithography Services, UK) in a MA 6 mask aligner (Süss MicroTec, Germany). After a post exposure bake (95 $^{\circ}\text{C}$, 270 s) the photoresist was developed using mr-DEV600 developer (210 s). The wafers were hard baked (200 $^{\circ}\text{C}$, 2 h) and the final heights were verified (step profiler, Dektax XT advanced, Bruker). The silanization process was carried out in a desiccator with 50 μL of 1H,1H,2H,2H-perfluorodecyltrichlorosilane (ABCR, Karlsruhe, Germany) under low atmospheric pressure (100 mbar, 24 h).

Basic material of the PDMS assembly was a 1:10 mixture of curing agent and PDMS monomer (Sylgard[®] 184 silicone elastomer kit, Dow Corning), which was degassed at a pressure of 50 mbar for 20 min before use. The fluid layer was produced by spin coating the previously prepared PDMS mixture on the corresponding master mold (2200 rpm, 60 s, Spin Coater WS-400-6NPP/LITE, Laurell technologies Corporation, North Wales) to build a 35 μm high PDMS layer. For curing the coated wafer was stored in the oven (80 $^{\circ}\text{C}$, 1 h). The control layer was produced by pouring a 5 mm thick layer of PDMS mixture on the corresponding master mold. Curing was also carried out in the oven (80 $^{\circ}\text{C}$, 3 h). Next, the control layer was cut out and inlets for the pressure valves were stamped out (Biopsy puncher, 1mm diameter, Miltex, York, PA). To assemble fluid- and control layer, both were activated by oxygen plasma (0.75 mbar, 18 W, 45 s, custom-made plasma cleaner). The subsequent alignment was performed under a microscope (Multizoom AZ100 M, Nikon Corporation, Japan).

To complete the bonding process, the assembled PDMS unit was stored in the oven (80 $^{\circ}\text{C}$, 1 h). The PDMS unit was removed from the master mold and an inlet and outlet were stamped out (Biopsy puncher, 1.5 mm diameter, Miltex, York, PA). Finally the PDMS unit was bonded onto a glass cover slip (Menzel Gläser # 1, Germany) by oxygen plasma activation (0.75 mbar, 45 s, 18 W, Harrick Plasma Cleaner PDC-32G) and placed on a hot plate (50 $^{\circ}\text{C}$, 15 min) to complete the bonding process. The final device was stored in a dust-free environment until usage.

4 Cultivation and quantitative single cell analysis of *Saccharomyces cerevisiae*

4.3.3 Cell culture

Saccharomyces cerevisiae of the strain YSBN6 were streaked out on YPD agar plates, incubated at 30 °C for 36 h and afterwards stored at 4 °C until usage. For on-chip cell cultivation experiments, a preculture was prepared by inoculating a 15 mL falcon tube containing 3 mL of YPD medium (1 % yeast extract, 2 % bacteriological peptone, 2 % D-glucose) with a single *Saccharomyces cerevisiae* colony of the YPD agar plate. The following incubation was performed at 30 °C with shaking at 200 rpm (KS 4000 i control, IKA, Staufen, Germany) until late log-phase growth was reached. For single cell analysis experiments, a preculture grown in YPD medium to an OD600 of 1 was inoculated in a 15 mL falcon tube containing 3 mL YPD medium at a dilution of 1 to 100. The following incubation was performed at 30 °C with shaking at 200 rpm until early log-phase growth was reached.

4.3.4 Cell cultivation

For cell cultivation experiments, the microfluidic device was placed in an aluminum holder equipped with a heating system, temperature sensor and tubing holders and positioned on an inverted microscope (Olympus IX70). The device was preheated to 30 °C. The *Saccharomyces cerevisiae* sample was diluted 1:2000 with PBS, filtered (Partec CellTrics 10 µm, LabForce AG, Switzerland) and loaded in the microfluidic chip using a syringe pump (NanoJet, CHEMYX, Stafford, USA) at a flow rate of 10 µL/min until sufficient single cells were captured by hydrodynamic trapping. The inner ring-shaped valve was closed for a 10 min washing step with PBS at a flow rate of 20 µL/min. As the trapped cells were isolated completely within the closed microchambers, they were not affected by the applied high flow rate. The washing step was carried out to remove yeast cells adhering to the glass or PDMS surface outside the microchamber. The further experimental procedure was varied according to the requirements of the three different test cases under investigation: (i) investigation of cells with nutrient supply; the inner ring-shaped valve was opened and instead, the outer ring-shaped valve was actuated. The device was continuously flushed with YPD medium (1 % yeast extract, 2 % bacteriological peptone, 2 % D-glucose) which was preheated to 30 °C. (ii) investigation of cells without nutrient supply; the inner ring-shaped valve was kept close. (iii) investigation of oxidatively stressed cells with nutrient supply; the cells were firstly incubated on-chip with 0.1 mM hydrogen peroxide for 15 min. After a 10 min washing step with PBS at a flow rate of 5 µL/min, the setting was changed to the conditions of the test case (i). For all cases under investigation cell growth was monitored in time intervals of 1.5 h corresponding to the minimal required doubling time in log-phase over a period of in total 6 h. Bright field pictures were taken of every microchamber at each point in time with an EMCCD camera (iXon Ultra, Andor Technologies, Ireland) in combination with a 60X water immersion objective and the internal zoom of the microscope (1.5X).

4.3.5 NAD(P)H assay

After positioning the microfluidic platform on an inverted microscope (Olympus IX70), the cell sample was introduced into the device through use of a syringe pump (NanoJet, CHEMYX, Stafford, USA) at a flow rate of 10 $\mu\text{L}/\text{min}$ until the great majority of cell traps was occupied by a single cell. After a subsequent 10 min washing step with PBS, the inner ring-shaped valve was actuated to close the microchambers and thereby isolate the captured cells. Bright field pictures were taken of every cell trap with an EMCCD camera (iXon Ultra, Andor Technologies, Ireland) in combination with a 60X water immersion objective. Thereby, the cell load status was confirmed, i.e. empty or double occupied traps were identified (Figure 31). In the test case investigating on-chip cultured cells previously exposed to hydrogen peroxide, the number of daughter cells originating from the same mother was determined. Next, the lysis buffer (10 mM Tris-HCl completed with 10 mM KCl, 1.5 mM MgCl_2 , 10 mg/mL lysozyme, 0.8 mg/mL lyticase, 0.5 U/mL diaphorase and 2 μM resazurin) was loaded on the platform at a flow rate of 10 $\mu\text{L}/\text{min}$ for 10 min. Then, the flow-rate was increased to 20 $\mu\text{L}/\text{min}$ and the lysis buffer was introduced to the inner microchambers by opening the inner ring-shaped valves for 750 ms. The opening time was controlled by LabView software. After 45 min of incubation time, the end-point fluorescence signal of resorufin was detected by taking images at 180 ms exposure time (gain $\times 150$) with a metal halid lamp (X-Cite 120 PC, Olympus) and an appropriate filter set (excitation: 546/12 and emission: 607/80, AHF Tübingen, Germany). Then, propidium iodide (10 $\mu\text{g}/\text{mL}$ in PBS) was flushed into the microchambers to verify the complete cell lysis (Figure 36) by DNA staining. For calibration, the assay performance was carried out with different known NAD(P)H concentrations instead of with yeast cells (Figure 37a). The assay conditions and the imaging settings were identical with those of the cell experiments. Every concentration was introduced into multiple microchambers of the same platform to test if the chamber position affects the end-point-fluorescence signal. Moreover, the assay was performed for every concentration on two different microfluidic chips to investigate if the device itself has an influence on the detected signal. For the same concentration of NAD(P)H no significant deviations in the fluorescence signal were detected regardless of the position or the device the analyzed chamber was located.

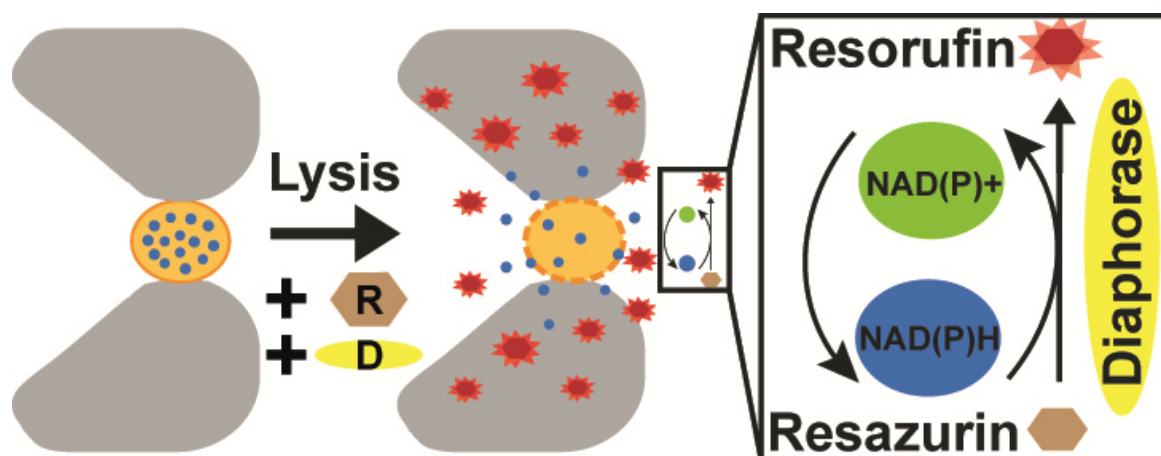


Figure 29: Scheme of the fluorimetric NAD(P)H assay.

4.4 Results and discussion

4.4.1 Chip design

The microfluidic platform is optimized for the specific requirements of cell cultivation as well as bioanalyte quantification in individual cells (Figure 28). The device is composed of 32 analysis units each equipped with the following main characteristics: (1) The micrometer-sized feature which is used for hydrodynamic capture of a single *S. cerevisiae* cell herein after referred to as cell trap and (2) the double-valve configuration which is centrally placed around it (Figure 30).

Channel height:	15 μm
Channel width [A]:	40 μm
Chamber dia. [B]:	140 μm
Chamber dia. [C]:	500 μm
Valve gap size [D]:	40 μm
Chamber volume:	230 pL
Cell trap gap size:	3.5 μm

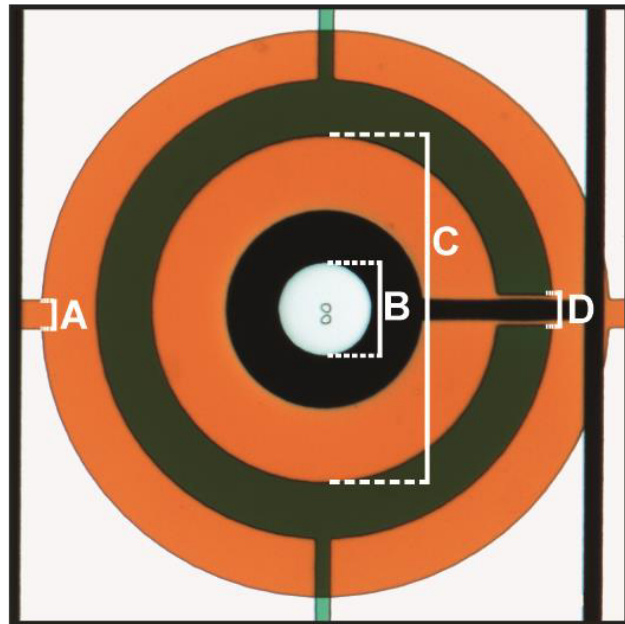


Figure 30: Construction details of the microfluidic platform. Size parameters of the basic structural elements that build up the analysis chamber.

The cell trap (1) consists of two PDMS piles that are arranged at a distance of 3.5 μm , as this interspace matches the size range of a single yeast cell. Consequently, individual cells get physically immobilized between the piles during cell sample load (flow rate $\geq 5 \mu\text{L}/\text{min}$). The optimum interspace size was determined by testing the cell trapping efficiency of four different trap designs with gap sizes varying from 5 μm , to 4 μm to 3.5 μm to 2 μm . The highest single cell occupancy was achieved for an interspace of 3.5 μm . Larger distances promoted the load of multiple cells whereas smaller reduced the overall cell load, i.e. the majority of the traps remained unoccupied (Figure 31).

Figure 31: Influence of the cell trap geometry on the cell load. Bright field micrographs from an actual experiment that illustrate the influence of the cell trap gap size on the cell load. a) In case the cell trap gap is significantly smaller ($\leq 2 \mu\text{m}$) than the expected diameter of a single yeast cell, the trapping efficiency is low, i.e. most traps remain empty or cells are only weakly attached to the PDMS piles but not trapped within the for this purpose intended gap. b) In case the cell trap gap size is minimal smaller than the expected diameter of a single yeast cell ($3 \mu\text{m} - 4 \mu\text{m}$), single yeast cells are captured within the gap in an extremely reliable and stable manner, i.e. even high flow-rates do not lead to cell loss. c) In case the cell trap gap is a little wider or the same size ($5 \mu\text{m} - 10 \mu\text{m}$) as a single yeast cell, the number of traps occupied by multiple cells increases. In addition, the cell capture is less stable with regard to the application of high fluid flow-rates.

The double-valve configuration (2) enables the straightforward switch between complete isolation (closure of the inner ring-shaped valve) and partial isolation (closure of the outer ring-shaped valve with integrated opening) of the captured cell. Both valves can be operated independently of each other within milliseconds. By actuation of the outer ring-shaped valve (Figure 28e, inner diameter of $500 \mu\text{m}$, gap size of $40 \mu\text{m}$) an ideal cell cultivation system is generated. The integrated gap plays a key role as it facilitates the slow, diffusion-based fluid exchange between the microchamber area and the surrounding. Thereby, a continuous, shear-stress free supply of fresh culture medium is guaranteed. Simulations of the fluid flow (COMSOL Multiphysics 5.0) prove that there is no flow within the gap-region under the prevailing flow conditions of the system (Figure 32a). Consequently, the experimentally observed fluid exchange has to be mainly diffusion-based, in contrast to most other microfluidic cell culture systems that induce shear stress due to the fluid flow. The time required for a full fluid exchange was determined in diffusion experiments with fluorescently labeled biotin (Figure 32b-c). Two different test cases were investigated. In a first test case the diffusion of Atto 565-Biotin into the analysis chamber was monitored. At the starting time inner- and outer valve were both actuated before the non-fluorescent buffer solution was replaced by the fluorescently labeled biotin solution (Figure 32c). In a second test case, the diffusion of Atto 565-Biotin out of the analysis chamber was monitored. First, the device was flushed with the fluorescently labeled biotin solution while the inner- and outer valve were still open. Afterwards, both valves were actuated and the non-fluorescent buffer solution was loaded into the device. The fluid exchange was the fastest within the first 20 min due to the initially high concentration gradient (Figure 32b). A complete fluid exchange was ensured after 45 min.

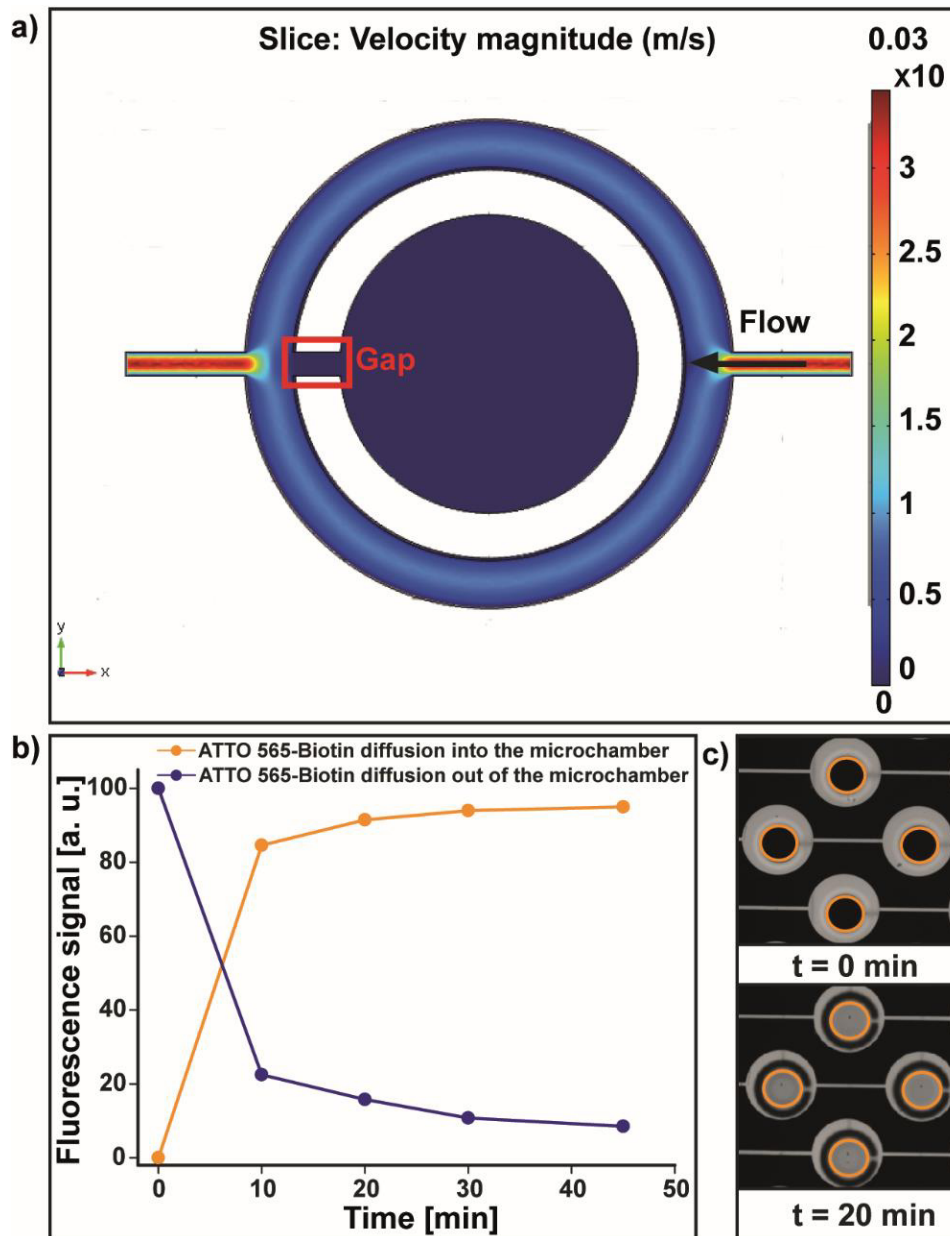


Figure 32: Diffusion-based fluid exchange. a) Simulation of the fluid flow in the microfluidic device in case the outer valve with integrated gap is actuated (COMSOL Multiphysics 5.0). Flow rate is $5 \mu\text{L}/\text{min}$ and the device is filled with water. The selected perspective shows the fluid flow in the analysis chamber from the top. b) Measurement of the diffusion rate of fluorescent labeled biotin (Atto 565-Biotin, $20 \mu\text{g}/\text{mL}$ in ultrapure water) into- (orange curve) and out (blue curve) of the analysis chamber, respectively. c) Fluorescent pictures of an actual experiment investigating the diffusion of fluorescent labeled biotin into the analysis chamber (orange curve). Top: Fluorescent picture at the starting time. Bottom: Fluorescent picture after 20 min.

In contrast, actuation of the inner ring-shaped valve (Figure 28f) creates ideal conditions for quantitative single cell biomolecule analysis, as complete enclosure of an analysis volume of only 230 pL is assured. Thereby, the analyte dilution after cell lysis is successfully prevented. The resulting high analyte concentrations within the analysis chamber affect positively the detection limits of the performed bioassays, as illustrated in a previous publication (234).

4.4.2 On-chip cell cultivation

The suitability of the system for cell cultivation was validated by on-chip cell culture studies. Individual *S. cerevisiae* cells were trapped and the on-chip growth was monitored over a time period of 6 h (Figure 33a, Figure 34). Three different test cases were investigated; (i) the cells had permanent access to fresh culture medium (outer ring-shaped valve with gap-design was actuated), (ii) the cells had no access to fresh culture medium (inner ring-shaped valve was actuated; i.e. no supply with culture medium), (iii) the cells were exposed to hydrogen peroxide for 15 min and then continuously supplied with fresh culture medium identical to the first test case.

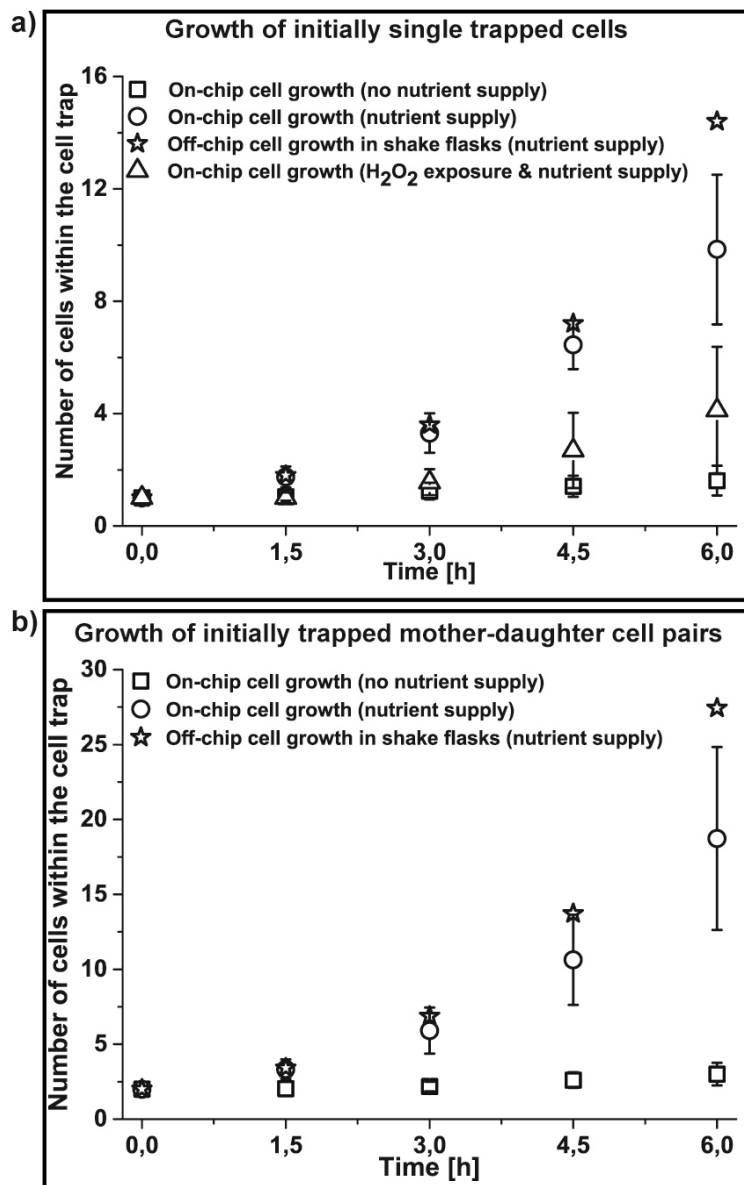


Figure 33: **On-chip cell cultivation.** a) Growth curves of single trapped yeast cells that were cultured under different nutrient conditions ($n = 53$). b) Growth curves of two yeast cells, i.e. a cell trap that was in the beginning of the experiment occupied by a mother yeast cell attached to one daughter cell ($n = 26$). For comparative purposes, literature values of *S. cerevisiae* growth in shake flask cultures in YPD medium were plotted (black stars).

4 Cultivation and quantitative single cell analysis of *Saccharomyces cerevisiae*

The average growth rate of cells with access to culture medium was $0.375 \pm 0.049 \text{ h}^{-1}$ (Figure 35). The corresponding average doubling time was 1.85 h and comparable to literature values of *S. cerevisiae* shake flask cultures indicating doubling times of 1.5 h (YPD medium) to 2.3 h (synthetic medium) (264). Interestingly, analysis of the growth of individual cells revealed a great heterogeneity in growth behavior as depicted by the rather large error bars in the growth curves (Figure 33a, open black rings) and growth rate values (Figure 35). As also cells originating from the same colony monitored under identical conditions (same device, same day, and same culture medium) differed in growth rates, a significant influence of the microfluidic device itself can be neglected. Thus, our findings confirm the heterogeneity in the growth behavior of individual *S. cerevisiae* cells, which has been reported previously (120, 264, 265).

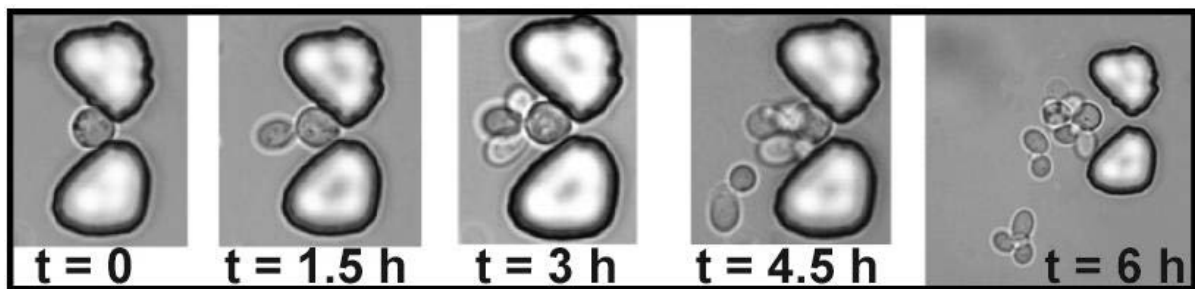


Figure 34: Example micrographs of on-chip cell cultivation. Micrographs of an actual experiment that show the growth behavior of a budding mother yeast cell over a time period of 6 h.

In general, the on-chip growth rates were slightly lower than the literature values of shake flask cultures in YPD medium (Figure 33, black stars). We assume that this observation could be attributed to the lack of the mechanical stresses induced by the movement of the shake flask system. The absence of these stresses could retard the separation of the daughter cell from the mother cell. In addition, the nutrient supply in shake flask cultures is, in contrast to our platform, not only based on diffusion but also on convection processes. In this respect, a recent study should be mentioned which confirmed that the way of nutrient supply, i.e., by diffusion or convection, significantly influences the cell growth and division behavior (266). The cells without nutrient supply (Figure 33a, open black squares) had considerably lower growth rates of in average $0.075 \pm 0.056 \text{ h}^{-1}$. Some cells did not undergo cell division at all (Figure 35), whereby negative propidium iodide staining proved intact cell walls and therefore implicated cell viability. The growth rates of oxidatively stressed cells of in average $0.189 \pm 0.129 \text{ h}^{-1}$ (Figure 33a, open black triangles) ranged between the growth rates of starving cells and of non-stressed cells with access to culture medium. Also under oxidative stress conditions, a great heterogeneity in the growth of single cells was observed. The ability to monitor the growth of individual cells and therefore to spot cells with specific characteristics differing from those of the main population is the essential advantage of our system over bulk measurements and demonstrated by these findings. In some cases, mother cells still attached to their daughters were captured coincidentally. Same as for the single trapped cells, cell pairs with access to fresh culture medium grew significantly better than cell pairs without access to fresh medium (Figure 33b, Figure 35).

4 Cultivation and quantitative single cell analysis of *Saccharomyces cerevisiae*

Growth rate μ [h ⁻¹] of single yeast cells in case of nutrient supply	Growth rate μ [h ⁻¹] of single yeast cells in case of no nutrient supply	Growth rate μ [h ⁻¹] of single yeast cells in case of H ₂ O ₂ exposure and nutrient supply
0.2507	0	0
0.2841	0	0
0.2986	0	0
0.3358	0	0.1155
0.3466	0	0.1831
0.3662	0	0.2088
0.3662	0	0.2507
0.3662	0.0676	0.2682
0.3662	0.0676	0.312
0.3662	0.0676	0.3662
0.3838	0.0676	Avg. growth rate: 0.189 ± 0.129 h ⁻¹
0.3838	0.1155	Avg. doubling time ~ 3.7 h
0.3919	0.1155	
0.3919	0.1155	
0.3996	0.1155	
0.3996	0.1155	
0.3996	0.1155	
0.3996	0.1155	
0.4275	0.1155	
0.4275	0.1155	
0.4275	0.1155	
0.4621	0.1155	
	0.1831	
Avg. growth rate: 0.375 ± 0.049 h ⁻¹ Avg. doubling time ~ 1.85 h	Avg. growth rate: 0.075 ± 0.056 h ⁻¹ Avg. doubling time ~ 9.2 h	
Growth rate μ [h ⁻¹] of mother daughter cell pairs in case of no nutrient supply	Growth rate μ [h ⁻¹] of mother daughter cell pairs in case of nutrient supply	
0	0.231	
0	0.2682	
0	0.3243	
0.0372	0.3242	
0.0372	0.3358	
0.0676	0.3567	
0.0676	0.3662	
0.0676	0.3752	
0.0676	0.3996	
0.0933	0.407	
0.0933	0.4337	
0.0933	0.4337	
0.1155		
0.1352		
Avg. growth rate: 0.063 ± 0.043 h ⁻¹ Avg. doubling time ~ 11.1 h	Avg. growth rate: 0.355 ± 0.062 h ⁻¹ Avg. doubling time ~ 1.95 h	

Figure 35: **Growth rates.** Growth rates of all analyzed single cells and mother-daughter cell pairs under the defined culture conditions.

4 Cultivation and quantitative single cell analysis of *Saccharomyces cerevisiae*

4.4.3 NAD(P)H assay

For quantification of the intracellular NAD(P)H levels of single *S. cerevisiae* cells, the enzyme diaphorase and its substrate resazurin were added to the lysis buffer. After cell lysis, the former intracellular NAD(P)H was released and was used as reductant for the diaphorase-catalyzed conversion of resazurin to resorufin (Figure 29). After an incubation time of 45 min ensuring a complete depletion of all available NAD(P)H, the end-point fluorescence signal of resorufin was detected. An on-chip background correction was performed on each device by detection of the fluorescence signal of cell-free microchambers (Figure 36). Complete cell lysis was verified by subsequent staining with propidium iodide (Figure 36).

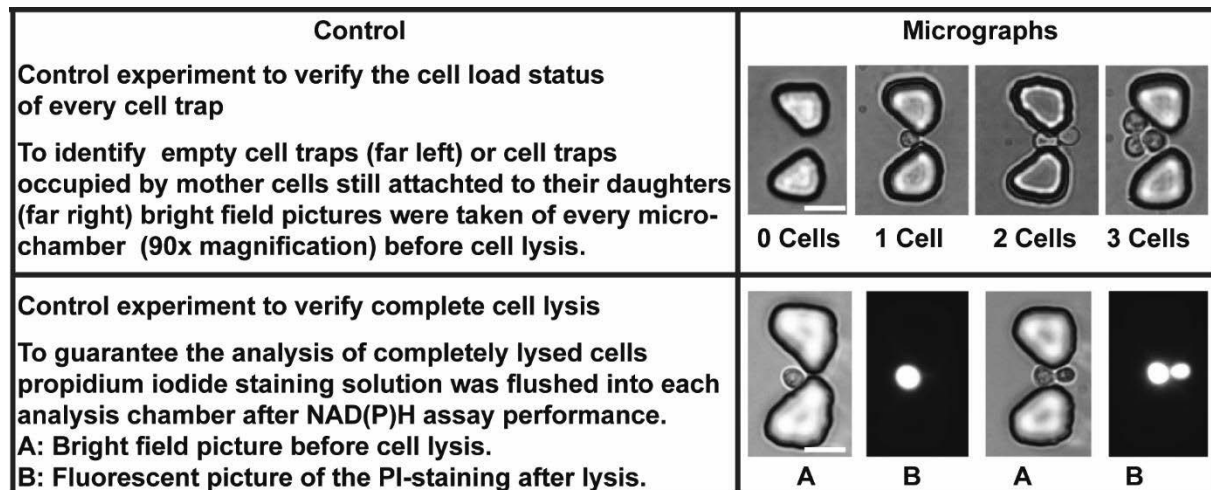


Figure 36: Control experiments to ensure single cell analysis and complete lysis. Control experiments that were carried out on each microfluidic platform. Left: Description. Right: Example micrographs of an actual experiment.

In addition, the assay was performed with 6 different known NAD(P)H concentrations instead of with yeast cells. The samples were prepared by adding the 6 different known NAD(P)H amounts to the lysis buffer. The fluorimetric NAD(P)H assay was carried out for each sample on multiple analysis chambers and on two different devices. The resulting linear calibration curve (Figure 37a) was used to determine the NAD(P)H amount of single cells (Figure 37b). Due to the small analysis volume of the microchamber and the high sensitivity of the fluorimetric assay, a limit of detection of 10 amol was reached allowing the quantification of low copy number analytes. The average NAD(P)H amount per cell was found to be 48 ± 22 amol and is in accordance with values from literature of healthy, i.e. not to oxidative stress exposed, yeast cells (267, 268).

Moreover, we analyzed mother cells that were still attached to one or two daughter cells. The obtained NAD(P)H levels were approximately two times (93 ± 38 amol) respectively three times (137 ± 25 amol) as high as the levels of corresponding single cell measurements.

We also performed the assay for yeast cells grown on-chip after exposure to hydrogen peroxide. In this case we analyzed multiple cells per microchamber; i.e. the mother yeast cells together with the corresponding daughters, and determined the NAD(P)H mean value per cell.

4 Cultivation and quantitative single cell analysis of *Saccharomyces cerevisiae*

For around 40 % of the in total 22 analyzed cells the NAD(P)H amount was below our limit of detection of 10 attomole. For the remaining 60 % of analyzed cells, the average NAD(P)H amount per cell ($45 \text{ amol} \pm 21 \text{ amol}$) was comparable to the corresponding value of non-stressed cells. The variations we found in the NAD(P)H levels of individual cells encourages the use of the device for further bioanalyte studies of isogenic cells subjected on-chip to varying cultivation conditions.

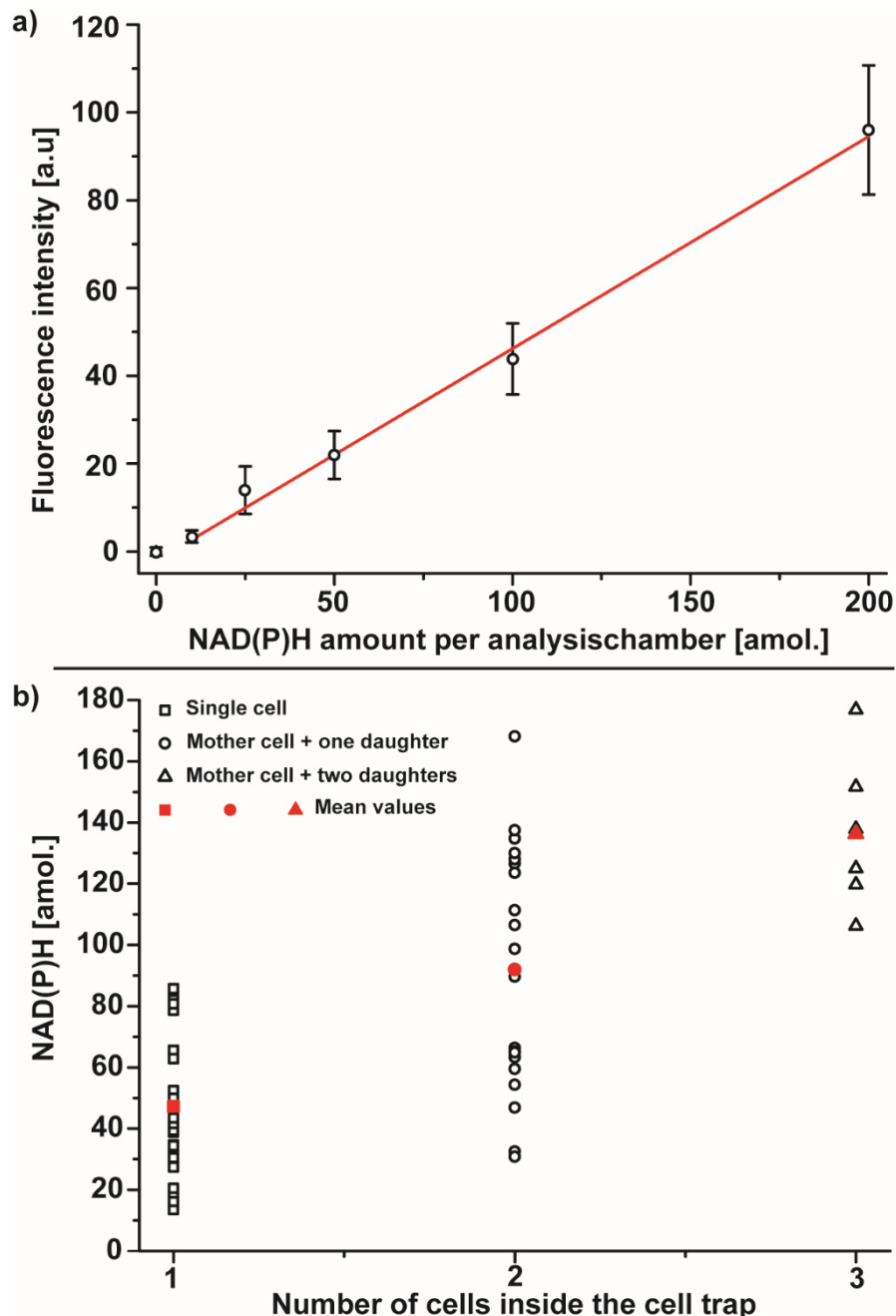


Figure 37: **Fluorimetric NAD(P)H assay.** a) On-chip calibration curve. The fluorescence end-point signal and the amount of NAD(P)H exhibit a linear correlation. The limit of detection was 10 attomole per analysis chamber what equates to a concentration of 45 nM ($LOD = \text{mean}_{\text{blank}} + 2 SD_{\text{blank}}$). b) Analysis of single yeast cells (open black squares; $n = 26$), budding mother cells still attached to one daughter (open black circles; $n = 20$) or two daughters (open black triangles; $n = 6$).

4.5 Conclusions

We successfully engineered a multifunctional microfluidic cell analysis platform. Key feature of the device is a convenient double-valve-construction surrounding a centrally placed micrometer-sized feature for single *S. cerevisiae* cell capture. The double-valve-construction enables the fast change from partial to complete isolation of the trapped cell. The thereby provided high experimental flexibility was proven by cell culture- and single cell analysis studies. Due to the small analysis chamber volume in the low picoliter range reliable bioanalyte quantification was possible up to a limit of detection of 10 attomole. Further developments will concentrate on the implementation of an automated optical readout and the capacity scale-up, e.g. increased number of microchambers, to enable parallelized high throughput measurements. Future projects will focus on the analysis of individual cells exposed on-chip to varying stress factors. Thereby, cell-to-cell differences in the adaptability to environmental changes can be investigated.

4.6 Acknowledgements

We gratefully acknowledge C. Bärtschi and H. Benz for the construction of the custom-built pressure control system and the clean room facility FIRST at the ETH Zurich. Furthermore, we would like to acknowledge Dr. Alfredo Ibanez who generously provided *Saccharomyces cerevisiae* YSBN6. The work was funded by the European Research Council (ERC Starting Grant, Project No. 203428, nμLIPIDs).

5 Separation & subsequent biomolecule analysis of single mother-daughter cell pairs

The content of this chapter is submitted in the following research article: On-chip separation and subsequent biomolecule analysis of single mother-daughter cell pairs, Simone Stratz, Pascal Emilio Verboket, and Petra S. Dittrich, Proceedings of the microTAS conference (MicroTAS), (2015).

Modifications made to the original publication

The figure numbering, the table numbering, and the reference numbering were changed. In addition, supplementary information was integrated that was not provided in the conference proceedings paper due to the limited number of words allowed. To be precise, section 5.2, 5.3.1, 5.3.2, 5.3.3, 5.5, and 5.7 were newly added. Moreover, additional text information was added to section 5.3.5, 5.4, and 5.6.

Contributions of the individual authors

Simone Stratz: Designed the research, planned and performed all experiments, analyzed the data, and wrote the publication.

Pascal Emilio Verboket: Provided advice on the development of the device design and fabricated the master molds in the clean room. In addition, he proofread the publication.

Petra Dittrich: Designed the research and wrote the publication.

5 Separation & subsequent biomolecule analysis of single mother-daughter cell pairs

5.1 Abstract

Individual cells of an isogenic population can exhibit significant differences in their phenotypes. Due to the great variety of factors contributing to the emergence of cellular heterogeneity, the investigation of the underlying mechanisms is a demanding task. In recent years, several devices for cell heterogeneity studies have been developed, although special effort has been directed towards the influence of environmental factors. In contrast, less emphasis has been put on inheritance noise studies requiring the separate analysis of individual mother cells from the associated daughters. Therefore, we designed a microfluidic platform for the separation and subsequent biomolecule analysis of single *Saccharomyces cerevisiae* mother-daughter cell pairs. Consequently, the particular influence of cell division, here the budding of the yeast cells, on the heterogeneity of a population can be studied.

5.2 Introduction

In the last decades, numerous studies confirmed the manifold influences inducing phenotypic heterogeneity among individual cells of an isogenic population. Nevertheless, the majority of projects performed in this field of research focused on the investigation of external impacts, for example, the effect of stress factors like reactive oxygen species (ROS) or the exposure to antibiotics. A hitherto less intensively studied source of cellular heterogeneity is related to the random distribution of biomolecules during cell division (269). This uneven partitioning is referred to as inheritance noise and has been reported for different biomolecules and cell types (270, 271). The effects of partitioning errors are particularly large for molecules that occur at low copy numbers and for mRNA molecules, as one single mRNA is transcribed into many proteins (231). Recent research results suggest that inheritance noise is not primarily a demonstration of the error tolerance of a biological system (272). On the contrary, it is an evolutionary strategy to generate diversity among cells of identical gene profile (273). The co-existence of subpopulations exhibiting characteristics differing from those of the main population can result in an increased fitness of the overall population. In this context, the mechanism of bet hedging (274), which can be found in many microbial populations like yeast (272) or *E. coli* (275), should be mentioned. The fundamental principle of bet hedging is based on the simultaneous occurrence of slow growing, multi-resistant phenotypes and fast growing ones. The latter flourish under ideal conditions while the former are capable of withstanding external perturbations and thereby hedge the survival of the entire population under stress conditions. In current studies, several mechanisms were discussed contributing to the emergence of partitioning noise. For example, variations in the copy numbers of plasmids and chromosomes have been shown to induce large heterogeneity in clonal populations (276). The plasmid copy number (PCN) determined by the replication system is an important factor concerning the overall plasmid stability (277-279). Low PCNs increase the probability of failure in plasmid partition to the daughter cells. As a result, plasmid-free cells occur generating a higher level of genetic and phenotypic heterogeneity within the population. Other investigated mechanisms causing inheritance noise include the segregated distribution of cellular storage components or cytoplasmic proteins related to cell age (280, 281).

5 Separation & subsequent biomolecule analysis of single mother-daughter cell pairs

Nevertheless, most of the molecular processes regulating the individual mechanisms remain to be elucidated. This requires systems that enable the comprehensive analysis of single mother and daughter cells. Therefore, we developed a microfluidic device that enables the separation and analysis of individual *S. cerevisiae* mother-daughter cell pairs (Figure 38). The device was adapted to the special requirements of *S. cerevisiae* as it commonly occurs in isogenic populations and, in addition, plays an important role in the biotechnology sector and as model organism for higher eukaryotic systems.

5.3 Experimental

5.3.1 Reagents

All reagents were utilized as received. All solutions were prepared by the use of ultrapurified water (Milli-Q System, Millipore®) if not mentioned otherwise. Silicon wafers were obtained from Si-Mat (Kaufering, Germany). Photoresist SU-8 2015 was obtained from Microchem (Newton, MA, USA). 1H,1H,2H,2H-perfluorodecyltrichlorosilane was supplied by ABCR (Karlsruhe, Germany). Sylgard® 184 silicone elastomer kit was purchased from Dow Corning (Midland, MI, USA). D(+)-glucose was obtained from Thermo Fisher Scientific (Geel, Belgium). YPD agar powder, YPD Broth powder microbial growth medium, lyticase lyophilized powder from *Arthrobacter luteus*, lysozyme powder from chicken egg white, resazurin sodium salt, diaphorase extracted from *Clostridium kluyveri*, magnesium chloride hexahydrate, potassium chloride, and β -nicotinamide adenine dinucleotide phosphate tetra(cyclo-hexylammonium) salt (NADPH, reduced) were supplied by Sigma-Aldrich (Buchs, Switzerland). Phosphate buffered saline (PBS) was purchased from Life Technologies Europe (Zug, Switzerland).

5.3.2 Device fabrication

The basic fabrication principle was explained in detail in former publications (62, 70, 220). Briefly summarized, the utilized device consisted of two polydimethylsiloxane (PDMS) layers which were bonded to a glass slide. Both PDMS layers, i.e. the fluid layer and the control layer containing the integrated microvalves, were fabricated separately by casting the polymer from master molds. The corresponding master molds were produced by standard microfabrication techniques in a clean room facility. The small design of the cell filter features and the microjunctions made the usage of a chrome-glass mask (Compugraphics Jena GmbH, Jena, Germany) instead of a film mask essential. The exact parameters of the photolithographic fabrication process are indicated in Table 2 of section 2.1.2. The finished master molds served the fabrication of PDMS replica which were subsequently assembled by oxygen plasma activation. In the last step, the completed PDMS assembly and the glass slide were exposed to oxygen plasma and bonded to form the final platform (Figure 38).

5 Separation & subsequent biomolecule analysis of single mother-daughter cell pairs

5.3.3 Cell culture

For short-term maintenance, *Saccharomyces cerevisiae* of the strain YSBN6 were streaked out on YPD agar plates. Subsequent incubation was carried out at 30 °C for 36 h. Storage of the parafilm-sealed culture plates was performed in a refrigerator at 4 °C. For the actual cell experiments, a preculture was prepared the day before. Therefore, a 15 mL falcon tube containing 3 mL of YPD medium (1 % yeast extract, 2 % bacteriological peptone, 2 % D-glucose) was inoculated with a single *S. cerevisiae* colony of the culture plate. The following incubation was carried out at 30 °C with shaking at 200 rpm (KS 4000 i control, IKA, Staufen, Germany) until the cell sample accomplished late log-phase growth. Next, the preculture was inoculated in a 15 mL falcon tube containing 3 mL YPD medium at a dilution of 1 to 100. The cell sample was incubated at 30 °C with shaking at 200 rpm until early log-phase growth was achieved. Shortly before introduction into the platform, the cell sample was diluted 1:200 with PBS and filtered (Partec CellTrics® 20 µm, LabForce AG, Switzerland) to prevent blockage of the microjunctions or cell filters by dust particles.

5.3.4 Mother-daughter cell pair capture and separation

The microfluidic device was placed on an inverted microscope (Olympus IX70) and the prepared cell sample was introduced by means of a syringe pump (NanoJet, CHEMYX, Stafford, USA) at a flow rate of 5 µL/min until each microjunction was occupied by a mother-daughter cell pair. The microchambers centrally surrounding the microjunctions were actuated and a 10 min washing step with PBS at a flow rate of 5 µL/min was performed. Thereby, yeast cells were removed which adhered to the PDMS or glass surfaces beyond the cell capture features. Afterwards, bright field pictures were taken of every microjunction with an EMCCD camera (iXon Ultra, Andor Technologies, Ireland) in combination with a 60X water immersion objective to confirm the capture of single mother-daughter cell pairs. Next, the microvalves were opened and fluid flow was applied in the main channel (flow rate: 5 µL/min) and in the side channel (flow rate: 1 µL/min) to induce the flow-based separation of the mother-daughter cell pair. After successful separation, the microvalves of the microjunctions and also of the filter system were actuated to isolate the separated cells from the surrounding.

5 Separation & subsequent biomolecule analysis of single mother-daughter cell pairs

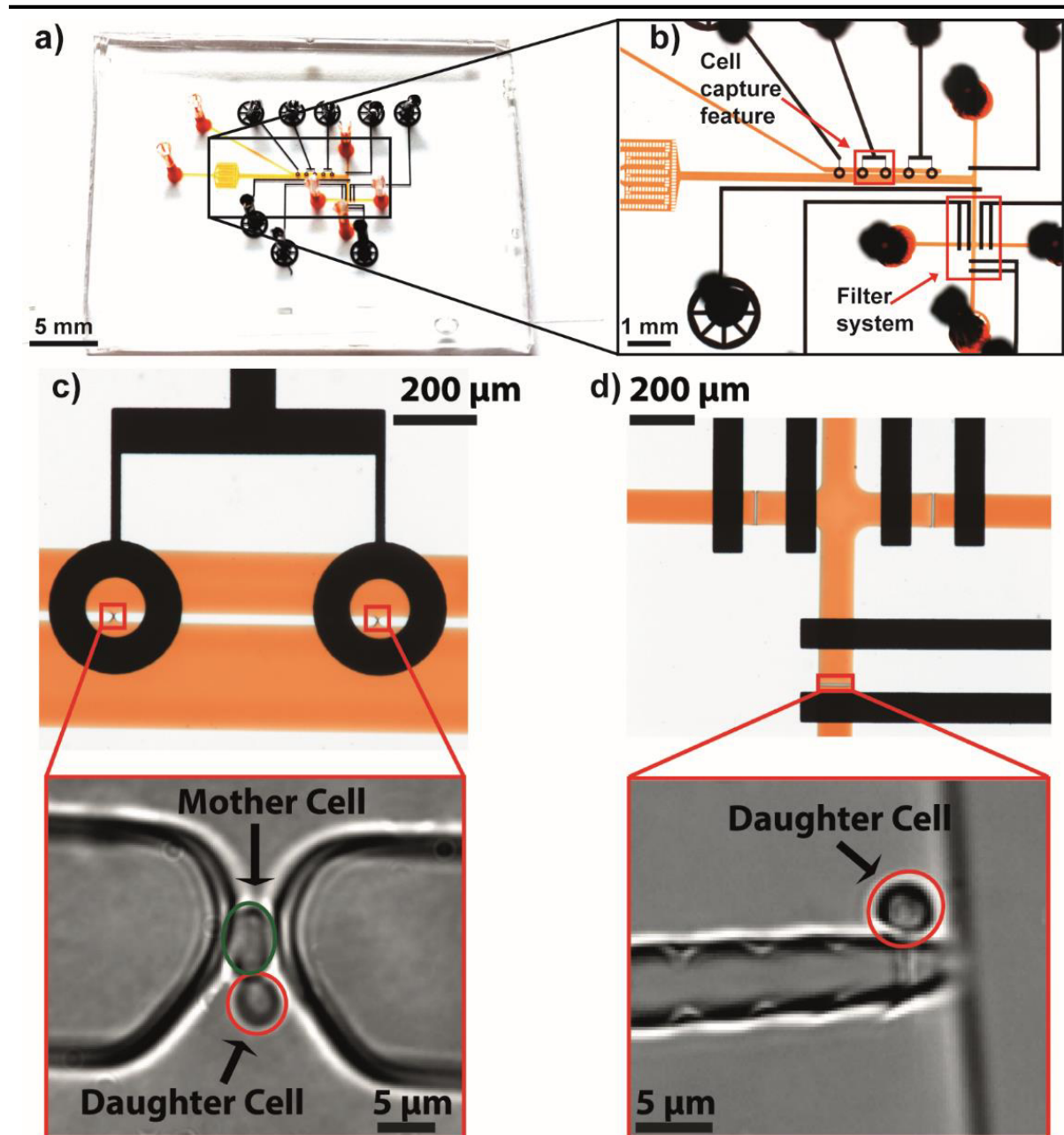


Figure 38: Design and functionality of the microfluidic device. a) Photograph of the platform. b) Micrograph of the entire fluid channel system. For visualization, the fluid channels are filled with orange food dye (inlets appear black) and the pressure lines with black ink. c & d) Close-up images of the design key features. c) Micrometer-sized junctions for trapping of single mother-daughter cell pairs, each surrounded by a ring-shaped valve. d) Micrograph of the filter system to capture the separated daughter cell.

5 Separation & subsequent biomolecule analysis of single mother-daughter cell pairs

5.3.5 NAD(P)H assay

The separated mother-daughter cell pairs were isolated from the adjacent chip environment by actuation of the microvalves. The lysis buffer (10 mM Tris-HCl completed with 10 mM KCl, 1.5 mM MgCl₂, 10 mg/mL lysozyme, 0.8 mg/mL lyticase, 0.5 U/mL diaphorase and 2 μM resazurin) was introduced into the device at a flow rate of 5 μL/min for 15 min. Next, the flow-rate was increased to 10 μL/min and the cell surrounding PBS solution was exchanged by lysis buffer. Therefore, the microvalves were opened for 750 ms. The opening time was regulated by LabView software. An incubation time of 45 min was carried out. Afterwards, the end-point fluorescence signal of the formed product resorufin was detected. Images were taken at 180 ms exposure time (gain ×150) with a metal halid lamp (X-Cite 120 PC, Olympus) and an adequate filter set (excitation: 546/12 and emission: 607/80, AHF Tübingen, Germany).

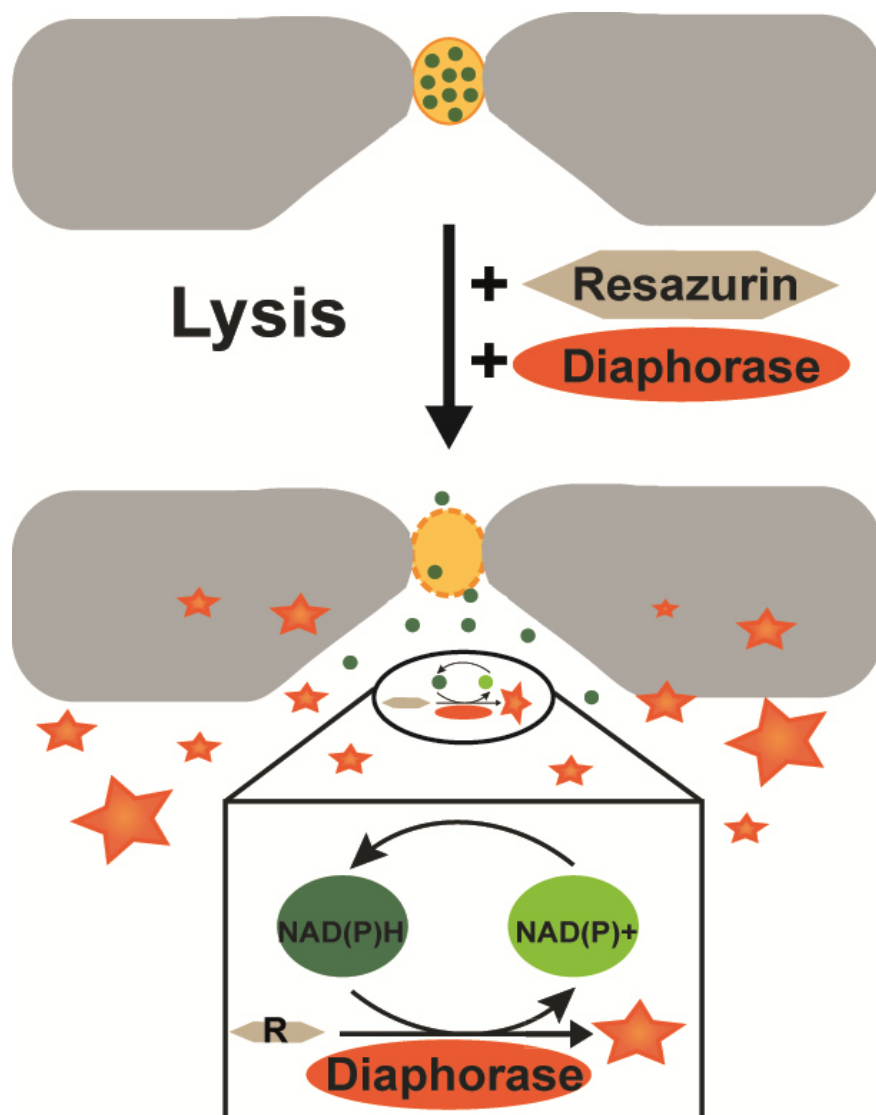


Figure 39: Schematic drawing of the fluorometric NAD(P)H assay. For detection of the NAD(P)H levels of single yeast cells the enzyme diaphorase (D) and its substrate resazurin (R) are added to the lysis buffer. After lysis, the released NAD(P)H is consumed as reductant for the conversion of resazurin to resorufin catalyzed by the enzyme diaphorase. After complete depletion of NAD(P)H, the end-point fluorescence signal of resorufin is detected.

5 Separation & subsequent biomolecule analysis of single mother-daughter cell pairs

5.4 Results

5.4.1 Mother-daughter cell pair separation

After successful trapping of a single budding mother yeast cell in the microjunction, the separation process was initiated. For separation of the mother-daughter cell pair, fluid flow was applied simultaneously in both fluid channels, as illustrated in Figure 40b. By pumping the fluid at low flow-rates ($\leq 1 \mu\text{L}/\text{min}$) out of the side channel, a gentle suction effect was generated that pressed the mother yeast cell into the cell trap and thereby strengthened stable cell capture. At the same time, fluid flow with higher flow rates ($5 \mu\text{L}/\text{min}$) was generated in the main channel. As a result, the smaller daughter cell directly facing the main channel was exposed to a strong flushing effect that caused the separation from the mother cell and subsequent flow-based transport to the filter system. However, reliable and fast separation of mother-daughter cell pairs by fluid flow remained difficult due to the small difference in size and weight. Consequently, major modifications of the presented prototype design should be implemented, as discussed in section 5.5.

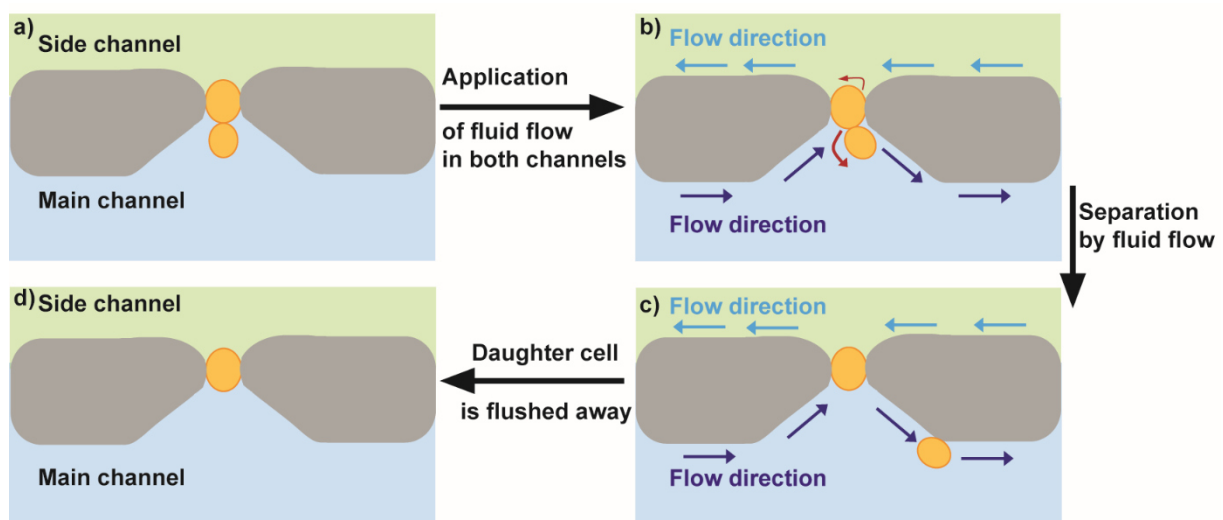


Figure 40: Scheme of the fluid-based mother-daughter cell pair separation process. a) Flow is applied in the main channel to introduce the cell sample into the device. The larger mother cell is physically captured within the micrometer-sized junction while the significantly smaller daughter cell remains directed towards the main flow channel. After sufficient cell traps are loaded with mother-daughter cell pairs, the flow is stopped. b) Fluid flow is applied in the main and in the side channel. As a consequence of the thereby generated flow profile, the mother cell is pressed into the cell trap while the daughter cell is fully exposed to the fluid flow of the main channel. c) The daughter cell is flushed away and thereby separated from the mother cell. d) The flow is stopped in both channels, and it remains a single mother cell within the cell trap.

5 Separation & subsequent biomolecule analysis of single mother-daughter cell pairs

5.4.2 Biomolecule analysis

After separation, the single mother and daughter cells were analyzed individually by a fluorometric assay (Figure 39). For this purpose, diaphorase and resazurin containing lysis buffer was introduced into the microjunctions and cell filter compartments. Thereby, cell lysis was induced and the former intracellular NAD(P)H was released. After an incubation time of 45 min which guaranteed complete consumption of all available NAD(P)H, the end-point fluorescence signal of resorufin was recorded. In addition, a background correction was performed on each platform. Therefore, the fluorescence signal of cell-free microjunctions and filter compartments was detected. As depicted in Figure 41a, the relative fluorescence intensity was higher for single mother cells than for the corresponding daughters. However, if the significant differences in cell volume are taken into account, as illustrated in Figure 41b, the actual situation is reversed indicating higher NAD(P)H concentrations in the daughter cells than in the mothers. These findings are in good agreement with literature values supposing age-associated reduction in cellular fitness of mother cells (270, 282). Nevertheless, for a substantiated statement, the acquisition of more data is required.

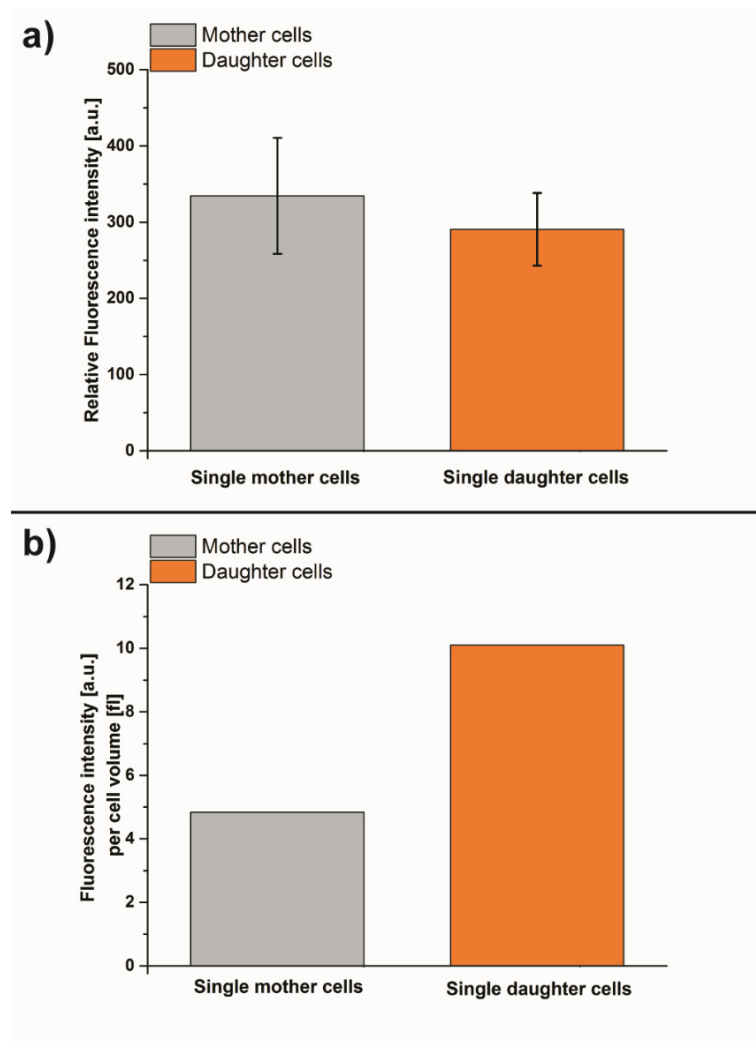


Figure 41: Biomolecule analysis of separated mother and daughter cells. a) Fluorescence end-point signal of resorufin of mother and daughter cells ($n=6$). b) Fluorescence end-point signal related to the volume of the analyzed cells.

5 Separation & subsequent biomolecule analysis of single mother-daughter cell pairs

5.5 Discussion - Improvement and modification of the existing prototype

The only small difference in cell size and weight made the exclusively flow-based separation of the mother-daughter cell pairs on the existing prototype to a challenging task. For a more reliable and faster separation process, that is less prone to the generation of cell stress, major modifications must be implemented. In this context, one main issue is the resolution of the small cell filter structures and microjunctions covering a size range from 2 μm to 3.5 μm . As illustrated in Figure 38d, the majority of the cell filter features were not resolved completely. Consequently, the channel part located in front of the filter system was only connected by a few small gaps, i.e. the minority of resolved filter features, to the channel part located behind the filter system. The undissolved features caused a partial blockage of the channel and thereby hindered fast fluid exchange or application of high flow-rates. A further related issue was the rather large gap of the microjunctions for physical capture of the mother cells. Instead of the 3.5 μm distance displayed on the chrome-glass mask, the actual distance on the fabricated silicon master mold was 5 μm in size. As discussed in section 4.4.1, larger cell trap gap sizes result in less stable cell capture. To overcome the problems caused by the incomplete resolution of key design features, the photolithographic production process of the master molds must be optimized. Moreover, the device design itself could be further developed. The two main suggestions for improvement are illustrated in Figure 42 and will be discussed in more detail in the following.

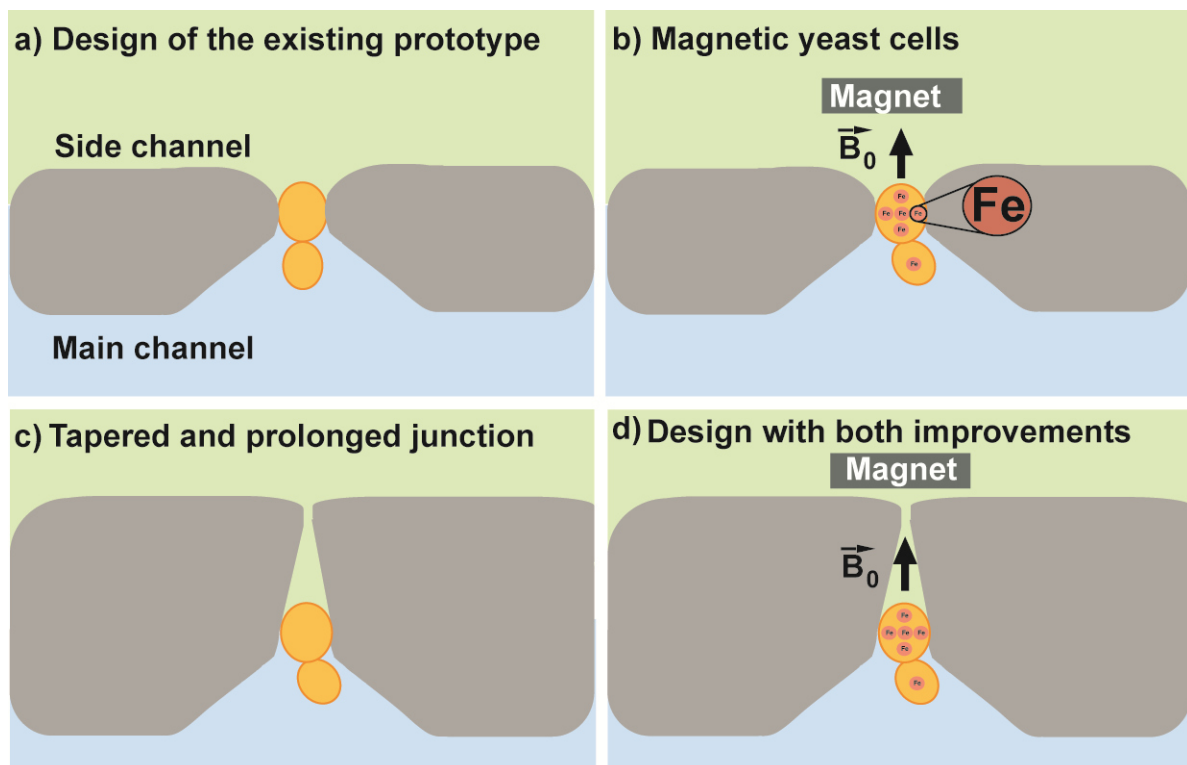


Figure 42: Scheme of potential improvements related to the current device design. a) Microjunction design of the existing device. b) Modified set-up suited for the use of magnetic yeast cells. c) Tapered and prolonged microjunction design for the improved physical capture of the mother yeast cell. d) Possible set-up in case both improvements are integrated in one device.

5 Separation & subsequent biomolecule analysis of single mother-daughter cell pairs

One possibility is the additional implementation of magnetic forces either by functionalization of the cell membrane with magnetic beads or by the use of genetically modified iron-enriched yeast strains (283, 284). In the latter case, the mother yeast cell would be cultured in iron-enriched medium which would be replaced by standard medium before budding. The previous difference in medium composition in combination with the larger cell volume of the mother yeast would lead to a higher iron concentration in the mother cell than in the corresponding daughter (285). Consequently, the mother cell would be more strongly affected by the magnetic force than the daughter cell (Figure 42b). The same effect could be generated by functionalization of the mother cell membrane with magnetic beads before bud formation. As the membrane of the daughter yeast cell is newly produced during budding, the magnetic bead modification would not be inherited (283). A further improvement option is related to the microjunction geometry. To enable a more stable cell capture, the microjunction shape could be changed towards a prolonged and tapered design (Figure 42c). Thereby, the risk of flushing away the entire mother-daughter cell pair could be reduced. Depending on the testing and evaluation results of the above mentioned enhancements, the implementation of both strategies on the same device could be taken into consideration (Figure 42d). In this context, a recent study should be mentioned that used soft PDMS micropads to trap a single mother yeast cell (286). Therefore, the mother cell was captured between the bottom glass slide and the top PDMS part. Due to the significantly smaller size, the daughter cell was not affected by the PDMS part and could be removed by fluid flow. Inspired by this system, a further interesting design idea would include the implementation of PDMS based micro-pillars acting as valves which under pressurization would enable the physical capture of the mother cell from the top.

Apart from magnetic forces, a further approach is the implementation of optical tweezers. So far, several studies reported the successful use of highly focused laser beams for the manipulation of individual cells (270, 287). However, related drawbacks are the sophisticated and comparatively expensive technical equipment and the difficulty to carry out automated high throughput single cell measurements. In addition, undesired radical formation or heat generation could affect the subsequent biomolecule analysis. For instance, oxygen radicals could induce cell stress and consequently falsify the NAD(P)H measurements.

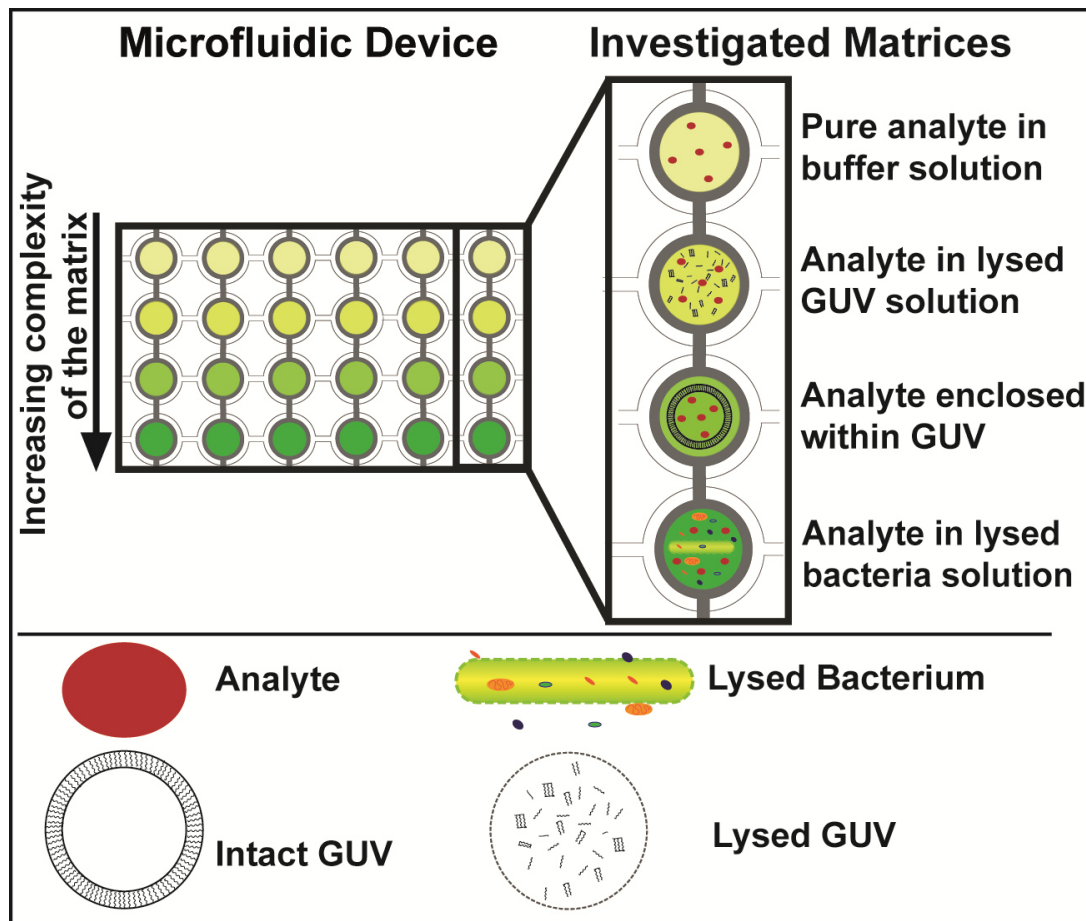
5.6 Conclusions

These first results prove that our device allows the separation and biomolecule analysis of mother and daughter cells. Future work will focus on the further development of the existing prototype towards reliable high throughput analysis. In addition, the acquisition of more data is aimed to obtain a better statistic validation of the results.

5.7 Acknowledgements

We gratefully acknowledge C. Bärtschi and H. Benz for the construction of the custom-built pressure control system and the clean room facility FIRST at the ETH Zurich. Furthermore, we would like to acknowledge Dr. Alfredo Ibanez who generously provided *Saccharomyces cerevisiae* YSN6. The work was funded by the European Research Council (ERC Starting Grant, Project No. 203428, n μ LIPIDs).

6 The influence of matrix effects on the analyte detection in immunoassays



The content of this chapter is prepared in the following research article: The influence of matrix effects on the analyte detection in immunoassays, [Simone Stratz](#), Karina Hasler, and Petra S. Dittrich, (2015).

Modifications made to the original publication

The figure numbering, the table numbering, and the reference numbering were changed. In addition, the supplementary information was integrated into the text of the main publication. Therefore, a few connecting sentences, which were not included in the original publication, were added to simplify the reading flow.

Contributions of the individual authors

Simone Stratz: Designed the research, planned and performed experiments, analyzed the data, and wrote the publication.

Karina Hasler: Planned and performed experiments, and analyzed the data.

Petra Dittrich: Designed the research and wrote the publication.

6.1 Abstract

Due to the provided high selectivity and sensitivity, immunoassays are widely used in a variety of applications like medical diagnostics, environmental safety testing, and research. So far, several studies reported the successful implementation of this powerful analytical method in microfluidic platforms, for example, for the biomolecule quantification in single mammalian cells or bacteria (chapter 3). The achieved low detection limits and high assay sensitivities demonstrate the advantages of combining both techniques. Nevertheless, comprehensive studies on the effect of different matrices in immunoassays performed on microfluidic devices are rarely found. With respect to the mentioned cell biological projects, the influence of membrane lipids and other cellular components on the assay signal are of particular interest. Therefore, we utilized the previously developed device and assay protocol to investigate the impact of cell-based matrices on the target analyte detection in PDMS microchips.

6.2 Introduction

Immunoassays have already been used since decades in laboratory medicine as they contribute in many cases significantly to the rapid and reliable diagnosis of disease, for example by the detection of specific antibodies related to HIV or tuberculosis in blood samples. Consequently, early and targeted patient treatment is facilitated. In recent years, the integration of immunoassays into miniaturized systems has been further developed (288, 289). In this context, an important driving force is the trend towards portable point-of-care (POC) diagnostic devices, that enable to perform fast medical testing under non-laboratory conditions (290, 291). Despite the reduction in size and weight of the final testing unit, performance of immunoassays on microchips provides further important benefits (292). The high surface area to volume ratio and the short distances lead to fast antibody antigen interactions and shorter assay times (293). In addition, the reagent consumption is greatly reduced contributing to much lower testing costs. A further important point concerning in particular cell biological research is related to the small well sizes that are ideally suited for single cell studies. Due to these advantages, several promising microfluidic devices for immunoassay-based analysis have already been reported. For instance, a recent study presented a POC microfluidic platform for the coinstantaneous diagnosis of HIV and syphilis antibodies from whole blood samples within a quarter of an hour (294). Loading of the reagents was performed by the use of prefilled tubing in combination with a bubble-based delivery method, that did not require motorized equipment (295). For the analyte detection, a silver-nitrate reagent solution and detection antibodies labeled with gold nanoparticles were used (296). The gold particles catalyzed the reduction of the silver ions to elemental silver. The resulting silver film was detectable by the human eye. Sensitivity and specificity of the microchip immunoassay were comparable to standard HIV tests with the key difference that no expensive laboratory equipment was required. This example illustrates on the one hand the great potential of miniaturized assay systems, but on the other clarifies a major challenge, namely the reliable detection of small analyte amounts in complex biological samples (297).

6 The influence of matrix effects on the analyte detection in immunoassays

In this context, the term matrix effect, which is defined as the sum of all sample components that have an impact on the assay performance apart from the analyte itself (298), should be discussed in more detail. The nature and extent of interferences depend strongly on the matrix type. In the field of biology, blood, urine and saliva are among the most common matrices (297). Typical interferences are related to unspecific binding of sample components to the antibody or to the target analyte. For example, numerous studies reported interferences in immunoassays caused by serum proteins such as the masking of the chromosomal protein HMGB1 associated with inflammatory diseases by IgG and IGM based autoantibodies (299). Aside from unspecific binding events, another main source of interferences are indirect disturbing factors such as matrix components inducing a change of the pH value or the ionic strength of the buffer solution and thereby reducing the strength of the antibody-antigen-complex (300). For instance, reduced binding-affinity caused by fluctuations in the pH of the matrix are a well-known issue in case of urine samples (301, 302).

Since ELISA systems are widely used, there are several well-established matrix management strategies available such as solid phase extraction (303), centrifugation (304), alternating current electrokinetics (305), or surface coatings (306). However, not all of these methods are compatible with the conditions of automated and miniaturized systems. This issue can be illustrated by the example of the above-mentioned POC device for the diagnosis of HIV and syphilis. The described assay was performed with unprocessed whole blood which is considered as a challenging matrix due to the complex composition including serum proteins, lipids, erythrocytes, leukocytes, platelets, amino acids, hormones, and various electrolytes. A standard matrix management strategy in case of blood samples is the performance of sample pretreatment steps such as centrifugation to remove cell debris. However, implementation of this method on a miniaturized POC device is rather difficult. Instead, the following precautions were undertaken to minimize matrix interferences. The used reagent delivery tubing was coated with BSA-Tween to prevent adsorption of serum proteins (294). Furthermore, sample dilution and washing steps were implemented. Both procedures are applied routinely in standard ELISA protocols. Especially washing steps can significantly reduce the background signal, since most non-specific binding events are based on relatively weak interactions. In the described study, the taken measures enabled to achieve an assay sensitivity that was comparable to commercial laboratory tests. Nevertheless, detection of low copy number analytes on POC ELISA systems remains challenging. This is, among other reasons, due to the difficulty to implement equipment-intensive sample preparation techniques on the devices. In addition, the data basis concerning matrix effects in microfluidic devices could be further broadened. Aim of the following project was therefore to study the particular influence of cell-based matrices on the analyte detection in immunoassays performed on PDMS microchips. For this purpose, the previously developed assay protocol for the detection of the intracellular enzyme β -galactosidase was performed with different test matrices and the impact on the analyte detection was analyzed.

6.3 Experimental

6.3.1 Reagents

All reagents were utilized as received. All solutions were prepared with ultrapurified water (Milli-Q System, Millipore®) if not mentioned otherwise. Silicon wafers were obtained from Si-Mat (Kaufering, Germany). Photoresist SU-8 2015 was obtained from Microchem (Newton, MA, USA). 1*H*,1*H*,2*H*,2*H*-perfluorodecyltrichlorosilane was supplied by ABCR (Karlsruhe, Germany). Sylgard® 184 silicone elastomer kit was purchased from Dow Corning (Midland, MI, USA). D(+)-glucose was obtained from Thermo Fisher Scientific (Geel, Belgium). LB agar powder, LB broth (Lennox) powder microbial growth medium, lysozyme powder from chicken egg white, trichloromethane, ethylenedinitrilotetraacetic acid disodium salt dihydrate (EDTA), fluorescein di- β -D-galactopyranoside (FDG), and protein G-biotin conjugate were supplied by Sigma-Aldrich (Buchs, Switzerland). Phosphate buffered saline (PBS) was purchased from Life Technologies Europe (Zug, Switzerland). Biotin-derivatized poly(l-lysine)-grafted poly(ethylene glycol) (PLL-g-PEG-biotin) and poly(l-lysine)-grafted poly(ethylene glycol) (PLL-g-PEG) were obtained from SuSoS AG (Dübendorf, Switzerland). Avidin was obtained from AppliChem (Gatersleben, Germany). Monoclonal anti- β -galactosidase antibody (mAB) was supplied by Santa Cruz Biotechnology (Dallas, TX, USA). Tris(hydroxymethyl)aminomethane hydrochloride (TRIS-HCl) was purchased from Bio-Rad (Richmond, CA, USA). 1,2-Dioleoyl-sn-glycero-3-phosphocholine (DOPC) and 1-Palmitoyl-2-oleoyl-sn-glycero-3-phosphocholine (POPC) were obtained from Avanti Polar Lipids (Alabaster, AL, USA).

6.3.2 Device fabrication

The experiments of this project were performed on a previously developed device for single mammalian cell analysis studies. All details of the fabrication process can be found in the supporting information of the corresponding publication (70). Shortly summarized, the used platform was constructed of two polydimethylsiloxane (PDMS) layers that formed the PDMS part of the device, which was assembled with a glass slide to seal off the fluid channels. The PDMS layers were produced independently by soft lithographic methods. The silicon master molds required for this purpose were fabricated by standard microfabrication techniques in a clean room facility. The precise parameters of the process steps performed in the clean room are indicated in Table 2 of section 2.1.2. The generated PDMS replica were bonded by oxygen plasma activation. Finally, the finished PDMS part and the glass slide were exposed to oxygen plasma and assembled resulting in the completed measurement device.

6.3.3 Bacteria cultivation and lysate preparation

All experiments of this project were carried out with *E. coli* of the strain MG1655. Detailed information about the long-term and short-term maintenance are provided in section 2.3. For performance of the *E. coli* matrix experiments, a preculture was prepared the day before. Therefore, 3 mL LB medium completed with 20 mM glucose were inoculated with a single *E. coli* colony of the LB agar plate. The following incubation was performed in a 15 mL falcon tube at 37 °C with constant shaking at 220 rpm (KS 4000 i control, IKA, Staufen, Germany) until the optical density measured at 600 nm (OD₆₀₀) was approximately 1. For preparation of the lysate, 100 µL of the *E. coli* culture were added to 1 mL lysis buffer (10 mM Tris-HCl completed with 1 mM EDTA, 0.1 mM NaCl, and 10 mg/mL lysozyme, pH 8.0) and incubated under constant shaking at 300 rpm (Eppendorf® Thermomixer Compact, Eppendorf, Germany) at 37 °C for 30 min. Next, the lysate mixture was washed twice with PBS by centrifugation (14,100g, 4 min, Eppendorf® MiniSpin plus, Eppendorf, Germany) to remove remaining lysis buffer components. Finally, the lysate precipitate was dilute with 1 mL PBS before introduction into the device.

6.3.4 Giant unilamellar vesicle preparation by electroformation

The first set of experiments was performed with giant unilamellar vesicles (GUVs) that did not incorporate the target analyte. The GUVs were immobilized in a separate step after the β-galactosidase incubation phase. The GUVs used in these measurements were prepared according to the electroformation method as described in previous publications of the Dittrich group (307, 308). For this purpose, a custom-built, temperature-regulated device was utilized consisting of two indium tin oxide (ITO) coated glass slides (15-25 Ω sq⁻¹, Sigma-Aldrich), which were separated by a 1.5 mm thick silicone spacer. The device was embedded in an aluminum holder. The required AC field was created by a function generator (HMF2525, HAMEG Instruments, Mainhausen, Germany), which was connected to the ITO coated glass slides by copper strips. The lipid solution (mixture of DOPC (1 mM in methanol) and chloroform (1:10 (v/v))) was dried overnight on the ITO glass slide surfaces under vacuum and afterwards rehydrated by ultrapure water (Milli-Q System, Millipore®). Next, the chamber was completely sealed by the use of silicone paste and the device was fully assembled. For GUV formation, the power generator was set to 0.1 V at a frequency of 10 Hz. Next, the voltage was increased by 0.2 V in time intervals of 10 min until a final voltage of 0.7 V was reached. The voltage was applied for 4 h at room temperature (RT). In a final step, the AC field was turned off and the GUVs were collected by gentle pipetting. The obtained GUV solution was stored at 4 °C until usage.

6.3.5 Giant unilamellar vesicle preparation by water-oil emulsion transfer

A further set of measurements was carried out with GUVs directly incorporating the target analyte β -galactosidase. The GUVs utilized in these experiments were prepared by the water-oil emulsion transfer method, as this protocol, unlike the above mentioned one, allowed to wash the completed GUVs by centrifugation. In a first step, an oil-water interface was generated. Therefore, 500 μ L hosting solution (1 osmol glucose in ultrapure water) was pipetted into a 2 mL Eppendorf tube. Next, 200 μ L of phospholipid solution (200 μ M POPC dissolved in mineral oil) were carefully added on top of the hosting solution. An incubation phase was carried out at RT until the curvature of the interface flattened. In the meantime, 50 μ L of the β -galactosidase-sucrose solution (β -galactosidase (2 μ M in ultrapure water) and sucrose (3 osmol in ultrapure water) (2:1)) and 500 μ L phospholipid solution were pipetted into a 2 mL Eppendorf tube, which was subsequently agitated by scratching 5 times over a rack. Afterwards, 500 μ L of the thereby generated water-oil-emulsion were pipetted on top of the interphase. Subsequent centrifugation was carried out at 4729 rpm (Eppendorf® MiniSpin plus, Eppendorf, Germany) at RT. The supernatant was removed by an aspirator and 100 μ L of hosting solution were added to the remaining pellet localized at the bottom of the tube. After several aspiration steps performed by gentle pipetting, the mixture was centrifuged again (4729 rpm, 3 min, RT). To eliminate the remaining oil residue, 150 μ L of fluid were removed from the top of the tube. To remove excess β -galactosidase molecules, the vesicles were washed three times with hosting solution by centrifugation (4729 rpm, 3 min, RT). The obtained GUVs solution was stored at 4 °C until usage.

6.3.6 Performance of the immunoassay for β -galactosidase

The surface modification required for the performance of the β -galactosidase assay was performed as described in section 3.3.3. First, the microfluidic platform was placed on an inverted microscope (Olympus IX70) and complete closure of all microchamber subsets was ensured. Next, the different β -galactosidase concentrations were introduced successively into the device starting with the lowest concentration. Fluid flow was generated by means of a syringe pump (Nanojet, CHEMYX, Stafford, USA). The flow rate was set to 10 μ L/min. The previous described pressure control system operated by a custom-made LabVIEW software was used to immobilize different β -galactosidase concentrations in discrete microchamber subsets. Consequently, it was possible to measure different β -galactosidase concentrations on the same device. After β -galactosidase immobilization, a 10 min washing step with PBS (flow rate of 5 μ L/min, closed microchambers) was carried out. Next, the freshly prepared substrate solution (250 nM fluorescein di- β -D-galactopyranoside (FDG) in PBS) was loaded into the device and subsequently into the microchambers (10 μ L/min, 750 ms opening time, 5 s delay time between opening different chambers). Data acquisition was started directly after the substrate was added. Therefore, fluorescent images were taken every 15 min of every microchamber subset for a period of 1h (4X objective, exposure time 300 ms, gain X100, excitation filter: 470/40, and emission filter: 525/50).

6 The influence of matrix effects on the analyte detection in immunoassays

Each β -galactosidase concentration was immobilized on multiple microchambers and devices to analyze if the chamber position within the image area or the device itself strongly affect the fluorescence signal. As only minor deviations were detected, a significant influence of the above mentioned aspects can be excluded. The protocol described here refers to the assay performance with pure analyte solution. To study the influence of the different matrix effects, additional immobilization steps were required which are explained in detail in the following sections.

6.3.7 Performance of the immunoassay with *E. coli* lysate as matrix component

To analyze the effect of the *E. coli* lysate matrix on the analyte detection, the following test case was evaluated. The *E. coli* lysate was introduced into the device in the final step of the assay protocol. Therefore, the lysate was added directly to the substrate solution to a final OD600 of 0.1 corresponding to around 50 bacteria per microchamber. The remaining steps and parameters of the immunoassay protocol were performed as described in section 6.3.6.

6.3.8 Performance of the immunoassay with GUVs as matrix component

To investigate the influence of the GUV matrix on the analyte detection, two different test cases were evaluated. In a first test case under investigation, the GUVs were immobilized in a separate step after the 30 min incubation time of the target analyte β -galactosidase and before substrate addition. Despite the attempt to trap only a single GUV per microchamber, the load of multiple GUVs frequently occurred, and the corresponding microchambers were also analyzed. To confirm the GUV load, bright field pictures were taken of every microchamber using an EMCCD camera (iXon Ultra, Andor Technologies, Ireland) in combination with a 60X water immersion objective. In a second test case under investigation, the analyte β -galactosidase was directly enclosed in the GUVs in a final concentration of 2 μ M corresponding in case of a single GUV with a diameter of 10 μ m to around 600000 enzyme copies. The β -galactosidase immobilization step was replaced by the GUV immobilization step. Next, bright field pictures were taken of every microchamber to confirm the GUV load. Afterwards, lysis buffer (10 mM Tris-HCl completed with 1 mM EDTA, 0.1 mM NaCl, and 10 mg/mL lysozyme, pH 8.0) was introduced to the microchambers to induce GUV membrane rupture followed by a 30 min incubation time. The remaining steps and parameters of the immunoassay protocol were performed as described in section 6.3.6.

6.3.9 Data analysis

The acquired fluorescence images were analyzed by the image processing software ImageJ. The fluorescence signal of the whole chamber area was measured. For background correction, an area of identical pixel size situated in the PDMS region next to the corresponding microchamber was analyzed. Thereby, small intensity deviations of the fluorescence signal within the image and device-to-device variations were balanced out. A detailed description of this data evaluation step is provided in section 3.3.6. The corrected fluorescent values were plotted against time, as illustrated in Figure 43.

6.4 Results

6.4.1 Immunoassay performed without additional matrix

In a first set of experiments, the immunoassay for β -galactosidase was performed with pure analyte solutions. The assay was carried out for different known β -galactosidase concentrations. Each concentration was measured in multiple microchambers and devices. The resulting calibration curve was used to determine the dynamic range of the assay over which the β -galactosidase concentrations could be quantified with acceptable precision and accuracy. Main evaluation criteria were thereby the coefficient of determination (R^2) of the performed linear regression and the standard deviations of the underlying fluorescent signal over time curves (Figure 43).

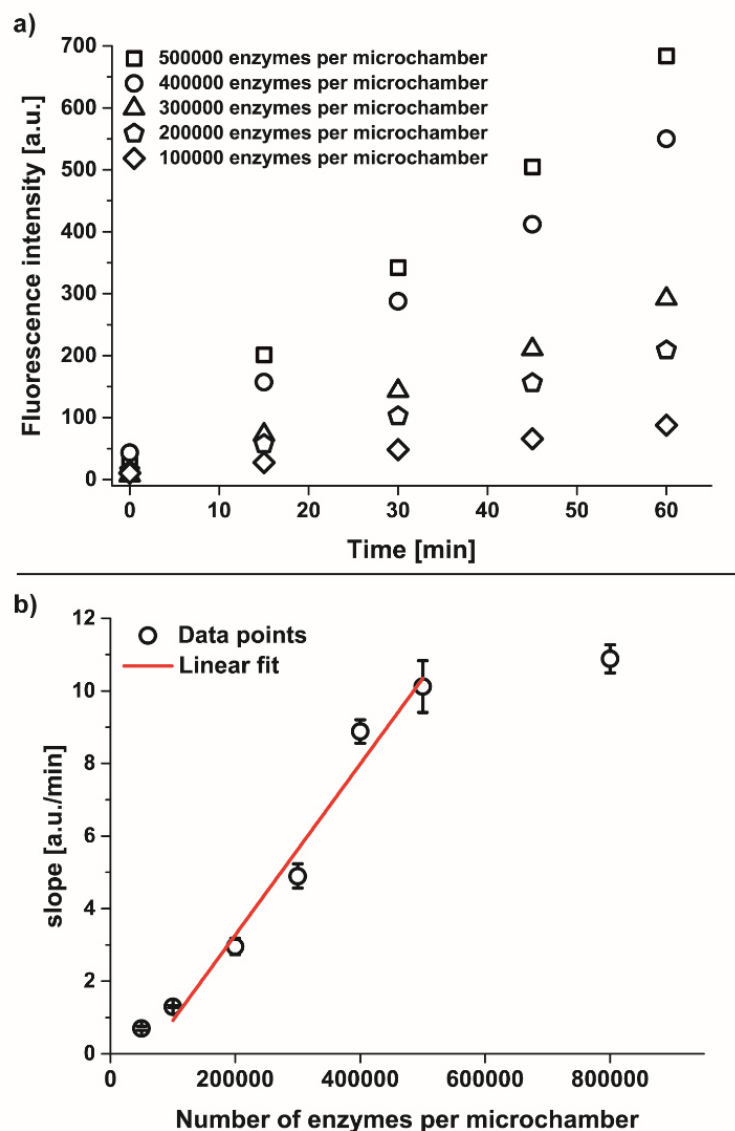


Figure 43: **Performance of the β -galactosidase immunoassay without additional matrix.** a) Example curves. Fluorescence signal over time plots for the different β -galactosidase concentrations defining the dynamic range of the assay. b) On-chip calibration curve. The slopes of the different fluorescence signal over time curves were plotted against the corresponding number of enzymes. In the dynamic range of the assay, a linear correlation is exhibited (red line, $R^2 = 0.97$). For enzyme concentrations outside of the dynamic range, the curve flattened and reliable analyte quantification was not anymore possible.

6.4.2 Immunoassay performed with *E. coli* lysate as additional matrix

In a next series of experiments, the immunoassay for β -galactosidase was carried out with *E. coli* lysate instead of with pure analyte solution as matrix. For this purpose, the *E. coli* lysate was immobilized together with the substrate FDG during the last step of the assay protocol. Consequently, the lysate affected mostly the substrate conversion process and not the antibody-antigen binding interactions, as the β -galactosidase immobilization was performed previously in the absence of the *E. coli* lysate. For the lower enzyme concentrations, no significant matrix effect was observed. The detected fluorescence signals (Figure 44, first four data points (counted from the left), open black squares) were comparable to those obtained for the immunoassay performed without additional matrix (Figure 44, first four data points (counted from the left), open red circles). For higher enzyme concentrations (last two data points corresponding to 400000 and 500000 enzymes per microchamber, respectively), slightly weaker fluorescence signals were detected. A possible explanation is that the lysate components affect in particular the small amount of unbound enzymes. It is assumed that the access to fresh substrate molecules is hindered by the high density of lysate particles diffusing throughout the substrate solution. Although the position of the dynamic equilibrium lies strongly on the side of the bound enzymes, the small number of free enzymes has an impact on the product formation rate due to the higher activity. In this context, reference is made to several studies demonstrating reduced enzyme activity in the bound β -galactosidase fraction due to steric hindrance (309, 310). As the absolute amount of free enzymes is higher for higher enzyme concentrations, this could be an explanation why the effect was not observed to the same extend for the lower β -galactosidase copy numbers.

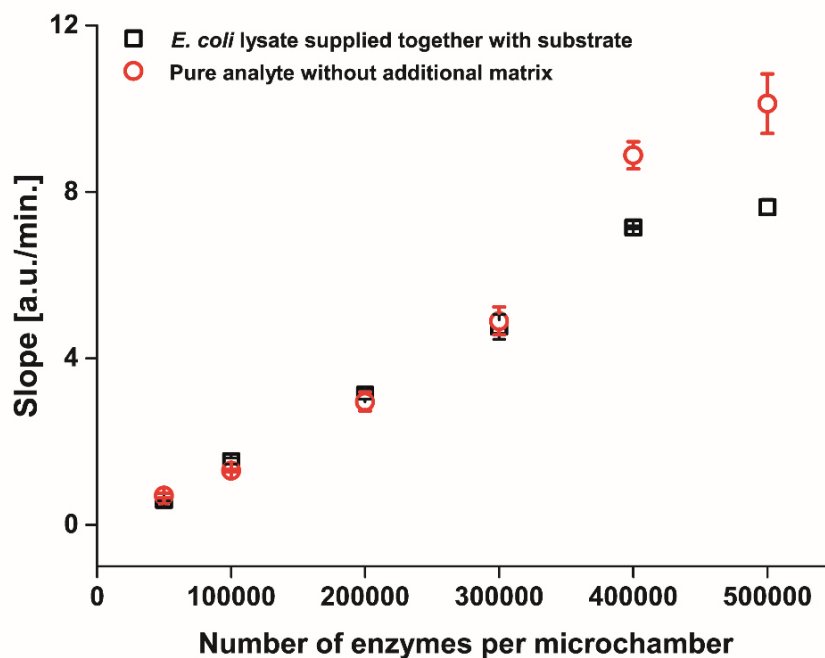


Figure 44: **On-chip calibration curves illustrating the influence of the *E. coli* matrix on the detected fluorescence signal.** In case of the *E. coli* lysate spiked substrate solution, a slight decrease in the fluorescent signal was observed for the high β -galactosidase concentrations (open black squares) compared to the data of the pure analyte samples (open red circles).

6.4.3 Immunoassay performed with GUVs as additional matrix

In a further step, the influence of the GUV matrix on the immunoassay for β -galactosidase was investigated. Therefore, single or a few GUVs were immobilized within the microchambers before the substrate FGD was added. As depicted in Figure 45, the GUV matrix affected the measurements of all analyzed β -galactosidase concentrations resulting in a decrease of the fluorescence signal (open black rectangles) compared to the test cases performed without additional matrix (open red circles) or with *E. coli* matrix (open black squares), respectively. This effect is most likely caused by physical masking of the antibody or the target analyte by the phospholipids as documented in literature on the subject (311, 312). The correlation of the number of immobilized GUVs and extend of signal decrease did not lead to unambiguous results. Nevertheless, the overall trend of the evaluated measurement data clearly confirmed a weakening of the fluorescence signal.

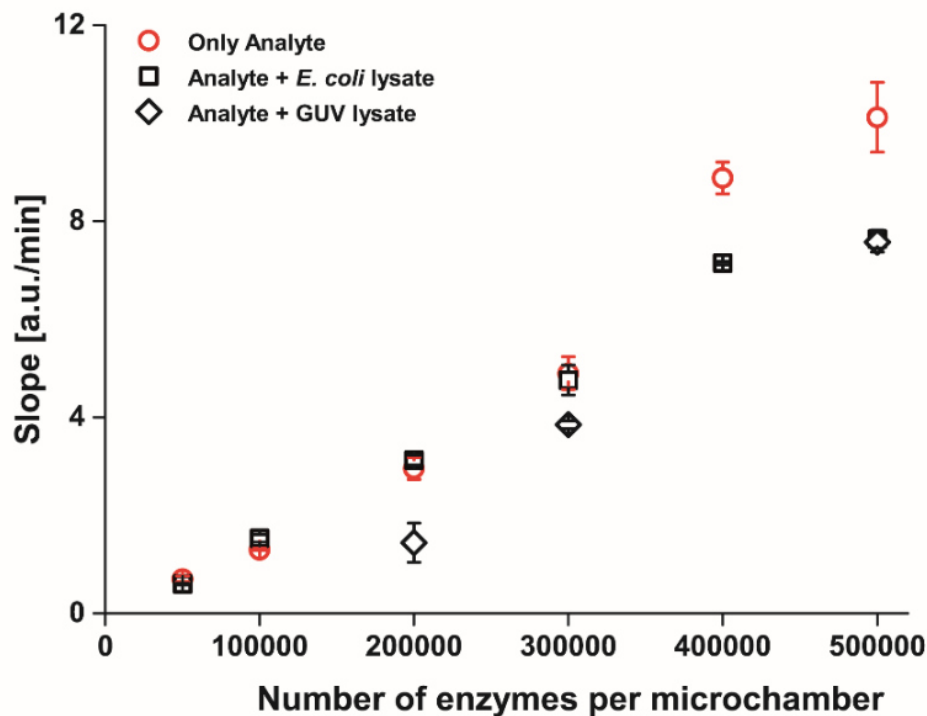


Figure 45: **On-chip calibration curve illustrating the influence of the GUV matrix on the detected fluorescence signal.** In case the immunoassay was performed with GUVs as additional matrix, a decrease in the fluorescent signal was measured for all analyzed β -galactosidase concentrations (open black rectangles) in comparison to the data of the matrix free samples (open red circles). In addition, the GUV matrix had a greater impact than the *E. coli* lysate matrix (open black squares).

6 The influence of matrix effects on the analyte detection in immunoassays

In addition, a protocol was established that enabled the direct immobilization of the analyte β -galactosidase within the GUVs. Therefore, the GUV formation method was changed from electroformation to water-oil-emulsion transfer, as the latter allowed to wash the freshly prepared GUVs by centrifugation. The washing step was crucial, as otherwise large amounts of excess analyte remained in the GUV solution resulting in high background signals. The implemented adaptations described in detail in section 6.3.5 significantly reduced the background signal. As a result, it was possible to distinguish between microchambers occupied by a single GUV enclosing the analyte β -galactosidase and empty, GUV-free microchambers (Figure 46).

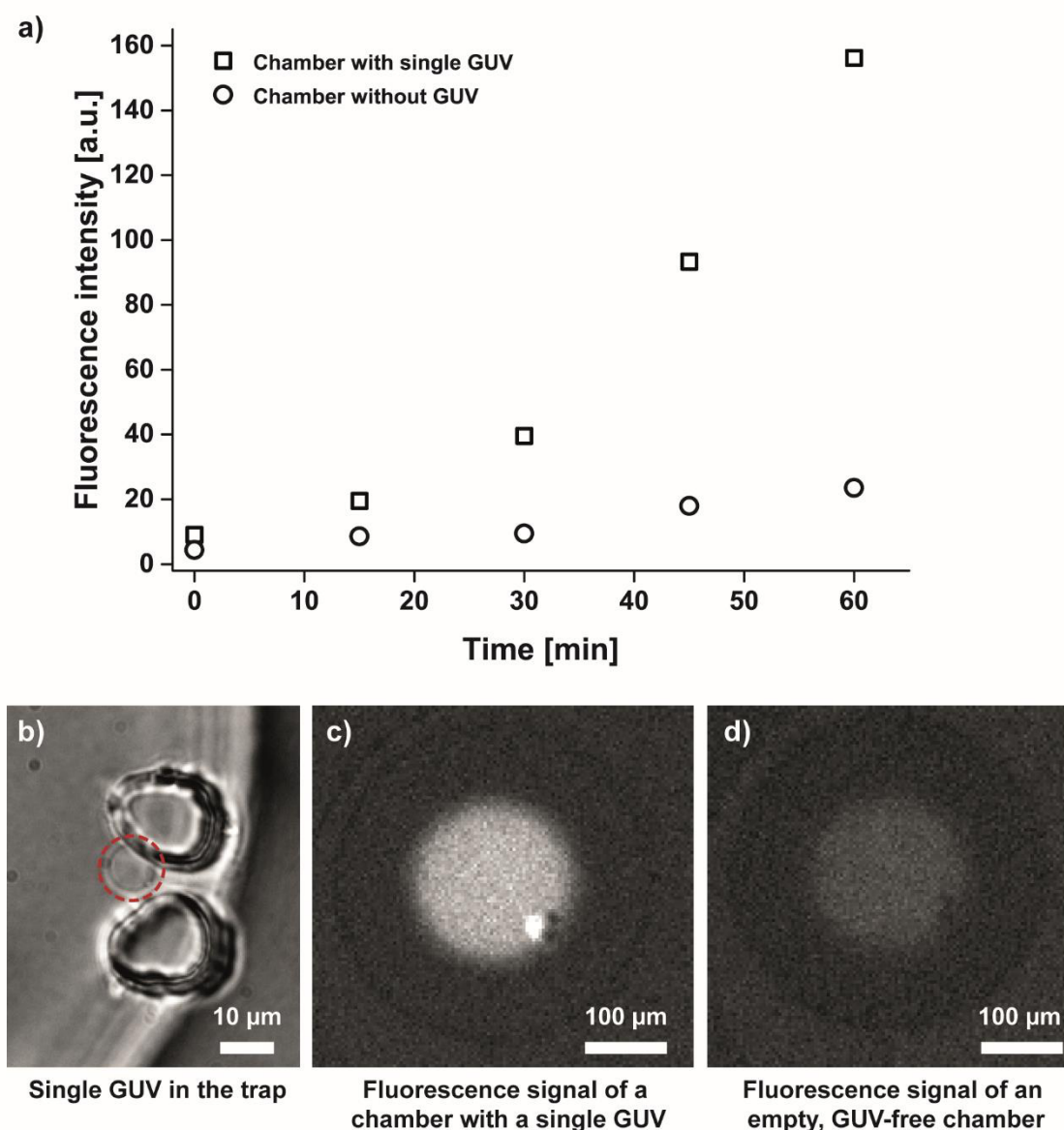


Figure 46: Immunoassay performed with single GUVs directly enclosing the target analyte β -galactosidase. a) Example plots of the fluorescence signal over time curves in case of an empty microchamber (open black circles) and in case of a single trapped GUV (open black squares), respectively. b) Bright field picture of a single GUV physically captured within the cell trap. c) Fluorescent picture of a microanalysis chamber enclosing the lysate of a single GUV ($t = 60$ min). d) Fluorescent picture of an empty, GUV-free microanalysis chamber ($t = 60$ min).

6.5 Conclusions

These first results indicate a significant impact of cell-based matrices on analyte detection in immunoassays. In addition, a main advantage of the microanalysis chamber design, namely the straightforward implementation of washing steps, is nicely illustrated. Consequently, the obtained findings confirm that the multiple flushing steps integrated in previous assay protocols (Table 4) contributed to the achieved low detection limits and high assay sensitivities. Future work will focus on the testing of further matrices like yeast lysate and the acquisition of more data to receive a comprehensive overview of the effect of a particular matrix on the assay outcome.

6.6 Acknowledgements

We gratefully acknowledge C. Bärtschi and H. Benz for the construction of the custom-built pressure control system and the clean room facility FIRST at the ETH Zurich. Furthermore, we would like to acknowledge Bernhard Sebastian and Pascal Verboket for providing advice on vesicle formation. The work was funded by the European Research Council (ERC Starting Grant, Project No. 203428, n μ LIPIDs).

7 Conclusion and outlook

The main focus of this thesis was on the development of microfluidic devices suitable for the quantification of biomolecules in single microbes. For realization of this research objective, four different projects were carried out. In the following, the development potential of each project is discussed separately with regard to the overarching goal of comprehensive high throughput single cell analysis. Particular emphasis is on the further development opportunities concerning the microfluidic platform itself as well as the optimization and expansion of the current applications.

The first performed study focused on the development of a microfluidic platform adapted to the requirements of microbes significantly smaller than the former analyzed mammalian cells. The completed prototype was successfully used for the analysis of individual *E. coli* bacteria. The analysis of the single cell lysates was performed in microchambers enclosing a volume in the low picoliter range. Due to the small volume and the high sensitivity of the implemented immunoassay, a very low limit of quantification of a few hundred analyte molecules was achieved. Thereby, the obtained results demonstrated the suitability of the device for biomolecule quantification in single microbes. Possible technical improvements are related to the automation and parallelization of the platform, for example by the use of a programmable motorized microscope stage together with automated image acquisition and processing methods. In combination with an increased number of microanalysis chambers, the simultaneous analysis of several hundred cells could be feasible. In addition, the analyte detection method should be changed, as the use of enzymes producing fluorescent products is not well-suited for multiple analyte measurements. Even the utilization of fluorophores with very narrow excitation and emission spectra would not allow to detect more than a few analytes in parallel. A promising alternative are DNA-labeled detection antibodies for PCR-based target molecule quantification. On-chip performance of the required polymerase chain reaction should be possible by minor modifications of the existing chip design. The resulting multiple analyte detection technique would enable to explore more complex systems, for example entire cell signaling pathways involving numerous different biomolecules. Possible applications after successful implementation of the discussed enhancements concern, for instance, the investigation of the emergence of multi-resistant phenotypes in bacteria populations.

The second project aimed the development of a multifunctional platform optimized for *Saccharomyces cerevisiae* cells. Key characteristic of the fully developed system was a convenient double-valve configuration that enabled the successful combination of cell culture experiments with quantitative biomolecule analysis. Further development options include the expansion of the existing number of analysis chambers to increase the throughput of the performed measurements. In future applications the platform could be used to simulate on one device varying nutrient conditions. This would enable to cultivate subsets of individual cells under differing microenvironments. The subsequently performed biomolecule analysis would enable to investigate in a highly controlled and differentiated manner the influence of different stress stimuli or environmental factors on the proteome.

7 Conclusion and outlook

In the first instance, the impact of a particular stress factor could be analyzed. Furthermore, it would be possible to study if individual cells exposed to the same stress factor show a dissimilar biological response behavior. As all experiments would be performed on one single device with cells originating from the same preculture, influences of the set-up or the cell cultivation itself could be minimized. To draw meaningful conclusions on how homogeneous or heterogeneous a population responds to environmental fluctuations, a substantial number of cells has to be analyzed. Consequently, optimization of the device design towards high throughput measurements is given priority.

The objective of the third project was to investigate the impact of inheritance noise on the emergence of cellular heterogeneity. For this purpose, a platform was designed that enabled the on-chip separation and subsequent analysis of single *S. cerevisiae* mother-daughter cell pairs. The short-term goal is the improvement of the existing prototype with regard to the number of cell pairs that can be analyzed in parallel and the efficiency of the cell separation process. In this context, the existing cell separation procedure mainly based on physical cell capture and the dynamic forces of the applied fluid flows should be complemented by, for example, the use of magnetic forces or additional PDMS stamps located directly above the corresponding cell capture microjunctions. The long-term goal is the expansion of the current scope of applications towards the investigation of yet not fully explored and explained processes taking place during cell division. For example, it was reported in several studies that aged-mother yeast cells produce daughters with shorten life-span. It is assumed, that certain substances and mRNA molecules accumulating in aged cells induce the observed reduced life span potential. So far, the exact underlying molecular mechanisms are not completely elucidated. Since the developed device enables the quantitative biomolecule analysis of separated mother and daughter cell pairs, this could be an interesting research issue to be addressed. In addition, the implementation of slight modifications could enable the analysis of inheritance noise in further cell types, for example in bacteria or mammalian cells.

In the fourth study, the impact of matrix effects on analyte detection in immunoassays was investigated. The obtained findings indicate a significant influence of different cell-based matrices on the target molecule quantification. In the next project phase, the developed protocol for the enclosure of the target analyte in single GUVs could be optimized with regard to the stability and uniformity of the generated GUVs. Further studies could be performed with GUVs differing in their membrane composition. The ultimate objective is to reliably estimate the effect of a particular matrix component, for example a distinct membrane lipid, on the detected assay signal. In this context, the use of GUVs instead of real cells is advantageous. First, the composition of a GUV serving as minimalistic artificial cell model is less complex than the composition of a real cell. Second, the variations between individual GUVs are expected to be much smaller than between individual cells. The focus of the performed experiments should be on GUVs as the thereby created test system would be less susceptible to variations not related to the matrix effect itself. Thereby, a comprehensive picture of the impact of matrix effects on immunoassays would be provided.

In a nutshell, the challenge of future work is to bundle the new knowledge acquired from the above presented projects to develop a multifunctional device suitable for high throughput proteomics and metabolomics of single cells originating from various cell types.

8 References

1. E. K. Sackmann, A. L. Fulton, D. J. Beebe, The present and future role of microfluidics in biomedical research. *Nature* **507**, 181-189 (2014).
2. G. M. Whitesides, The origins and the future of microfluidics. *Nature* **442**, 368-373 (2006).
3. J. Melin, S. R. Quake, Microfluidic large-scale integration: the evolution of design rules for biological automation. *Annual Review of Biophysics and Biomolecular Structure* **36**, 213-231 (2007).
4. G. Karniadakis, A. Beskok, N. Aluru, Basic Concepts and Technologies. In *Microflows and nanoflows: fundamentals and simulation*, vol. 29, Springer Science & Business Media, New York, 2005.
5. S. C. Terry, J. H. Jerman, J. B. Angell, A gas chromatographic air analyzer fabricated on a silicon wafer. *IEEE Transactions on Electron Devices* **26**, 1880-1886 (1979).
6. M. Esashi, S. Shoji, A. Nakano, in *Micro Electro Mechanical Systems, 1989, Proceedings, An Investigation of Micro Structures, Sensors, Actuators, Machines and Robots. IEEE.* (1989), pp. 29-34.
7. F. C. M. Van de Pol, H. T. G. Van Lintel, M. Elwenspoek, J. H. J. Fluitman, A thermopneumatic micropump based on micro-engineering techniques. *Sensors and Actuators A: Physical* **21**, 198-202 (1990).
8. A. Manz, Y. Miyahara, J. Miura, Y. Watanabe, H. Miyagi, K. Sato, Design of an open-tubular column liquid chromatograph using silicon chip technology. *Sensors and Actuators B: Chemical* **1**, 249-255 (1990).
9. A. Manz, N. Graber, H. M. Widmer, Miniaturized total chemical analysis systems: A novel concept for chemical sensing. *Sensors and Actuators B: Chemical* **1**, 244-248 (1990).
10. Y. Xia, G. M. Whitesides, Soft Lithography. *Angewandte Chemie International Edition* **37**, 550-575 (1998).
11. P. S. Dittrich, A. Manz, Lab-on-a-chip: microfluidics in drug discovery. *Nature Reviews Drug Discovery* **5**, 210-218 (2006).
12. P. Neuži, S. Giselbrecht, K. Länge, T. J. Huang, A. Manz, Revisiting lab-on-a-chip technology for drug discovery. *Nature Reviews Drug Discovery* **11**, 620-632 (2012).
13. C. D. Chin, V. Linder, S. K. Sia, Commercialization of microfluidic point-of-care diagnostic devices. *Lab on a Chip* **12**, 2118-2134 (2012).
14. F. Lautenschläger, M. Piel, Microfabricated devices for cell biology: all for one and one for all. *Current Opinion in Cell Biology* **25**, 116-124 (2013).
15. P. N. Nge, C. I. Rogers, A. T. Woolley, Advances in Microfluidic Materials, Functions, Integration, and Applications. *Chemical Reviews* **113**, 2550-2583 (2013).

8 References

16. K. S. Elvira, X. C. i Solvas, R. C. R. Wootton, A. J. deMello, The past, present and potential for microfluidic reactor technology in chemical synthesis. *Nature Chemistry* **5**, 905-915 (2013).
17. T. M. Squires, S. R. Quake, Microfluidics: Fluid physics at the nanoliter scale. *Reviews of Modern Physics* **77**, 977-1026 (2005).
18. D. J. Beebe, G. A. Mensing, G. M. Walker, Physics and applications of microfluidics in biology. *Annual Review of Biomedical Engineering* **4**, 261-286 (2002).
19. D. Janasek, J. Franzke, A. Manz, Scaling and the design of miniaturized chemical-analysis systems. *Nature* **442**, 374-380 (2006).
20. O. Reynolds, An Experimental Investigation of the Circumstances Which Determine Whether the Motion of Water Shall Be Direct or Sinuous, and of the Law of Resistance in Parallel Channels. *Philosophical Transactions of the Royal Society of London* **174**, 935-982 (1883).
21. H. Chanson, Part 1 Basic Principles of Open Channel Flows. In *Hydraulics of Open Channel Flow: An Introduction*, Butterworth-Heinemann, Oxford, 2004.
22. K. Avila, D. Moxey, A. de Lozar, M. Avila, D. Barkley, B. Hof, The Onset of Turbulence in Pipe Flow. *Science* **333**, 192-196 (2011).
23. S. Pennathur, C. D. Meinhart, H. T. Soh, How to exploit the features of microfluidics technology. *Lab on a Chip* **8**, 20-22 (2008).
24. K. W. Overton, S. L. Spencer, W. L. Noderer, T. Meyer, C. L. Wang, Basal p21 controls population heterogeneity in cycling and quiescent cell cycle states. *Proceedings of the National Academy of Sciences of the United States of America* **111**, E4386-E4393 (2014).
25. S. J. Altschuler, L. F. Wu, Cellular heterogeneity: when do differences make a difference? *Cell* **141**, 559-563 (2010).
26. I. Keren, D. Shah, A. Spoering, N. Kaldalu, K. Lewis, Specialized Persister Cells and the Mechanism of Multidrug Tolerance in *Escherichia coli*. *Journal of Bacteriology* **186**, 8172-8180 (2004).
27. K. Lewis, Persister cells, dormancy and infectious disease. *Nature Reviews Microbiology* **5**, 48-56 (2007).
28. B. W. Kwan, N. Chowdhury, T. K. Wood, Combatting bacterial infections by killing persister cells with mitomycin C. *Environmental Microbiology*, doi: 10.1111/1462-2920.12873 (2015).
29. A. Y. Mitrophanov, E. A. Groisman, Positive feedback in cellular control systems. *BioEssays : news and reviews in molecular, cellular and developmental biology* **30**, 542-555 (2008).
30. N. T. Ingolia, A. W. Murray, Positive-Feedback Loops as a Flexible Biological Module. *Current Biology* **17**, 668-677 (2007).

8 References

31. C. E. Meacham, S. J. Morrison, Tumour heterogeneity and cancer cell plasticity. *Nature* **501**, 328-337 (2013).
32. R. A. Burrell, N. McGranahan, J. Bartek, C. Swanton, The causes and consequences of genetic heterogeneity in cancer evolution. *Nature* **501**, 338-345 (2013).
33. K. M. Gligorich, R. M. Vaden, D. N. Shelton, G. Wang, C. B. Matsen, R. E. Looper, M. S. Sigman, B. E. Welm, Development of a screen to identify selective small molecules active against patient-derived metastatic and chemoresistant breast cancer cells. *Breast Cancer Research : BCR* **15**, R58-R58 (2013).
34. M. Leewenhoek, R. de Graaf, A Specimen of Some Observations Made by a Microscope, Contrived by M. Leewenhoek in Holland, Lately Communicated by Dr. Regnerus de Graaf. *Philosophical Transactions* **8**, 6037-6038 (1673).
35. M. Minsky, Memoir on inventing the confocal scanning microscope. *Scanning* **10**, 128-138 (1988).
36. A. L. Mattheyses, S. M. Simon, J. Z. Rappoport, Imaging with total internal reflection fluorescence microscopy for the cell biologist. *Journal of Cell Science* **123**, 3621-3628 (2010).
37. B. Valeur, J.-C. Brochon, in *New trends in fluorescence spectroscopy: applications to chemical and life sciences*, vol. 1, Springer Science & Business Media, New York, 2001.
38. X. Michalet, A. N. Kapanidis, T. Laurence, F. Pinaud, S. Doose, M. Pflughoefft, S. Weiss, The power and prospects of fluorescence microscopies and spectroscopies. *Annual review of biophysics and biomolecular structure* **32**, 161-182 (2003).
39. J. W. Lichtman, J.-A. Conchello, Fluorescence microscopy. *Nature Methods* **2**, 910-919 (2005).
40. A. A. Cohen, N. Geva-Zatorsky, E. Eden, M. Frenkel-Morgenstern, I. Issaeva, A. Sigal, R. Milo, C. Cohen-Saidon, Y. Liron, Z. Kam, L. Cohen, T. Danon, N. Perzov, U. Alon, Dynamic Proteomics of Individual Cancer Cells in Response to a Drug. *Science* **322**, 1511-1516 (2008).
41. A. Manz, P. S. Dittrich, N. Pamme, D. Iossifidis, OPTICAL SPECTROSCOPY. In *Bioanalytical Chemistry*, Imperial College Press, London, 2015.
42. J.-Q. Wu, T. D. Pollard, Counting Cytokinesis Proteins Globally and Locally in Fission Yeast. *Science* **310**, 310-314 (2005).
43. A. Meunier, O. Jouannot, R. Fulcrand, I. Fanget, M. Bretou, E. Karatekin, S. Arbault, M. Guille, F. Darchen, F. Lemaître, C. Amatore, Coupling Amperometry and Total Internal Reflection Fluorescence Microscopy at ITO Surfaces for Monitoring Exocytosis of Single Vesicles. *Angewandte Chemie* **123**, 5187-5190 (2011).

8 References

44. M. Brown, C. Wittwer, Flow Cytometry: Principles and Clinical Applications in Hematology. *Clinical Chemistry* **46**, 1221-1229 (2000).
45. A. L. Givan, in *Flow Cytometry: First Principles*, John Wiley & Sons, Inc., New York, 2001.
46. A. Moldavan, PHOTO-ELECTRIC TECHNIQUE FOR THE COUNTING OF MICROSCOPICAL CELLS. *Science* **80**, 188-189 (1934).
47. M. D. Graham, The Coulter Principle: Foundation of an Industry. *Journal of the Association for Laboratory Automation* **8**, 72-81 (2003).
48. W. H. Coulter. (Google Patents, 1953).
49. L. S. Cram, D. Arndt-Jovin, Mack Jett Fulwyler, pioneer of flow cytometry and flow sorting (1936–2001). *Cytometry Part A* **67A**, 53-60 (2005).
50. R. C. Leif, Practical flow cytometry. *Cytometry* **19**, 376-376 (1995).
51. L. A. Herzenberg, R. G. Sweet, L. A. Herzenberg, FLUORESCENCE-ACTIVATED CELL SORTING. *Scientific American* **234**, 108-117 (1976).
52. L. A. Herzenberg, D. Parks, B. Sahaf, O. Perez, M. Roederer, L. A. Herzenberg, The History and Future of the Fluorescence Activated Cell Sorter and Flow Cytometry: A View from Stanford. *Clinical Chemistry* **48**, 1819-1827 (2002).
53. S. C. Bendall, G. P. Nolan, M. Roederer, P. K. Chattopadhyay, A deep profiler's guide to cytometry. *Trends in Immunology* **33**, 323-332 (2012).
54. W. Kern, U. Bacher, C. Haferlach, T. Alpermann, S. Schnittger, T. Haferlach, Multiparameter flow cytometry provides independent prognostic information in patients with suspected myelodysplastic syndromes: A study on 804 patients. *Cytometry Part B: Clinical Cytometry* **88**, 154-164 (2015).
55. Y. Hu, L. Fan, J. Zheng, R. Cui, W. Liu, Y. He, X. Li, S. Huang, Detection of circulating tumor cells in breast cancer patients utilizing multiparameter flow cytometry and assessment of the prognosis of patients in different CTCs levels. *Cytometry Part A* **77A**, 213-219 (2010).
56. P. Dalerba, S. J. Dylla, I.-K. Park, R. Liu, X. Wang, R. W. Cho, T. Hoey, A. Gurney, E. H. Huang, D. M. Simeone, A. A. Shelton, G. Parmiani, C. Castelli, M. F. Clarke, Phenotypic characterization of human colorectal cancer stem cells. *Proceedings of the National Academy of Sciences of the United States of America* **104**, 10158-10163 (2007).
57. S. Fraser, M. Cameron, E. O'Connor, M. Schwickart, M. Tanen, M. Ware, Next Generation Ligand Binding Assays—Review of Emerging Real-Time Measurement Technologies. *The AAPS Journal* **16**, 914-924 (2014).
58. S. H. Cho, C. H. Chen, F. S. Tsai, J. M. Godin, Y.-H. Lo, Human mammalian cell sorting using a highly integrated micro-fabricated fluorescence-activated cell sorter (microFACS). *Lab on a Chip* **10**, 1567-1573 (2010).

8 References

59. H. Bow, I. V. Pivkin, M. Diez-Silva, S. J. Goldfless, M. Dao, J. C. Niles, S. Suresh, J. Han, A microfabricated deformability-based flow cytometer with application to malaria. *Lab on a Chip* **11**, 1065-1073 (2011).
60. M. Charnley, M. Textor, A. Khademhosseini, M. P. Lutolf, Integration column: microwell arrays for mammalian cell culture. *Integrative Biology* **1**, 625-634 (2009).
61. I. Biran, D. R. Walt, Optical Imaging Fiber-Based Single Live Cell Arrays: A High-Density Cell Assay Platform. *Analytical Chemistry* **74**, 3046-3054 (2002).
62. K. Eyer, P. Kuhn, C. Hanke, P. S. Dittrich, A microchamber array for single cell isolation and analysis of intracellular biomolecules. *Lab on a Chip* **12**, 765-772 (2012).
63. J. L. Connell, A. K. Wessel, M. R. Parsek, A. D. Ellington, M. Whiteley, J. B. Shear, Probing Prokaryotic Social Behaviors with Bacterial “Lobster Traps”. *mBio* **1**, e00202-00210 (2010).
64. M. Yang, C. W. Li, J. Yang, Cell docking and on-chip monitoring of cellular reactions with a controlled concentration gradient on a microfluidic device. *Analytical Chemistry* **74**, 3991-4001 (2002).
65. D. Di Carlo, N. Aghdam, L. P. Lee, Single-cell enzyme concentrations, kinetics, and inhibition analysis using high-density hydrodynamic cell isolation arrays. *Analytical Chemistry* **78**, 4925-4930 (2006).
66. M. Théry, Micropatterning as a tool to decipher cell morphogenesis and functions. *Journal of Cell Science* **123**, 4201-4213 (2010).
67. M. Jang, Y. Nam, Aqueous micro-contact printing of cell-adhesive biomolecules for patterning neuronal cell cultures. *BioChip Journal* **6**, 107-113 (2012).
68. N. M. Rodriguez, R. A. Desai, B. Trappmann, B. M. Baker, C. S. Chen, Micropatterned Multicolor Dynamically Adhesive Substrates to Control Cell Adhesion and Multicellular Organization. *Langmuir* **30**, 1327-1335 (2014).
69. G. D. Nicodemus, S. J. Bryant, Cell Encapsulation in Biodegradable Hydrogels for Tissue Engineering Applications. *Tissue Engineering. Part B, Reviews* **14**, 149-165 (2008).
70. K. Eyer, S. Stratz, P. Kuhn, S. K. Küster, P. S. Dittrich, Implementing Enzyme-Linked Immunosorbent Assays on a Microfluidic Chip To Quantify Intracellular Molecules in Single Cells. *Analytical Chemistry* **85**, 3280-3287 (2013).
71. Z. Zhu, O. Frey, D. S. Ottoz, F. Rudolf, A. Hierlemann, Microfluidic single-cell cultivation chip with controllable immobilization and selective release of yeast cells. *Lab on a Chip* **12**, 906-915 (2012).

8 References

72. M.-C. Kim, B. C. Isenberg, J. Sutin, A. Meller, J. Y. Wong, C. M. Klapperich, Programmed trapping of individual bacteria using micrometre-size sieves. *Lab on a Chip* **11**, 1089-1095 (2011).
73. N. Bryan, P. Birch, C. Stanley, D. Bond, J. A. Hunt, The use of acoustic force capture to ultra-purify lymphocyte subpopulations from human adult whole blood. *Journal of Tissue Engineering and Regenerative Medicine* **7**, 812-818 (2013).
74. X. Ding, Z. Peng, S.-C. S. Lin, M. Geri, S. Li, P. Li, Y. Chen, M. Dao, S. Suresh, T. J. Huang, Cell separation using tilted-angle standing surface acoustic waves. *Proceedings of the National Academy of Sciences of the United States of America* **111**, 12992-12997 (2014).
75. J. Nilsson, M. Evander, B. Hammarström, T. Laurell, Review of cell and particle trapping in microfluidic systems. *Analytica Chimica Acta* **649**, 141-157 (2009).
76. J. Gimsa, T. Müller, T. Schnelle, G. Fuhr, Dielectric spectroscopy of single human erythrocytes at physiological ionic strength: dispersion of the cytoplasm. *Biophysical Journal* **71**, 495-506 (1996).
77. A. Ashkin, J. M. Dziedzic, T. Yamane, Optical trapping and manipulation of single cells using infrared laser beams. *Nature* **330**, 769-771 (1987).
78. A. M. Klein, L. Mazutis, I. Akartuna, N. Tallapragada, A. Veres, V. Li, L. Peshkin, D. A. Weitz, M. W. Kirschner, Droplet Barcoding for Single-Cell Transcriptomics Applied to Embryonic Stem Cells. *Cell* **161**, 1187-1201 (2015).
79. J. F. Edd, D. Di Carlo, K. J. Humphry, S. Köster, D. Irimia, D. A. Weitz, M. Toner, Controlled encapsulation of single cells into monodisperse picoliter drops. *Lab on a chip* **8**, 1262-1264 (2008).
80. C.-P. Jen, J.-H. Hsiao, N. A. Maslov, Single-Cell Chemical Lysis on Microfluidic Chips with Arrays of Microwells. *Sensors* **12**, 347-358 (2011).
81. J. R. Rettig, A. Folch, Large-Scale Single-Cell Trapping And Imaging Using Microwell Arrays. *Analytical Chemistry* **77**, 5628-5634 (2005).
82. K. Bernath, M. Hai, E. Mastrobattista, A. D. Griffiths, S. Magdassi, D. S. Tawfik, In vitro compartmentalization by double emulsions: sorting and gene enrichment by fluorescence activated cell sorting. *Analytical Biochemistry* **325**, 151-157 (2004).
83. P. S. Dittrich, Cell and Vesicle Analysis in Microchambers. *Biophysical Journal* **108**, 371a (2015).
84. A. Khademhosseini, R. Langer, J. Borenstein, J. P. Vacanti, Microscale technologies for tissue engineering and biology. *Proceedings of the National Academy of Sciences of the United States of America* **103**, 2480-2487 (2006).

8 References

85. V. I. Chin, P. Taupin, S. Sanga, J. Scheel, F. H. Gage, S. N. Bhatia, Microfabricated platform for studying stem cell fates. *Biotechnology and Bioengineering* **88**, 399-415 (2004).
86. H. Bachmann, M. Fischlechner, I. Rabbers, N. Barfa, F. Branco dos Santos, D. Molenaar, B. Teusink, Availability of public goods shapes the evolution of competing metabolic strategies. *Proceedings of the National Academy of Sciences of the United States of America* **110**, 14302-14307 (2013).
87. A. Rakszewska, J. Tel, V. Chokkalingam, W. T. S. Huck, One drop at a time: toward droplet microfluidics as a versatile tool for single-cell analysis. *NPG Asia Materials* **6**, e133 (2014).
88. H. N. Joensson, H. Andersson Svahn, Droplet Microfluidics—A Tool for Single-Cell Analysis. *Angewandte Chemie International Edition* **51**, 12176-12192 (2012).
89. J. Clausell-Tormos, D. Lieber, J.-C. Baret, A. El-Harrak, O. J. Miller, L. Frenz, J. Blouwolff, K. J. Humphry, S. Köster, H. Duan, C. Holtze, D. A. Weitz, A. D. Griffiths, C. A. Merten, Droplet-Based Microfluidic Platforms for the Encapsulation and Screening of Mammalian Cells and Multicellular Organisms. *Chemistry & Biology* **15**, 427-437 (2008).
90. D. Dressman, H. Yan, G. Traverso, K. W. Kinzler, B. Vogelstein, Transforming single DNA molecules into fluorescent magnetic particles for detection and enumeration of genetic variations. *Proceedings of the National Academy of Sciences of the United States of America* **100**, 8817-8822 (2003).
91. M. M. Kiss, L. Ortoleva-Donnelly, N. R. Beer, J. Warner, C. G. Bailey, B. W. Colston, J. M. Rothberg, D. R. Link, J. H. Leamon, High-Throughput Quantitative PCR in Picoliter Droplets. *Analytical chemistry* **80**, 8975-8981 (2008).
92. A. Salehi-Reyhani, E. Burgin, O. Ces, K. R. Willison, D. R. Klug, Addressable droplet microarrays for single cell protein analysis. *The Analyst* **139**, 5367-5374 (2014).
93. B. L. Wang, A. Ghaderi, H. Zhou, J. Agresti, D. A. Weitz, G. R. Fink, G. Stephanopoulos, Microfluidic high-throughput culturing of single cells for selection based on extracellular metabolite production or consumption. *Nature Biotechnology* **32**, 473-478 (2014).
94. M. A. Unger, H.-P. Chou, T. Thorsen, A. Scherer, S. R. Quake, Monolithic Microfabricated Valves and Pumps by Multilayer Soft Lithography. *Science* **288**, 113-116 (2000).
95. R. A. Kellogg, R. Gómez-Sjöberg, A. A. Leyrat, S. Tay, High-throughput microfluidic single-cell analysis pipeline for studies of signaling dynamics. *Nature Protocols* **9**, 1713-1726 (2014).

8 References

96. A. M. Streets, X. Zhang, C. Cao, Y. Pang, X. Wu, L. Xiong, L. Yang, Y. Fu, L. Zhao, F. Tang, Y. Huang, Microfluidic single-cell whole-transcriptome sequencing. *Proceedings of the National Academy of Sciences of the United States of America* **111**, 7048-7053 (2014).
97. S. R. Bates, S. R. Quake, Highly parallel measurements of interaction kinetic constants with a microfabricated optomechanical device. *Applied Physics Letters* **95**, 073705 (2009).
98. L. Nan, Z. Jiang, X. Wei, Emerging microfluidic devices for cell lysis: a review. *Lab on a Chip* **14**, 1060-1073 (2014).
99. R. Kotlowski, A. Martin, A. Ablordey, K. Chemlal, P.-A. Fonteyne, F. Portaels, One-tube cell lysis and DNA extraction procedure for PCR-based detection of *Mycobacterium ulcerans* in aquatic insects, molluscs and fish. *Journal of Medical Microbiology* **53**, 927-933 (2004).
100. X. Chen, D. Cui, C. Liu, H. Li, J. Chen, Continuous flow microfluidic device for cell separation, cell lysis and DNA purification. *Analytica Chimica Acta* **584**, 237-243 (2007).
101. M. F. Santillo, M. L. Heien, A. G. Ewing, Temporal analysis of protozoan lysis in a microfluidic device. *Lab on a Chip* **9**, 2796-2802 (2009).
102. C.-P. Jen, T. G. Amstislavskaya, Y.-H. Liu, J.-H. Hsiao, Y.-H. Chen, Single-Cell Electric Lysis on an Electroosmotic-Driven Microfluidic Chip with Arrays of Microwells. *Sensors (Basel, Switzerland)* **12**, 6967-6977 (2012).
103. A. S. Johnson, A. Selimovic, R. S. Martin, Microchip-based electrochemical detection for monitoring cellular systems. *Analytical and Bioanalytical Chemistry* **405**, 3013-3020 (2013).
104. H. Y. Wang, P. Banada, A. K. Bhunia, C. Lu, in *Microchip-Based Assay Systems: Methods and Applications*, Humana Press, Totowa, 2007.
105. H. Y. Wang, P. P. Banada, A. K. Bhunia, C. Lu, Rapid electrical lysis of bacterial cells in a microfluidic device. *Methods in Molecular Biology* **385**, 23-35 (2007).
106. Z. G. Li, A. Q. Liu, E. Klaseboer, J. B. Zhang, C. D. Ohl, Single cell membrane poration by bubble-induced microjets in a microfluidic chip. *Lab on a Chip* **13**, 1144-1150 (2013).
107. P. A. Quinto-Su, C. Kuss, P. R. Preiser, C.-D. Ohl, Red blood cell rheology using single controlled laser-induced cavitation bubbles. *Lab on a Chip* **11**, 672-678 (2011).
108. P. A. Quinto-Su, H.-H. Lai, H. H. Yoon, C. E. Sims, N. L. Allbritton, V. Venugopalan, Examination of laser microbeam cell lysis in a PDMS microfluidic channel using time-resolved imaging. *Lab on a Chip* **8**, 408-414 (2008).

8 References

109. H. Reinhardt, P. S. Dittrich, A. Manz, J. Franzke, Micro-Hotplate enhanced optical heating by infrared light for single cell treatment. *Lab on a Chip* **7**, 1509-1514 (2007).
110. C.-Y. Lee, G.-B. Lee, J.-L. Lin, F.-C. Huang, C.-S. Liao, Integrated microfluidic systems for cell lysis, mixing/pumping and DNA amplification. *Journal of Micromechanics and Microengineering* **15**, 1215 (2005).
111. D. Di Carlo, K.-H. Jeong, L. P. Lee, Reagentless mechanical cell lysis by nanoscale barbs in microchannels for sample preparation. *Lab on a Chip* **3**, 287-291 (2003).
112. H. Kortmann, F. Kurth, L. M. Blank, P. S. Dittrich, A. Schmid, Towards real time analysis of protein secretion from single cells. *Lab on a Chip* **9**, 3047-3049 (2009).
113. A. Walter, A. Marz, W. Schumacher, P. Rosch, J. Popp, Towards a fast, high specific and reliable discrimination of bacteria on strain level by means of SERS in a microfluidic device. *Lab on a Chip* **11**, 1013-1021 (2011).
114. M. Li, J. Xu, M. Romero-Gonzalez, S. A. Banwart, W. E. Huang, Single cell Raman spectroscopy for cell sorting and imaging. *Current Opinion in Biotechnology* **23**, 56-63 (2012).
115. T. A. Nguyen, T.-I. Yin, D. Reyes, G. A. Urban, Microfluidic Chip with Integrated Electrical Cell-Impedance Sensing for Monitoring Single Cancer Cell Migration in Three-Dimensional Matrixes. *Analytical Chemistry* **85**, 11068-11076 (2013).
116. A. R. Wu, N. F. Neff, T. Kalisky, P. Dalerba, B. Treutlein, M. E. Rothenberg, F. M. Mburu, G. L. Mantalas, S. Sim, M. F. Clarke, S. R. Quake, Quantitative assessment of single-cell RNA-sequencing methods. *Nature Methods* **11**, 41-46 (2014).
117. S. S. Agasti, M. Liang, V. M. Peterson, H. Lee, R. Weissleder, Photocleavable DNA Barcode–Antibody Conjugates Allow Sensitive and Multiplexed Protein Analysis in Single Cells. *Journal of the American Chemical Society* **134**, 18499-18502 (2012).
118. Q. Shi, L. Qin, W. Wei, F. Geng, R. Fan, Y. Shik Shin, D. Guo, L. Hood, P. S. Mischel, J. R. Heath, Single-cell proteomic chip for profiling intracellular signaling pathways in single tumor cells. *Proceedings of the National Academy of Sciences of the United States of America* **109**, 419-424 (2012).
119. K. J. Boggio, E. Obasuyi, K. Sugino, S. B. Nelson, N. Y. R. Agar, J. N. Agar, Recent advances in single-cell MALDI mass spectrometry imaging and potential clinical impact. *Expert Review of Proteomics* **8**, 591-604 (2011).
120. A. J. Ibáñez, S. R. Fagerer, A. M. Schmidt, P. L. Urban, K. Jefimovs, P. Geiger, R. Dechant, M. Heinemann, R. Zenobi, Mass spectrometry-based metabolomics of single yeast cells. *Proceedings of the National Academy of Sciences of the United States of America* **110**, 8790-8794 (2013).

8 References

121. S. C. Bendall, E. F. Simonds, P. Qiu, E.-A. D. Amir, P. O. Krutzik, R. Finck, R. V. Bruggner, R. Melamed, A. Trejo, O. I. Ornatsky, R. S. Balderas, S. K. Plevritis, K. Sachs, D. Pe'er, S. D. Tanner, G. P. Nolan, Single-Cell Mass Cytometry of Differential Immune and Drug Responses Across a Human Hematopoietic Continuum. *Science* **332**, 687-696 (2011).
122. P. E. Verboket, O. Borovinskaya, N. Meyer, D. Günther, P. S. Dittrich, A New Microfluidics-Based Droplet Dispenser for ICPMS. *Analytical Chemistry* **86**, 6012-6018 (2014).
123. R. S. Yalow, S. A. Berson, Assay of Plasma Insulin in Human Subjects by Immunological Methods. *Nature* **184**, 1648-1649 (1959).
124. K. E. Rubenstein, R. S. Schneider, E. F. Ullman, "Homogeneous" enzyme immunoassay. A new immunochemical technique. *Biochemical and Biophysical Research Communications* **47**, 846-851 (1972).
125. M. E. Jolley, S. D. Stroupe, K. S. Schwenzler, C. J. Wang, M. Lu-Steffes, H. D. Hill, S. R. Popelka, J. T. Holen, D. M. Kelso, Fluorescence polarization immunoassay. iii. an automated system for therapeutic drug determination. *Clinical Chemistry* **27**, 1575-1579 (1981).
126. C. Dodeigne, L. Thunus, R. Lejeune, Chemiluminescence as diagnostic tool. A review. *Talanta* **51**, 415-439 (2000).
127. G. Kohler, C. Milstein, Continuous cultures of fused cells secreting antibody of predefined specificity. *Nature* **256**, 495-497 (1975).
128. D. A. A. Vignali, Multiplexed particle-based flow cytometric assays. *Journal of Immunological Methods* **243**, 243-255 (2000).
129. S. Park, H. J. Lee, W.-G. Koh, Multiplex Immunoassay Platforms Based on Shape-Coded Poly(ethylene glycol) Hydrogel Microparticles Incorporating Acrylic Acid. *Sensors (Basel, Switzerland)* **12**, 8426-8436 (2012).
130. C. M. Niemeyer, M. Adler, R. Wacker, Detecting antigens by quantitative immuno-PCR. *Nature Protocols* **2**, 1918-1930 (2007).
131. K. Ren, J. Wu, F. Yan, H. Ju, Ratiometric electrochemical proximity assay for sensitive one-step protein detection. *Scientific Reports* **4**, 4360-4365 (2014).
132. S. A. Kazane, D. Sok, E. H. Cho, M. L. Uson, P. Kuhn, P. G. Schultz, V. V. Smider, Site-specific DNA-antibody conjugates for specific and sensitive immuno-PCR. *Proceedings of the National Academy of Sciences of the United States of America* **109**, 3731-3736 (2012).
133. I. A. Darwish, Immunoassay Methods and their Applications in Pharmaceutical Analysis: Basic Methodology and Recent Advances. *International Journal of Biomedical Science : IJBS* **2**, 217-235 (2006).
134. B. B. Haab, Methods and applications of antibody microarrays in cancer research. *Proteomics* **3**, 2116-2122 (2003).

8 References

135. M. J. Wheeler, J. S. Morley Hutchinson, in *Hormone Assays in Biological Fluids*, vol. 324, Humana Press, Totowa, 2006.
136. S. H. Y. Wong, I. Sunshine, in *Handbook of analytical therapeutic drug monitoring and toxicology*, CRC Press, Boca Raton, 1996.
137. T. K. Christopoulos, E. P. Diamandis, IMMUNOASSAY CONFIGURATIONS. In *Immunoassay*, Academic Press, San Diego, 1996.
138. A. Oubiña, B. Ballesteros, P. Bou Carrasco, R. Galve, J. Gascón, F. Iglesias, N. Sanvicens, M.-P. Marco, Immunoassays for environmental analysis. In *Techniques and Instrumentation in Analytical Chemistry*, vol. 21, Elsevier, Amsterdam, 2000.
139. D. Goldblatt, Affinity of Antigen–Antibody Interactions. In *Encyclopedia of Life Sciences*, John Wiley & Sons, Ltd, Chichester, 2001.
140. T. K. Christopoulos, E. P. Diamandis, THEORY OF IMMUNOASSAYS. In *Immunoassay*, Academic Press, San Diego, 1996.
141. P. Tijssen, Kinetics and nature of antibody-antigen interactions. In *Laboratory Techniques in Biochemistry and Molecular Biology*, vol. 15, Elsevier, Amsterdam, 1985.
142. A. Salehi-Reyhani, S. Sharma, E. Burgin, M. Barclay, A. Cass, M. A. A. Neil, O. Ces, K. R. Willison, D. R. Klug, Scaling advantages and constraints in miniaturized capture assays for single cell protein analysis. *Lab on a Chip* **13**, 2066-2074 (2013).
143. R. M. Lequin, Enzyme Immunoassay (EIA)/Enzyme-Linked Immunosorbent Assay (ELISA). *Clinical Chemistry* **51**, 2415-2418 (2005).
144. Z. Qu, H. Xu, P. Xu, K. Chen, R. Mu, J. Fu, H. Gu, Ultrasensitive ELISA Using Enzyme-Loaded Nanospherical Brushes as Labels. *Analytical Chemistry* **86**, 9367-9371 (2014).
145. U. Resch-Genger, M. Grabolle, S. Cavaliere-Jaricot, R. Nitschke, T. Nann, Quantum dots versus organic dyes as fluorescent labels. *Nature Methods* **5**, 763-775 (2008).
146. F.-Y. Kong, B.-Y. Xu, J.-J. Xu, H.-Y. Chen, Simultaneous electrochemical immunoassay using CdS/DNA and PbS/DNA nanochains as labels. *Biosensors and Bioelectronics* **39**, 177-182 (2013).
147. I. Weeks, I. Beheshti, F. McCapra, A. K. Campbell, J. S. Woodhead, Acridinium esters as high-specific-activity labels in immunoassay. *Clinical Chemistry* **29**, 1474-1479 (1983).
148. G. Shan, W. Huang, S. J. Gee, B. A. Buchholz, J. S. Vogel, B. D. Hammock, Isotope-labeled immunoassays without radiation waste. *Proceedings of the National Academy of Sciences of the United States of America* **97**, 2445-2449 (2000).

8 References

149. R. C. Brown, Z. Li, A. J. Rutter, X. Mu, O. H. Weeks, K. Smith, I. Weeks, Development and application of a novel acridinium ester for use as a chemiluminescent emitter in nucleic acid hybridisation assays using chemiluminescence quenching. *Organic & Biomolecular Chemistry* **7**, 386-394 (2009).
150. A. Gadow, H. Fricke, C. J. Strasburger, W. G. Wood, Synthesis and evaluation of luminescent tracers and hapten-protein conjugates for use in luminescence immunoassays with immobilised antibodies and antigens. A critical study of macro solid phases for use in immunoassay systems, Part II. *Journal of clinical chemistry and clinical biochemistry* **22**, 337-347 (1984).
151. A. A. Prasse, T. Zauner, K. Büttner, R. Hoffmann, T. Zuchner, Improvement of an antibody-enzyme coupling yield by enzyme surface supercharging. *BMC Biotechnology* **14**, 88 (2014).
152. W. C. Davis, in *Monoclonal Antibody Protocols*, vol. 45, Humana Press, Totowa, 1995.
153. J. L. Guesdon, T. Ternynck, S. Avrameas, The use of avidin-biotin interaction in immunoenzymatic techniques. *Journal of Histochemistry & Cytochemistry* **27**, 1131-1139 (1979).
154. B. Akerström, T. Brodin, K. Reis, L. Björck, Protein G: a powerful tool for binding and detection of monoclonal and polyclonal antibodies. *The Journal of Immunology* **135**, 2589-2592 (1985).
155. N. Malou, D. Raoult, Immuno-PCR: a promising ultrasensitive diagnostic method to detect antigens and antibodies. *Trends in Microbiology* **19**, 295-302 (2011).
156. L. Song, D. Shan, M. Zhao, B. A. Pink, K. A. Minnehan, L. York, M. Gardel, S. Sullivan, A. F. Phillips, R. B. Hayman, D. R. Walt, D. C. Duffy, Direct Detection of Bacterial Genomic DNA at Sub-Femtomolar Concentrations Using Single Molecule Arrays. *Analytical Chemistry* **85**, 1932-1939 (2013).
157. D. M. Rissin, D. R. Fournier, T. Piech, C. W. Kan, T. G. Campbell, L. Song, L. Chang, A. J. Rivnak, P. P. Patel, G. K. Provuncher, E. P. Ferrell, S. C. Howes, B. A. Pink, K. A. Minnehan, D. H. Wilson, D. C. Duffy, Simultaneous Detection of Single Molecules and Singulated Ensembles of Molecules Enables Immunoassays with Broad Dynamic Range. *Analytical Chemistry* **83**, 2279-2285 (2011).
158. L. Chang, D. M. Rissin, D. R. Fournier, T. Piech, P. P. Patel, D. H. Wilson, D. C. Duffy, Single Molecule Enzyme-Linked Immunosorbent Assays: Theoretical Considerations. *Journal of Immunological Methods* **378**, 102-115 (2012).

8 References

159. D. M. Rissin, C. W. Kan, T. G. Campbell, S. C. Howes, D. R. Fournier, L. Song, T. Piech, P. P. Patel, L. Chang, A. J. Rivnak, E. P. Ferrell, J. D. Randall, G. K. Provuncher, D. R. Walt, D. C. Duffy, Single-molecule enzyme-linked immunosorbent assay detects serum proteins at subfemtomolar concentrations. *Nature Biotechnology* **28**, 595-599 (2010).
160. T. Escherich, Die Darmbakterien des Neugeborenen und Säuglings. *Fortschritte der Medizin* **3**, 515-522 (1885).
161. E. L. Tatum, J. Lederberg, Gene Recombination in the Bacterium *Escherichia coli*. *Journal of Bacteriology* **53**, 673-684 (1947).
162. J. Lederberg, Genetic recombination in bacteria: a discovery account. *Annual review of genetics* **21**, 23-46 (1987).
163. R. E. Lenski, M. R. Rose, S. C. Simpson, S. C. Tadler, Long-term experimental evolution in *Escherichia coli*. I. Adaptation and divergence during 2,000 generations. *American Naturalist*, 1315-1341 (1991).
164. P. D. Sniegowski, P. J. Gerrish, R. E. Lenski, Evolution of high mutation rates in experimental populations of *E. coli*. *Nature* **387**, 703-705 (1997).
165. V. S. Cooper, R. E. Lenski, The population genetics of ecological specialization in evolving *Escherichia coli* populations. *Nature* **407**, 736-739 (2000).
166. R. Lenski, J. Mongold, P. Sniegowski, M. Travisano, F. Vasi, P. Gerrish, T. Schmidt, Evolution of competitive fitness in experimental populations of *E. coli*: What makes one genotype a better competitor than another? *Antonie van Leeuwenhoek Journal of Microbiology* **73**, 35-47 (1998).
167. S. N. Cohen, A. C. Y. Chang, H. W. Boyer, R. B. Helling, Construction of Biologically Functional Bacterial Plasmids In Vitro. *Proceedings of the National Academy of Sciences of the United States of America* **70**, 3240-3244 (1973).
168. J. S. Huston, D. Levinson, M. Mudgett-Hunter, M. S. Tai, J. Novotný, M. N. Margolies, R. J. Ridge, R. E. Brucoleri, E. Haber, R. Crea, Protein engineering of antibody binding sites: recovery of specific activity in an anti-digoxin single-chain Fv analogue produced in *Escherichia coli*. *Proceedings of the National Academy of Sciences of the United States of America* **85**, 5879-5883 (1988).
169. I. Johnson, Human insulin from recombinant DNA technology. *Science* **219**, 632-637 (1983).
170. R. Chen, Bacterial expression systems for recombinant protein production: *E. coli* and beyond. *Biotechnology Advances* **30**, 1102-1107 (2012).
171. N. Blanco, M. Reidy, J. Arroyo, E. Cabib, Crosslinks in the cell wall of budding yeast control morphogenesis at the mother-bud neck. *Journal of Cell Science* **125**, 5781-5789 (2012).

8 References

172. J.-L. Legras, D. Merdinoglu, J.-M. Cornuet, F. Karst, Bread, beer and wine: *Saccharomyces cerevisiae* diversity reflects human history. *Molecular Ecology* **16**, 2091-2102 (2007).
173. P. E. McGovern, J. Zhang, J. Tang, Z. Zhang, G. R. Hall, R. A. Moreau, A. Nuñez, E. D. Butrym, M. P. Richards, C.-S. Wang, G. Cheng, Z. Zhao, C. Wang, Fermented beverages of pre- and proto-historic China. *Proceedings of the National Academy of Sciences of the United States of America* **101**, 17593-17598 (2004).
174. A. Goffeau, B. G. Barrell, H. Bussey, R. W. Davis, B. Dujon, H. Feldmann, F. Galibert, J. D. Hoheisel, C. Jacq, M. Johnston, E. J. Louis, H. W. Mewes, Y. Murakami, P. Philippsen, H. Tettelin, S. G. Oliver, Life with 6000 Genes. *Science* **274**, 546-567 (1996).
175. D. Botstein, G. R. Fink, Yeast: an experimental organism for modern biology. *Science* **240**, 1439-1443 (1988).
176. E. A. Winzeler, D. D. Shoemaker, A. Astromoff, H. Liang, K. Anderson, B. Andre, R. Bangham, R. Benito, J. D. Boeke, H. Bussey, A. M. Chu, C. Connelly, K. Davis, F. Dietrich, S. W. Dow, M. El Bakkoury, F. Foury, S. H. Friend, E. Gentalen, G. Giaever, J. H. Hegemann, T. Jones, M. Laub, H. Liao, N. Liebundguth, D. J. Lockhart, A. Lucau-Danila, M. Lussier, N. M'Rabet, P. Menard, M. Mittmann, C. Pai, C. Rebischung, J. L. Revuelta, L. Riles, C. J. Roberts, P. Ross-MacDonald, B. Scherens, M. Snyder, S. Sookhai-Mahadeo, R. K. Storms, S. Veronneau, M. Voet, G. Volckaert, T. R. Ward, R. Wysocki, G. S. Yen, K. Yu, K. Zimmermann, P. Philippsen, M. Johnston, R. W. Davis, Functional characterization of the *S. cerevisiae* genome by gene deletion and parallel analysis. *Science* **285**, 901-906 (1999).
177. G. Giaever, A. M. Chu, L. Ni, C. Connelly, L. Riles, S. Veronneau, S. Dow, A. Lucau-Danila, K. Anderson, B. Andre, A. P. Arkin, A. Astromoff, M. El-Bakkoury, R. Bangham, R. Benito, S. Brachat, S. Campanaro, M. Curtiss, K. Davis, A. Deutschbauer, K. D. Entian, P. Flaherty, F. Foury, D. J. Garfinkel, M. Gerstein, D. Gotte, U. Guldener, J. H. Hegemann, S. Hempel, Z. Herman, D. F. Jaramillo, D. E. Kelly, S. L. Kelly, P. Kotter, D. LaBonte, D. C. Lamb, N. Lan, H. Liang, H. Liao, L. Liu, C. Luo, M. Lussier, R. Mao, P. Menard, S. L. Ooi, J. L. Revuelta, C. J. Roberts, M. Rose, P. Ross-Macdonald, B. Scherens, G. Schimmack, B. Shafer, D. D. Shoemaker, S. Sookhai-Mahadeo, R. K. Storms, J. N. Strathern, G. Valle, M. Voet, G. Volckaert, C. Y. Wang, T. R. Ward, J. Wilhelmy, E. A. Winzeler, Y. Yang, G. Yen, E. Youngman, K. Yu, H. Bussey, J. D. Boeke, M. Snyder, P. Philippsen, R. W. Davis, M. Johnston, Functional profiling of the *Saccharomyces cerevisiae* genome. *Nature* **418**, 387-391 (2002).

8 References

178. D. Salk, K. Au, H. Hoehn, G. M. Martin, Cytogenetics of Werner's syndrome cultured skin fibroblasts: variegated translocation mosaicism. *Cytogenetics and cell genetics* **30**, 92-107 (1981).
179. D. A. Sinclair, K. Mills, L. Guarente, Accelerated Aging and Nucleolar Fragmentation in Yeast *sgs1* Mutants. *Science* **277**, 1313-1316 (1997).
180. M. Strand, T. A. Prolla, R. M. Liskay, T. D. Petes, Destabilization of tracts of simple repetitive DNA in yeast by mutations affecting DNA mismatch repair. *Nature* **365**, 274-276 (1993).
181. R. S. Aiyar, M. Bohnert, S. Duvezin-Caubet, C. Voisset, J. Gagneur, E. S. Fritsch, E. Couplan, K. von der Malsburg, C. Funaya, F. Soubigou, F. Courtin, S. Suresh, R. Kucharczyk, J. Evrard, C. Antony, R. P. St-Onge, M. Blondel, J.-P. di Rago, M. van der Laan, L. M. Steinmetz, Mitochondrial protein sorting as a therapeutic target for ATP synthase disorders. *Nature Communications* **5**, 5585 (2014).
182. N. Dhungel, S. Eleuteri, L.-B. Li, N. J. Kramer, J. W. Chartron, B. Spencer, K. Kosberg, J. A. Fields, K. Stafa, A. Adame, H. Lashuel, J. Frydman, K. Shen, E. Masliah, A. D. Gitler, Parkinson's Disease Genes VPS35 and EIF4G1 Interact Genetically and Converge on α -Synuclein. *Neuron* **85**, 76-87
183. R. Mustacchi, S. Hohmann, J. Nielsen, Yeast systems biology to unravel the network of life. *Yeast* **23**, 227-238 (2006).
184. L. Hood, R. M. Perlmutter, The impact of systems approaches on biological problems in drug discovery. *Nature Biotechnology* **22**, 1215-1217 (2004).
185. N. A. Buijs, V. Siewers, J. Nielsen, Advanced biofuel production by the yeast *Saccharomyces cerevisiae*. *Current opinion in chemical biology* **17**, 480-488 (2013).
186. B. Pscheidt, A. Glieder, Yeast cell factories for fine chemical and API production. *Microbial Cell Factories* **7**, 25 (2008).
187. M. E. Lidstrom, M. C. Konopka, The role of physiological heterogeneity in microbial population behavior. *Nature Chemical Biology* **6**, 705-712 (2010).
188. F. Buettner, K. N. Natarajan, F. P. Casale, V. Proserpio, A. Scialdone, F. J. Theis, S. A. Teichmann, J. C. Marioni, O. Stegle, Computational analysis of cell-to-cell heterogeneity in single-cell RNA-sequencing data reveals hidden subpopulations of cells. *Nature Biotechnology* **33**, 155-160 (2015).
189. M. Kaern, T. C. Elston, W. J. Blake, J. J. Collins, Stochasticity in gene expression: from theories to phenotypes. *Nature Reviews Genetics* **6**, 451-464 (2005).
190. Y. Ito, H. Toyota, K. Kaneko, T. Yomo, How selection affects phenotypic fluctuation. *Molecular Systems Biology* **5**, 1-7 (2009).
191. B. Munsky, G. Neuert, A. Van Oudenaarden, Using gene expression noise to understand gene regulation. *Science* **336**, 183-187 (2012).

8 References

192. S. V. Avery, Microbial cell individuality and the underlying sources of heterogeneity. *Nature Reviews Microbiology* **4**, 577-587 (2006).
193. C. Cecała, S. S. Rubakhin, J. W. Mitchell, M. U. Gillette, J. V. Sweedler, A hyphenated optical trap capillary electrophoresis laser induced native fluorescence system for single-cell chemical analysis. *The Analyst* **137**, 2965-2972 (2012).
194. S. Abel, T. Bucher, M. Nicollier, I. Hug, V. Kaefer, P. Abel zur Wiesch, U. Jenal, Bi-modal Distribution of the Second Messenger c-di-GMP Controls Cell Fate and Asymmetry during the *Caulobacter* Cell Cycle. *PLOS Genetics* **9**, 1 (2013).
195. M. Kwak, L. Mu, Y. Lu, J. J. Chen, K. Brower, R. Fan, Single-cell protein secretomic signatures as potential correlates to tumor cell lineage evolution and cell-cell interaction. *Frontiers in Oncology* **3**, 1-8 (2013).
196. M. Wu, A. K. Singh, Single-cell protein analysis. *Current Opinion in Biotechnology* **23**, 83-88 (2012).
197. A. V. Ullal, V. Peterson, S. S. Agasti, S. Tuang, D. Juric, C. M. Castro, R. Weissleder, Cancer Cell Profiling by Barcoding Allows Multiplexed Protein Analysis in Fine-Needle Aspirates. *Science Translational Medicine* **6**, 219ra219 (2014).
198. J. R. S. Newman, S. Ghaemmamghami, J. Ihmels, D. K. Breslow, M. Noble, J. L. DeRisi, J. S. Weissman, Single-cell proteomic analysis of *S. cerevisiae* reveals the architecture of biological noise. *Nature* **441**, 840-846 (2006).
199. A. Eldar, M. B. Elowitz, Functional roles for noise in genetic circuits. *Nature* **467**, 167-173 (2010).
200. L. M. F. Merlo, J. W. Pepper, B. J. Reid, C. C. Maley, Cancer as an evolutionary and ecological process. *Nature Reviews Cancer* **6**, 924-935 (2006).
201. A. Marusyk, V. Almendro, K. Polyak, Intra-tumour heterogeneity: a looking glass for cancer? *Nature Reviews Cancer* **12**, 323-334 (2012).
202. M. Gerlinger, C. Swanton, How Darwinian models inform therapeutic failure initiated by clonal heterogeneity in cancer medicine. *British Journal of Cancer* **103**, 1139-1143 (2010).
203. N. C. Turner, J. S. Reis-Filho, Genetic heterogeneity and cancer drug resistance. *The Lancet Oncology* **13**, e178-e185 (2012).
204. N. Dhar, J. D. McKinney, Microbial phenotypic heterogeneity and antibiotic tolerance. *Current Opinion in Microbiology* **10**, 30-38 (2007).
205. E. Drenkard, F. M. Ausubel, *Pseudomonas* biofilm formation and antibiotic resistance are linked to phenotypic variation. *Nature* **416**, 740-743 (2002).
206. R. C. MacLean, A. R. Hall, G. G. Perron, A. Buckling, The population genetics of antibiotic resistance: integrating molecular mechanisms and treatment contexts. *Nature Reviews Genetics* **11**, 405-414 (2010).

8 References

207. N. Q. Balaban, K. Gerdes, K. Lewis, J. D. McKinney, A problem of persistence: still more questions than answers? *Nature Reviews Microbiology* **11**, 587-591 (2013).
208. J. S. Marcus, W. F. Anderson, S. R. Quake, Microfluidic Single-Cell mRNA Isolation and Analysis. *Analytical Chemistry* **78**, 3084-3089 (2006).
209. J. F. Zhong, Y. Chen, J. S. Marcus, A. Scherer, S. R. Quake, C. R. Taylor, L. P. Weiner, A microfluidic processor for gene expression profiling of single human embryonic stem cells. *Lab on a Chip* **8**, 68-74 (2008).
210. K. H. Cheong, D. K. Yi, J. G. Lee, J. M. Park, M. J. Kim, J. B. Edel, C. Ko, Gold nanoparticles for one step DNA extraction and real-time PCR of pathogens in a single chamber. *Lab on a Chip* **8**, 810 (2008).
211. K. Leung, H. Zahn, T. Leaver, K. M. Konwar, N. W. Hanson, A. P. Pagé, C. C. Lo, P. S. Chain, S. J. Hallam, C. L. Hansen, A programmable droplet-based microfluidic device applied to multiparameter analysis of single microbes and microbial communities. *Proceedings of the National Academy of Sciences of the United States of America* **109**, 7665-7670 (2012).
212. M. He, J. S. Edgar, G. D. M. Jeffries, R. M. Lorenz, J. P. Shelby, D. T. Chiu, Selective Encapsulation of Single Cells and Subcellular Organelles into Picoliter- and Femtoliter-Volume Droplets. *Analytical Chemistry* **77**, 1539-1544 (2005).
213. Y. Taniguchi, P. J. Choi, G. W. Li, H. Chen, M. Babu, J. Hearn, A. Emili, X. S. Xie, Quantifying *E. coli* proteome and transcriptome with single-molecule sensitivity in single cells. *Science* **329**, 533-538 (2010).
214. M. Beck, A. Schmidt, J. Malmstroem, M. Claassen, A. Ori, A. Szymborska, F. Herzog, O. Rinner, J. Ellenberg, R. Aebersold, The quantitative proteome of a human cell line. *Molecular Systems Biology* **7**, 1 (2011).
215. S. Busby, R. H. Ebright, Transcription activation by catabolite activator protein (CAP). *Journal of Molecular Biology* **293**, 199-213 (1999).
216. R. W. Wheatley, S. Lo, L. J. Jancewicz, M. L. Dugdale, R. E. Huber, Structural Explanation for Allolactose (lac Operon Inducer) Synthesis by lacZ β -Galactosidase and the Evolutionary Relationship between Allolactose Synthesis and the lac Repressor. *Journal of Biological Chemistry* **288**, 12993 (2013).
217. J. Stülke, W. Hillen, Carbon catabolite repression in bacteria. *Current Opinion in Microbiology* **2**, 195-201 (1999).
218. B. Llanes, E. McFall, Effect of Galactose on β -Galactosidase Synthesis in *Escherichia coli* K-12. *Journal of Bacteriology* **97**, 217-222 (1969).
219. L. Cai, N. Friedman, X. S. Xie, Stochastic protein expression in individual cells at the single molecule level. *Nature* **440**, 358-362 (2006).
220. K. Eyer, P. Kuhn, S. Stratz, P. S. Dittrich, A Microfluidic Chip for the Versatile Chemical Analysis of Single Cells. e50618 (2013).

8 References

221. C. A. Schneider, W. S. Rasband, K. W. Eliceiri, NIH Image to ImageJ: 25 years of image analysis. *Nature Methods* **9**, 671-675 (2012).
222. R. Marie, J. P. Beech, J. Vörös, J. O. Tegenfeldt, F. Höök, Use of PLL-g-PEG in Micro-Fluidic Devices for Localizing Selective and Specific Protein Binding. *Langmuir* **22**, 10103-10108 (2006).
223. H. Vaisocherová, Z. Zhang, W. Yang, Z. Cao, G. Cheng, A. D. Taylor, M. Piliarik, J. Homola, S. Jiang, Functionalizable surface platform with reduced nonspecific protein adsorption from full blood plasma—Material selection and protein immobilization optimization. *Biosensors and Bioelectronics* **24**, 1924-1930 (2009).
224. I. Banerjee, R. C. Pangule, R. S. Kane, Antifouling Coatings: Recent Developments in the Design of Surfaces That Prevent Fouling by Proteins, Bacteria, and Marine Organisms. *Advanced Materials* **23**, 690-718 (2011).
225. M. Charnley, M. Textor, C. Acikgoz, Designed polymer structures with antifouling–antimicrobial properties. *Reactive and Functional Polymers* **71**, 329-334 (2011).
226. N. Nakashima, T. Kunitake, Drastic fluorescence enhancement of cyanine dyes bound to synthetic bilayer membranes. Its high sensitivity to the chemical structure and the physical state of the membrane. *Journal of the American Chemical Society* **104**, 4261-4262 (1982).
227. S. Tyagi, *E. coli*, what a noisy bug. *Science* **329**, 518-519 (2010).
228. A. Sanchez, I. Golding, Genetic Determinants and Cellular Constraints in Noisy Gene Expression. *Science* **342**, 1188-1193 (2013).
229. D. Levens, D. R. Larson, A New Twist on Transcriptional Bursting. *Cell* **158**, 241-242 (2014).
230. D. R. Larson, What do expression dynamics tell us about the mechanism of transcription? *Current Opinion in Genetics and Development* **21**, 591-599 (2011).
231. D. Huh, J. Paulsson, Random partitioning of molecules at cell division. *Proceedings of the National Academy of Sciences of the United States of America* **108**, 15004-15009 (2011).
232. S. Behjati, M. Huch, R. van Boxtel, W. Karthaus, D. C. Wedge, A. U. Tamuri, I. Martincorena, M. Petljak, L. B. Alexandrov, G. Gudem, P. S. Tarpey, S. Roerink, J. Blokker, M. Maddison, L. Mudie, B. Robinson, S. Nik-Zainal, P. Campbell, N. Goldman, M. van de Wetering, E. Cuppen, H. Clevers, M. R. Stratton, Genome sequencing of normal cells reveals developmental lineages and mutational processes. *Nature* **513**, 422-425 (2014).
233. P. Nemes, A. M. Knolhoff, S. S. Rubakhin, J. V. Sweedler, Metabolic Differentiation of Neuronal Phenotypes by Single-cell Capillary Electrophoresis–Electrospray Ionization–Mass Spectrometry. *Analytical Chemistry* **83**, 6810-6817 (2011).

8 References

234. S. Stratz, K. Eyer, F. Kurth, P. S. Dittrich, On-Chip Enzyme Quantification of Single *Escherichia coli* Bacteria by Immunoassay-based Analysis. *Analytical Chemistry* **86**, 12375-12381 (2014).
235. R. B. Brown, J. A. Hewel, A. Emili, J. Audet, Single amino acid resolution of proteolytic fragments generated in individual cells. *Cytometry Part A* **77A**, 347-355 (2010).
236. Y. Wakamoto, N. Dhar, R. Chait, K. Schneider, F. Signorino-Gelo, S. Leibler, J. D. McKinney, Dynamic Persistence of Antibiotic-Stressed Mycobacteria. *Science* **339**, 91-95 (2013).
237. S. L. Holland, T. Reader, P. S. Dyer, S. V. Avery, Phenotypic heterogeneity is a selected trait in natural yeast populations subject to environmental stress. *Environmental Microbiology* **16**, 1729-1740 (2014).
238. M. A. Sánchez-Romero, J. Casadesús, Contribution of phenotypic heterogeneity to adaptive antibiotic resistance. *Proceedings of the National Academy of Sciences of the United States of America* **111**, 355-360 (2014).
239. S. Chauhan, P. Bhatnagar, Future of Biotechnology Companies: A Global Perspective. In *Advances in Biotechnology*, Springer India, 2014.
240. A. Demain, Importance of microbial natural products and the need to revitalize their discovery. *Journal of Industrial Microbiology & Biotechnology* **41**, 185-201 (2014).
241. M. Novo, R. Gonzalez, E. Bertran, M. Martínez, M. Yuste, P. Morales, Improved fermentation kinetics by wine yeast strains evolved under ethanol stress. *LWT - Food Science and Technology* **58**, 166-172 (2014).
242. A. Cadière, A. Ortiz-Julien, C. Camarasa, S. Dequin, Evolutionary engineered *Saccharomyces cerevisiae* wine yeast strains with increased in vivo flux through the pentose phosphate pathway. *Metabolic Engineering* **13**, 263-271 (2011).
243. D. Libkind, C. T. Hittinger, E. Valério, C. Gonçalves, J. Dover, M. Johnston, P. Gonçalves, J. P. Sampaio, Microbe domestication and the identification of the wild genetic stock of lager-brewing yeast. *Proceedings of the National Academy of Sciences of the United States of America* **108**, 14539-14544 (2011).
244. J. Wang, N. Shen, H. Yin, C. Liu, Y. Li, Q. Li, Development of Industrial Brewing Yeast with Low Acetaldehyde Production and Improved Flavor Stability. *Applied Biochemistry and Biotechnology* **169**, 1016-1025 (2013).
245. Y. Sasano, Y. Haitani, K. Hashida, I. Ohtsu, J. Shima, H. Takagi, Simultaneous accumulation of proline and trehalose in industrial baker's yeast enhances fermentation ability in frozen dough. *Journal of Bioscience and Bioengineering* **113**, 592-595 (2012).

8 References

246. Y. Sasano, Y. Haitani, K. Hashida, S. Oshiro, J. Shima, H. Takagi, Improvement of fermentation ability under baking-associated stress conditions by altering the POG1 gene expression in baker's yeast. *International Journal of Food Microbiology* **165**, 241-245 (2013).
247. F. Randez-Gil, I. Córcoles-Sáez, J. A. Prieto, Genetic and Phenotypic Characteristics of Baker's Yeast: Relevance to Baking. *Annual Review of Food Science and Technology* **4**, 191-214 (2013).
248. D. Botstein, G. R. Fink, Yeast: An Experimental Organism for 21st Century Biology. *Genetics* **189**, 695-704 (2011).
249. H. Karathia, E. Vilaprinyo, A. Sorribas, R. Alves, *Saccharomyces cerevisiae* as a Model Organism: A Comparative Study. *PLOS ONE* **6**, e16015 (2011).
250. C. Faria, C. D. Jorge, N. Borges, S. Tenreiro, T. F. Outeiro, H. Santos, Inhibition of formation of α -synuclein inclusions by mannosylglycerate in a yeast model of Parkinson's disease. *Biochimica et Biophysica Acta (BBA) - General Subjects* **1830**, 4065-4072 (2013).
251. E. Couplan, R. S. Aiyar, R. Kucharczyk, A. Kabala, N. Ezkurdia, J. Gagneur, R. P. St. Onge, B. Salin, F. Soubigou, M. Le Cann, L. M. Steinmetz, J.-P. di Rago, M. Blondel, A yeast-based assay identifies drugs active against human mitochondrial disorders. *Proceedings of the National Academy of Sciences of the United States of America* **108**, 11989-11994 (2011).
252. S. Tenreiro, M. C. Munder, S. Alberti, T. F. Outeiro, Harnessing the power of yeast to unravel the molecular basis of neurodegeneration. *Journal of Neurochemistry* **127**, 438-452 (2013).
253. S. Lambert, A. M. Carr, Replication stress and genome rearrangements: lessons from yeast models. *Current Opinion in Genetics & Development* **23**, 132-139 (2013).
254. M. Breitenbach, S. M. Jazwinski, P. Laun, in *Aging Research in Yeast*, vol. 57, Springer Netherlands, Dordrecht, 2012.
255. A. X. S. Santos, H. Riezman, Yeast as a model system for studying lipid homeostasis and function. *FEBS Letters* **586**, 2858-2867 (2012).
256. J. Avesar, T. B. Arye, S. Levenberg, Frontier microfluidic techniques for short and long-term single cell analysis. *Lab on a Chip* **14**, 2161-2167 (2014).
257. A. Grünberger, W. Wiechert, D. Kohlheyer, Single-cell microfluidics: opportunity for bioprocess development. *Current Opinion in Biotechnology* **29**, 15-23 (2014).
258. D. H. E. W. Huberts, S. S. Lee, J. González, G. E. Janssens, I. A. Vizcarra, M. Heinemann, Construction and use of a microfluidic dissection platform for long-term imaging of cellular processes in budding yeast. *Nature Protocols* **8**, 1019-1027 (2013).

8 References

259. H. Kortmann, L. M. Blank, A. Schmid, Single cell analysis reveals unexpected growth phenotype of *S. cerevisiae*. *Cytometry. Part A : the journal of the International Society for Analytical Cytology* **75**, 130-139 (2009).
260. E. Sato, T. Mokudai, Y. Niwano, M. Kohno, Kinetic analysis of reactive oxygen species generated by the in vitro reconstituted NADPH oxidase and xanthine oxidase systems. *Journal of Biochemistry* **150**, 173-181 (2011).
261. T. Yao, H. Ogawa, T. Nakahara, Highly selective and sensitive detection of NADP coenzymes using co-immobilized glucose-6-phosphate dehydrogenase/diaphorase reactors as on-line amplifiers based on substrate recycling in a chemiluminometric flow-injection system. *Talanta* **42**, 1297-1303 (1995).
262. C. Le Goffe, G. Vallette, L. Charrier, T. Candelon, C. Bou-Hanna, J. F. Bouhours, C. L. Labois, Metabolic control of resistance of human epithelial cells to H₂O₂ and NO stresses. *Biochemical Journal* **364**, 349-359 (2002).
263. P. P. Pandolfi, F. Sonati, R. Rivi, P. Mason, F. Grosveld, L. Luzzatto, Targeted disruption of the housekeeping gene encoding glucose 6-phosphate dehydrogenase (G6PD): G6PD is dispensable for pentose synthesis but essential for defense against oxidative stress. *The EMBO Journal* **14**, 5209-5215 (1995).
264. F. Sherman, Getting started with yeast. In *Methods in Enzymology*, vol. 194, Academic Press, San Diego, 1991.
265. E. R. Sumner, S. V. Avery, Phenotypic heterogeneity: differential stress resistance among individual cells of the yeast *Saccharomyces cerevisiae*. *Microbiology* **148**, 345-351 (2002).
266. C. Dusny, A. Grunberger, C. Probst, W. Wiechert, D. Kohlheyer, A. Schmid, Technical bias of microcultivation environments on single-cell physiology. *Lab on a Chip* **15**, 1822-1834 (2015).
267. C. Evans, K. Bogan, P. Song, C. Burant, R. Kennedy, C. Brenner, NAD⁺ metabolite levels as a function of vitamins and calorie restriction: evidence for different mechanisms of longevity. *BMC Chemical Biology* **10**, 2 (2010).
268. S. Lin, E. Ford, M. Haigis, G. Liszt, L. Guarente, Calorie restriction extends yeast life span by lowering the level of NADH. *Genes & Development* **18**, 12 - 16 (2004).
269. D. Huh, J. Paulsson, Non-genetic heterogeneity from stochastic partitioning at cell division. *Nature Genetics* **43**, 95-100 (2011).
270. H. Aguilaniu, L. Gustafsson, M. Rigoulet, T. Nyström, Asymmetric Inheritance of Oxidatively Damaged Proteins During Cytokinesis. *Science* **299**, 1751-1753 (2003).
271. N. Brenner, K. Farkash, E. Braun, Dynamics of protein distributions in cell populations. *Physical Biology* **3**, 172 (2006).

8 References

272. S. F. Levy, N. Ziv, M. L. Siegal, Bet Hedging in Yeast by Heterogeneous, Age-Correlated Expression of a Stress Protectant. *PLOS Biology* **10**, e1001325 (2012).
273. M. Jahn, S. Günther, S. Müller, Non-random distribution of macromolecules as driving forces for phenotypic variation. *Current Opinion in Microbiology* **25**, 49-55 (2015).
274. W. C. Ratcliff, R. F. Denison, Bacterial persistence and bet hedging in *Sinorhizobium meliloti*. *Communicative & Integrative Biology* **4**, 98-100 (2011).
275. J.-W. Veening, E. J. Stewart, T. W. Berngruber, F. Taddei, O. P. Kuipers, L. W. Hamoen, Bet-hedging and epigenetic inheritance in bacterial cell development. *Proceedings of the National Academy of Sciences of the United States of America* **105**, 4393-4398 (2008).
276. Y. Chai, T. Norman, R. Kolter, R. Losick, Evidence that metabolism and chromosome copy number control mutually exclusive cell fates in *Bacillus subtilis*. *The EMBO Journal* **30**, 1402-1413 (2011).
277. D. K. Summers, Stability of Genetic Material in Prokaryotes. *Biologicals* **21**, 91-93 (1993).
278. D. K. Summers, C. W. H. Beton, H. L. Withers, Multicopy plasmid instability: the dimer catastrophe hypothesis. *Molecular Microbiology* **8**, 1031-1038 (1993).
279. J. Wong Ng, D. Chatenay, J. Robert, M. G. Poirier, Plasmid copy number noise in monoclonal populations of bacteria. *Physical Review E* **81**, 011909 (2010).
280. D. Jendrossek, D. Pfeiffer, New insights in the formation of polyhydroxyalkanoate granules (carbonosomes) and novel functions of poly(3-hydroxybutyrate). *Environmental Microbiology* **16**, 2357-2373 (2014).
281. J. Stubbe, J. Tian, Polyhydroxyalkanoate (PHA) homeostasis: the role of PHA synthase. *Natural product reports* **20**, 445-457 (2003).
282. J. R. McFaline-Figueroa, J. Vevea, T. C. Swayne, C. Zhou, C. Liu, G. Leung, I. R. Boldogh, L. A. Pon, Mitochondrial quality control during inheritance is associated with lifespan and mother-daughter age asymmetry in budding yeast. *Aging cell* **10**, 885-895 (2011).
283. F. Gaensly, G. Picheth, D. Brand, T. M. B. Bonfim, The uptake of different iron salts by the yeast *Saccharomyces cerevisiae*. *Brazilian Journal of Microbiology* **45**, 491-494 (2014).
284. Y.-M. Shin, T.-H. Kwon, K.-S. Kim, K.-S. Chae, D.-H. Kim, J.-H. Kim, M.-S. Yang, Enhanced Iron Uptake of *Saccharomyces cerevisiae* by Heterologous Expression of a Tadpole Ferritin Gene. *Applied and Environmental Microbiology* **67**, 1280-1283 (2001).

8 References

285. F. Raguzzi, E. Lesuisse, R. R. Crichton, Iron storage in *Saccharomyces cerevisiae*. *FEBS Letters* **231**, 253-258 (1988).
286. S. S. Lee, I. Avalos Vizcarra, D. H. Huberts, L. P. Lee, M. Heinemann, Whole lifespan microscopic observation of budding yeast aging through a microfluidic dissection platform. *Proceedings of the National Academy of Sciences of the United States of America* **109**, 4916-4920 (2012).
287. H. Zhang, K.-K. Liu, Optical tweezers for single cells. *Journal of the Royal Society Interface* **5**, 671-690 (2008).
288. K. N. Han, C. A. Li, G. H. Seong, Microfluidic Chips for Immunoassays. *Annual Review of Analytical Chemistry* **6**, 119-141 (2013).
289. K. F. Lei, Microfluidic Systems for Diagnostic Applications A Review. *Journal of laboratory automation* **17**, 330-347 (2012).
290. K. M. Schilling, D. Jauregui, A. W. Martinez, Paper and toner three-dimensional fluidic devices: programming fluid flow to improve point-of-care diagnostics. *Lab on a Chip* **13**, 628-631 (2013).
291. A. M. Foudeh, T. F. Didar, T. Veres, M. Tabrizian, Microfluidic designs and techniques using lab-on-a-chip devices for pathogen detection for point-of-care diagnostics. *Lab on a Chip* **12**, 3249-3266 (2012).
292. A. H. Ng, U. Uddayasankar, A. R. Wheeler, Immunoassays in microfluidic systems. *Analytical and Bioanalytical Chemistry* **397**, 991-1007 (2010).
293. S. Xue, H. Zeng, J. Yang, H. Nakajima, K. Uchiyama, A Compact Immunoassay Platform Based on a Multicapillary Glass Plate. *Sensors (Basel, Switzerland)* **14**, 9132-9144 (2014).
294. C. D. Chin, T. Laksanasopin, Y. K. Cheung, D. Steinmiller, V. Linder, H. Parsa, J. Wang, H. Moore, R. Rouse, G. Umvilighozo, E. Karita, L. Mwambarangwe, S. L. Braunstein, J. van de Wijgert, R. Sahabo, J. E. Justman, W. El-Sadr, S. K. Sia, Microfluidics-based diagnostics of infectious diseases in the developing world. *Nature Medicine* **17**, 1015-1019 (2011).
295. V. Linder, S. K. Sia, G. M. Whitesides, Reagent-loaded cartridges for valveless and automated fluid delivery in microfluidic devices. *Analytical Chemistry* **77**, 64-71 (2005).
296. S. K. Sia, V. Linder, B. A. Parviz, A. Siegel, G. M. Whitesides, An Integrated Approach to a Portable and Low-Cost Immunoassay for Resource-Poor Settings. *Angewandte Chemie International Edition* **43**, 498-502 (2004).
297. M. L. Chiu, W. Lawi, S. T. Snyder, P. K. Wong, J. C. Liao, V. Gau, Matrix Effects—A Challenge toward Automation of Molecular Analysis. *Journal of the Association for Laboratory Automation* **15**, 233-242 (2010).
298. W. G. Wood, "Matrix effects" in immunoassays. *Scandinavian Journal of Clinical and Laboratory Investigation* **51**, 105-112 (1991).

8 References

299. V. Urbonaviciute, B. G. Fürrohr, C. Weber, M. Haslbeck, S. Wilhelm, M. Herrmann, R. E. Voll, Factors masking HMGB1 in human serum and plasma. *Journal of Leukocyte Biology* **81**, 67-74 (2007).
300. R. Reverberi, L. Reverberi, Factors affecting the antigen-antibody reaction. *Blood Transfusion* **5**, 227-240 (2007).
301. M. W. Wood, S. K. Nordone, S. L. Vaden, E. B. Breitschwerdt, Assessment of urine solute and matrix effects on the performance of an enzyme-linked immunosorbent assay for measurement of interleukin-6 in dog urine. *Journal of veterinary diagnostic investigation* **23**, 316-320 (2011).
302. M. A. Johansson, K. E. Hellenas, Matrix effects in immunobiosensor determination of clenbuterol in urine and serum. *The Analyst* **129**, 438-442 (2004).
303. I. Marchi, S. Rudaz, J. L. Veuthey, Sample preparation development and matrix effects evaluation for multianalyte determination in urine. *Journal of pharmaceutical and biomedical analysis* **49**, 459-467 (2009).
304. K. E. Mach, C. B. Du, H. Phull, D. A. Haake, M.-C. Shih, E. J. Baron, J. C. Liao, Multiplex Pathogen Identification for Polymicrobial Urinary Tract Infections Using Biosensor Technology: A Prospective Clinical Study. *The Journal of Urology* **182**, 2735-2741 (2009).
305. W. Pak Kin, W. Tza-Huei, J. H. Deval, H. Chih-Ming, Electrokinetics in micro devices for biotechnology applications. *Mechatronics, IEEE/ASME Transactions on* **9**, 366-376 (2004).
306. C. Situ, A. R. Wylie, A. Douglas, C. T. Elliott, Reduction of severe bovine serum associated matrix effects on carboxymethylated dextran coated biosensor surfaces. *Talanta* **76**, 832-836 (2008).
307. T. Robinson, P. Kuhn, K. Eyer, P. S. Dittrich, Microfluidic trapping of giant unilamellar vesicles to study transport through a membrane pore. *Biomicrofluidics* **7**, 044105 (2013).
308. P. Kuhn, K. Eyer, T. Robinson, F. I. Schmidt, J. Mercer, P. S. Dittrich, A facile protocol for the immobilisation of vesicles, virus particles, bacteria, and yeast cells. *Integrative Biology* **4**, 1550-1555 (2012).
309. A. R. C. Braga, M. F. Silva, J. V. Oliveira, H. Treichel, S. J. Kalil, A new approach to evaluate immobilization of Beta-galactosidase on Eupergit® C: structural, kinetic, and thermal characterization. *Química Nova* **37**, 796-803 (2014).
310. E. Katchalski-Katzir, D. M. Kraemer, Eupergit® C, a carrier for immobilization of enzymes of industrial potential. *Journal of Molecular Catalysis B: Enzymatic* **10**, 157-176 (2000).
311. J. Schiettecatte, E. Anckaert, J. Smits, Interferences in immunoassays. In *Advances in Immunoassay Technology*, InTech, Rijeka, 2012.
312. J. Tate, G. Ward, Interferences in Immunoassay. *The Clinical Biochemist Reviews* **25**, 105-120 (2004).

9.2 Publications & conference posters

Publications

- **S. Stratz**, P. E. Verboket, K. Hasler, P. S. Dittrich.
Cultivation and quantitative single cell analysis of *Saccharomyces cerevisiae* on a multifunctional microfluidic device. Submitted.
- **S. Stratz**, P. S. Dittrich.
A microfluidic device for immunoassay-based protein analysis of single *E. coli* bacteria, *Methods in Molecular Biology*, Issue: Single Cell Protein Analysis, Springer Verlag, in print (2015).
- **S. Stratz**, K. Eyer, F. Kurth, P. S. Dittrich.
On-chip enzyme quantification of single *Escherichia coli* bacteria by immunoassay-based analysis, *Analytical Chemistry* **86**, 12375-12381 (2014).
- K. Eyer, P. Kuhn, **S. Stratz**, P. S. Dittrich.
A microfluidic chip for the versatile chemical analysis of single cells, *Journal of Visualized Experiments* **80**, (2013).
- K. Eyer, **S. Stratz**, P. Kuhn, S. K. Küster, P. S. Dittrich.
Implementing enzyme-linked immunosorbent assays on a microfluidic chip to quantify intracellular molecules in single cells, *Analytical Chemistry* **85**, 3280-3287 (2013).
- H. H. See, **S. Stratz**, P. C. Hauser.
Electro-driven extraction across a polymer inclusion membrane in a flow-through cell, *Journal of Chromatography A* **1300**, 79-84 (2013).

Conference posters

- MicroTAS, Freiburg, Germany, October 2013.
Poster title: Towards quantitative analysis of single *E. coli* lysates.
- 6th Symposium SSCI, Zurich, Switzerland, December 2013.
Poster title: Quantitative analysis of single *E. coli* lysates.
- Materials and Processes Day, Zurich, Switzerland, June 2014.
Poster title: A microfluidic device for proteomic analysis of single *E. coli* bacteria.
- EMBL Conference Microfluidics, Heidelberg, Germany, July 2014.
Poster title: On-chip proteomic analysis of single *E. coli* bacteria.
- MicroTAS, San Antonio, USA, October 2014.
Poster title: On-chip long-term cultivation and proteomic analysis of single yeast cells.